2012-01-01

Measurement And Analysis Of Turbulent Syngas/air And Methane Oxy-Combustion

Vishwanath Reddy Ardha
University of Texas at El Paso, vrardha@miners.utep.edu

MEASUREMENT AND ANALYSIS OF TURBULENT SYNGAS/AIR AND METHANE OXY-COMBUSTION

VISHWANATH REDDY ARDHA

Energy Science and Engineering Track

Environmental Science and Engineering PhD Program

Department of Mechanical Engineering

APPROVED:

Ahsan Choudhuri, Ph.D., Chair

Norman Love, Ph.D.

Vinod Kumar, Ph.D.

Evgeny Shafirovich, Ph.D.

Jose Espiritu, Ph.D.

Benjamin C. Flores, Ph.D.
Interim Dean of the Graduate School

Dedication

I would like to dedicate this Doctoral dissertation to my father, Pandu Ranga Reddy Ardha. There is no doubt in my mind that without his continued support and counsel I could not have completed this process.

MEASUREMENT AND ANALYSIS OF TURBULENT SYNGAS/AIR AND METHANE OXY-COMBUSTION

by

VISHWANATH REDDY ARDHA, M.S

DISSERTATION

Presented to the Faculty of the Graduate School of
The University of Texas at El Paso
in Partial Fulfillment
of the Requirements
for the Degree of

DOCTOR OF PHILOSOPHY

Energy Science and Engineering Track
Environmental Science and Engineering PhD Program
Department of Mechanical Engineering
THE UNIVERSITY OF TEXAS AT EL PASO
August 2012

Acknowledgements

I would never have been able to finish my dissertation without the guidance of my committee members, help from friends, and support from my family.

I would like to express my deepest gratitude to my advisor, Dr. Ahsan Choudhuri, for his excellent guidance, caring, patience, and providing me with an excellent atmosphere for doing research. I would like to thank US Department of Energy for financially supporting my research. I would like to thank Dr. Norman Love, who patiently corrected my writing and for guiding my research. I would also like to thank my final defense committee, Dr. Vinod kumar, Dr. Evgeny Shafirovich, and Dr. Jose Espiritu.

I would like to thank Bidhan Dam, who as a good friend was always willing to help and give his best suggestions. Many thanks to Gilberto Corona, Matin del La Torre and Rafique who helped me in setting up the experiments. I would like to thank the entire CSETR unit.

I would also like to thank my parents and elder brother. They were always supporting me and encouraging me with their best wishes.

Abstract

Development of a next generation gas turbine combustors for power production by using fossil fuels is increasing substantially in order to maintain energy sustainability. National Energy Technology Laboratory has made efforts for developing hydrogen and oxy-fuel based gas turbine combustors which could enhance plant efficiency and ensure low or zero NO_x production without sacrificing operational advantages. The current experimental work aims to characterize the turbulent flow-field of premixed syngas/air flames, methane/oxy flames and syngas/oxy flames in a laboratory scaled burner by varying the Reynolds numbers, blockage ratios, firing inputs and blockage ratios in the upstream of the burner. The effects of turbulence, firing input and operating conditions on the position, local flow-field dynamics of the flame front, laminar burning velocity and turbulent burning velocities are investigated in the present study. A recent progress in high speed particle image velocimetry enables to capture the turbulent flow field with high resolution which results in better understanding of phenomena like vortex shredding at the burner exit. An experimental setup is designed to visualize the turbulent flow field of both CO-H2/air, CH4/O2/CO2 and CO-H2/O2/CO2 mixtures by varying the above parameters using high speed particle image velocimetry. The burner used in the current study is a tubular burner (19mm in diameter) with a turbulence creator positioned at a distance of 15 mm downstream from top of the burner. The blockage ratio's that is considered for the current set of experimental study are 73%, 83% and 92% respectively. The turbulence flow field of CO-H_2/air, CH4/O2/CO2 and CO-H2/O2/CO2 combustion was recorded

at different locations from the burner exit using Particle Image Velocimetry (PIV) technique.

For CO-H_2/air flames at constant equivalence ratio of 0.9 and RE of 2000 the turbulent burning velocities not only increased with increase in hydrogen content but also increased when the BR's increased .Turbulent burning velocities increased with increase in BR's as the hydrogen content increased in syngas mixture at a constant laminar burning velocity for syngas compositions varying from 10%H_2 to 30 % H_2. Turbulent burning velocities increased with increase in the BR's along with the increase in N_2 and CO_2 in Syngas mixtures.CO_2 as diluents is more prominent than N_2, the increase of CO_2 in the Syngas mixtures decrease the turbulent burning velocity.

For CH4/O2/CO2 flames at constant equivalence ratio of 1 and RE of 2500, the local velocity fluctuations not only increases with increase in BR's but also increased with increase in the firing inputs. At higher recirculation ratios of CO2, there has been a significant reduction in the flame temperature thereby resulting in reduce in effective flame area.

Table of Contents

List of Tables

List of Figures

Chapter 1: Introduction and Background

Fossil fuels are considered as one of the most economically available energy source in today's society. Due to the increase in demand for energy, the usage of fossil fuels has become a necessity to meet the current energy demand. Whereas combustion of all fossil fuel results in CO2, which is considered to be a major source for the global warming and current climate changes. CO2 emissions have become a major concern due to the extensive use of fossil fuels. Limiting the CO2 emissions in a timely manner is the best solution to fight against the climate change. Some of the technological options to achieve this include switching to less carbon intensive fuels, nuclear energy, increase in use of renewable energy, reducing the energy consumption and combustion with capture and storage of CO2 (CCS).

1.1 Oxy-Fuel Combustion:

Oxy-Fuel combustion is one of efficient methods to achieve power production from fossil fuels with capture CO2; others include post-combustion and pre-combustion capture methods [Davison and Thambiathu, 2005]. In oxy-fuel combustion, the fuel is burnt with a mixture of O2, CO2 and steam as opposed to air resulting in zero NO_x emissions. The flue gases in oxy-fuel process mainly consist of CO2 and steam. The steam is condensed, leaving with a stream of high purity CO2 ready to capture. The major disadvantage in carbon capture methods is that it not only increases the fuel needs to capture and sequester and but also capital cost for extra equipment such as air separation units [Dardea et al, 2009]. Applying this technology to the existing plants which are far from the sequestration site will prove to be expensive than the ones

closer to the sequestration site. Thus it is important to improve the efficiency of Oxy-fuel plants. Since Oxy-fuel combustion is considered as one of the best and successful post combustion CO2 capture technique which is able to achieve higher plant efficiency, the US department of energy is considering implementing this technique either by retrofitting the existing plants or by building new plants to achieve its goal of capturing 90 percent of CO2 capture without significant increase in the cost of electricity [Davison and Thambiathu, 2005]. Oxy-fuel combustion can be implemented in current turbine cycles and pulverized coal plants. In pulverized coal oxy-fuel combustion, the fossil fuels are burnt in mixture of oxygen and recirculated flue gases. The remainder of non recirculated flue gases is rich in CO2 and steam, which is good candidate for treatment of steam and capture of CO2, thereby resulting in ultra-low emissions. In oxy-fuel turbine power cycles, natural gas or coal derived syngas is used for combustion. Extremely high temperatures are recorded when these fuels are combusted with pure oxygen, so temperatures are controlled by recirculating water/CO2 in the system [Dardea et al, 2009].

1.1.1 Effect of CO2 on combustion process:

Change of oxidizer in the combustion process not only affect the combustion dynamics of a system but also modifies its flame properties, such as adiabatic flame temperature, thermal and kinetic properties, mass and heat transport properties and radiative heat transfer .The specific heat of CO2 (47300 J/mol/k) is higher than of N2 (30009 J/mol/K) is higher than that of nitrogen, so the adiabatic flame temperature for

mixtures with O2/CO2 is lower than the O2/N2 at same equivalence ratio and same oxygen percentage in the oxidizer mixture. In order to achieve temperatures closer to air-fuel mixtures, oxygen concentration in oxy-fuel combustion process should be around 35 percent. The laminar flame speed and transport properties of oxy-fuel flames are greatly affected due to the high specific heat capacity and low mass diffusivity of CO2 in the oxidizer mixture.

Many experimental investigations stated that CO2 is kinetically active and participates in the reaction through CO2 + H ↔ CO + OH [Zhang et al, 1992 and Liu et al, 2003]. The above reaction completely reduces the pool of O and H radicals in the reaction thereby reducing the burning velocity of the mixture [Zhang et al, 1992 and Liu et al, 2003]. At high temperatures CO2 is chemically active as it increases the amount of CO emissions by participating in the reaction with a methylene group CH2 + CO2 ↔ CH2O + CO[Glaborg and Bentzen , 2008]. High concentrations of CO2 in the mixture results in increase in the radiative heat transfer [Wall, 2007 and Anderson et al, 2008].

1.1.2 Effect of Pressure on Oxy-fuel Combustion properties

Oxy-fuel power cycles have to operate at high pressures as the combustion efficiency of the combined cycle power plants are favorable under these conditions due to the change in the working fluid. Besides, the capture of N2 leakage in combustor and removal of significant amounts of SO2 after combustion can be achieved at high pressures. In addition, the CO2 capture becomes an easier as the volume occupied by CO2 at high pressures is lower. Heat capacity and the reaction rate increases with increase in pressure. Westbrook and Dyer stated that, increase in pressure enhances

the third body reactions which compete for O and H radicals in the reaction thereby reducing the reaction rate [Glaborg and Bentzen, 2008]. Studies show that non gray radiation tends to increase with increase in the pressure [Ashman and Haymes, 2008].

1.1.3 Stability of Oxy-fuel Flames:

Stability is one of the important parameter that dictates the operability limits of oxy-fuel flames. Flashback, blowout, combustion instabilities and auto-ignition are considered as major concerns that may affect the operability limits of flames. Flame flashback occurs when the flame velocity is greater than the bulk velocity of air/fuel stream causing the flame to propagate upstream resulting in a explosion in the fuel/air stream. Blowout occurs when the flame velocity is less than the bulk velocity of the air-fuel stream resulting in system failure. Combustion instabilities are generally referred to sustained pressure fluctuations caused by the unsteady combustion in the combustor [Amato et al, 2010]. Due to the presence of CO2, the laminar burning velocity is greatly reduced in oxy-fuel flames. So, blowout seems to be the most likely phenomena to occur [Dickens and Linett, 2007]. Some studies have indicated that the time scales related to oxy-fuel flames are high when lesser amounts of O2 is involved in the reaction [kobayashi et al, 2007].

1.2 PROBLEM STATEMENT:

Currently available and emerging modeling (fluid dynamics, heat transfer and combustion) tools can be effectively used to develop new oxy-fuel designs and analyze retrofits to meet the sequestration goals. However, computational tools are yet to be validated for oxy-fuel combustion systems and a suit of experimental data of

fundamental flame characteristics relevant to oxy-fuel combustion is needed for this purpose.

A central part in all gas turbines is the combustion chamber. Flame flashback is an inherent reliability problem in lean premixed combustion where the flame, instead of stabilizing completely within the combustion chamber, propagates upstream into the premixing zone against the gas stream. The flashback tendency in oxy-fuel combustion increases abruptly because of the increase in laminar burning velocities and flame temperature, so the oxy-fuel mixture is generally diluted with the flue gases (generally CO_2 and H_2O) to reduce the flame temperatures. Flashback involves coupled interactions of burning velocity, local flow-field quantities, and combustion instabilities [2]. Flashback is always unacceptable and must be avoided in all combustion conditions, since it increases pollutant emission and can also cause considerable damage to the hardware of the premixing zone and eventually to the entire combustion system. Since small changes in turbulent flame speed in a gas turbine combustor can greatly affect the combustor design and the amount of pollutants emitted, the present research is focused on measurement of turbulent burning velocities and understanding the flow field characteristics over a wide range of CH4-O2-CO2 fuel compositions.

1.3 OBJECTIVES:

The present PhD works focuses on oxy-fuel combustion in which the fuel compositions vary from natural gas to a broad range of syngas fuels. The primary objective of the current research is to broaden the fundamental knowledge of the turbulence-

chemistry interactions of the turbulent premixed oxy-fuel flames using a laboratory scaled burner and combustor at atmospheric conditions.

- Characterization of turbulent reacting flow-field with particle imaging velocimetry (PIV) on a laboratory scaled nozzle burner.
- Investigation of the effect of firing input on turbulent reacting flow-field at same turbulent intensity, same equivalence ratio and same Reynolds number.
- Investigation of the effect of turbulent intensity on turbulent reacting flow-field at same firing input, same equivalence ratio and same Reynolds number.
- Investigation of the effect of recirculation ratio ($RR_{CO_2} = \frac{m_{CO_2}}{m_{O_2}+m_{CO_2}+m_{H_2O}}$ and $RR_{H_2O} = \frac{m_{H_2O}}{m_{O_2}+m_{CO_2}+m_{H_2O}}$), on turbulent reacting flow-field at same firing input, turbulent intensity, same equivalence ratio and same Reynolds number.
- Investigation of the effect of fuel composition on turbulent reacting flow-field at same firing input, turbulent intensity, same equivalence ratio and same Reynolds number.
- Characterization of turbulent reacting flow-field with particle imaging velocimetry (PIV) on a laboratory scaled gas turbine combustor.
- Investigation of the influence of turbulence parameters, recirculation ratios, and firing inputs on the flame front position and turbulent flame speed.

1.3 PROJECT IMPACT:

The present work focuses on the current state of art oxy-fuel combustion research where the basic findings helps in analyzing physical phenomenon to identify the cause and effect relationship which are important for practical applications. The

knowledge gathered from the current research may be applied to retrofit the current gas turbine combustors without sacrificing the design and operational advantages, while still maintaining high efficiency and low emissions. The four major parameters that the current research is focuses and its impacts are described in brief in this section

1) Measurement of Laminar burning velocities of different compositions of syngas/air fuel mixtures. Investigated the effect of burner diameter and different imaging techniques on the laminar burning velocities. Investigated the effect of diluents (CO2 and N2) on laminar burning velocities.
    - The experimental values of laminar burning velocities are necessary for engine design, prevention from explosions or detonations, modeling of turbulent combustion and validation of chemical kinetic mechanisms.
2) Measurement and analysis of local flow field of premixed turbulent air-fuel combustion.
    - The flow field analysis gives the detailed information regarding the velocity, vorticity, turbulent intensity and turbulent kinetic energy distributions across the combustion chamber which helps in the combustor design and provides the experimental database to compare and validate with the numerical results.
3) Investigate the local turbulence flow field of oxy-fuel combustion
    - The effect of turbulent intensity and change of working fluid (i.e. oxidizer mixture concentrations) on the combustion flow field dynamics was extensively studied for efficient combustion process.

- The effect of diluents (CO_2 and H_2O) on the combustion process is extensively studied as they control the operability limits of the oxy-fuel combustion

4) Comparison Study of air-fuel and oxy-fuel combustion flow-field
    - This study gives an idea about the design parameters that has to be considered to achieve the fuel flexible combustion

Chapter 2: Theory and Literature Review

The current section focuses on the theory and basic concepts behind the premixed turbulent combustion. The chapter is divided into two parts. The properties and characteristics of turbulent flows are discussed in detail in the first section. The second part focuses on premixed combustion, which covers the topics of laminar and turbulent premixed flames.

2.1 Turbulent Flows

Most of the flows that occur in the physical world are turbulent. Some the examples of naturally occurring turbulent flows include water flow in rivers and canals, interstellar gas clouds, the photosphere of sun, clean air turbulence and clouds and the water currents below the Ocean. The same is true in case of engineering flows, e.g.; boundary layer generation on aircraft wings, ships etc, the wakes of ships, cars, aircrafts, submarines etc. [Lumley and Tennekes, 1972]

The characteristics of turbulence flows are randomness, chaotic, highly diffusive in nature, very high Reynolds number, rotational in nature (high level of vorticity) and it is three dimensional. In addition to it turbulence mainly depends on the type of flow or its surroundings. Moreover, since each and every flow is different, the turbulence of such flows is also different. Because of this it is very difficult to measure the turbulence for complex flows. For this reason, most of the researchers concentrated on the simple flows like jets, boundary layers and wakes [Lumley and Tennekes, 1972].

Turbulent flows are encountered in many engineering and environmental applications. In gas turbine combustors, the flows are highly turbulent because of high mass flow

rates of the fuel and oxidizers from the injection ports. The advantage of turbulence flows is that it enhances mixing between fuel and oxidizer, increases the mass and heat transfer rates thereby enhancing the combustion process. The current chapter focuses on some of the important statistical characteristics of turbulent flows that include length scales, turbulent kinetic energy, eddy cascade hypothesis and turbulent intensity.

Generally the flows are characterized by a non-dimensional factor, known as Reynolds number. It is given by the formulae

$$Re = \frac{UL}{\nu}$$

Where U and L are characteristic velocity and length scales of flow and ν is the kinematic viscosity. The transition from turbulent to laminar occurs when the flow irregularities are dampened by viscosity of a particular fluid. The transition point for flows varies with their geometries. For smooth pipe the transition point for a flow to change from laminar to turbulent is at Re =2300.

2.1.1 Statistical analysis of turbulent flows:

Turbulent flows are generally resolved by using statistical methods. Temperature, pressure and velocity are the main parameters that are to be resolved using Reynolds decomposition method to solve for the Navier- stoke equations. Generally in flows, turbulence causes eddies, which create fluctuations in the velocity which vary with time. So turbulent flows are characterized by the mean and fluctuating component. Figure 2.1.1 shows velocity recorded at a single point in a flow.

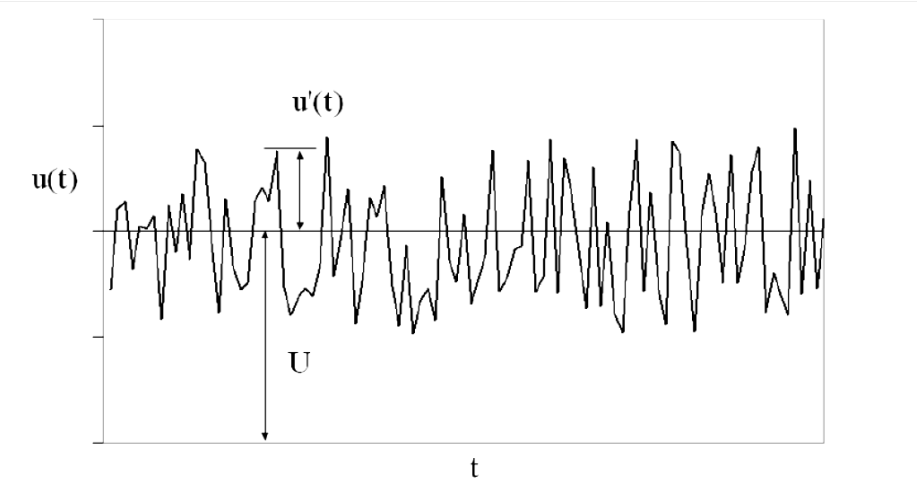

The mean velocity is given by the equation

$$U = \frac{1}{N}\sum u(t)$$

Turbulent fluctuation:

$$u'(t) = U - u(t)$$

Turbulence strength:

$$u_{rms} = \sqrt{\left[\frac{1}{N-1}\sum_{i}^{N}(u'(t))^2\right]}$$

Kinetic energy for three dimensional (3-D) flows:

$$k = \frac{1}{2}({u_{rms}}^2 + {v_{rms}}^2 + {w_{rms}}^2)$$

Where $u_{rms}, v_{rms}, w_{rms}$ are the fluctuating velocity components in x, y and z directions.

For isotropic flows

$$k = \frac{3}{2}({u_{rms}}^2)$$

2.1.2 Characteristic Length scales and Energy Cascade Hypothesis

Turbulent flows consists of eddies (vortices) of different length scales, turbulent length scale or integral length scale is considered as the largest energy containing eddies present in any flow, whereas Kolmograv scales are the smallest structures in a flow which are dissipated by viscosity of the fluid. The size of the kolmograv scales decreases with the increase in Reynolds number.

Correlation functions and integral length scale

The largest length scales in the flow are generally determined using two point correlations. Figure 2.2 shows the two dimensional flow field in which instantaneous velocities are sampled at two discrete spatial points which are separated by distance X_i

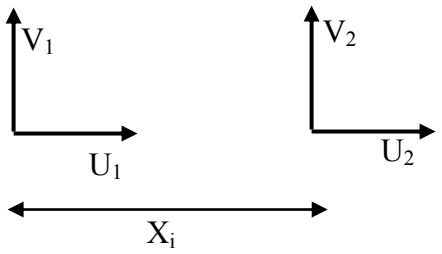

Figure 2.1.2: Two point velocity correlations

During the data sampling process, structures of same length scales pass through these points their velocities are related. The correlation $\overline{u(X)u(X_i)}$ between these two values of u at two different distances is called autocorrelation. The correlation coefficient is given by the equation below

$$R_{12} = \frac{\overline{\Delta u_1 . \Delta u_2}}{u_{1,rms} . u_{2,rms}}$$

The range of the autocorrelation varies from 0 to 1. 0 signifies that two are not correlated and whereas 1 signifies they are perfectly correlated. The size of the largest eddy is calculated by the equation shown below.

$$L_T = \int_0^\infty R_{12}\,(X_i)\,dX_i$$

The graphical representation of the integral length scale is shown in figure

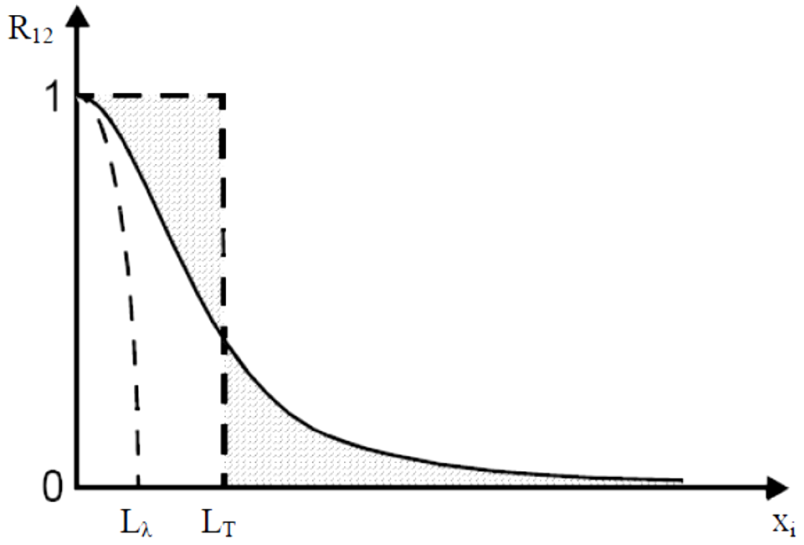

Figure 2.1.2: Spatial correlation coefficient and definition of integral length scale

2.1.3: Energy Cascade Hypothesis

Energy transfer in turbulent flows is carried out by large eddies, which are highly unstable and break up, transferring the energy to the smaller eddies by inviscid process. The process continues until the Reynolds number is sufficiently small that

energy is dissipated in the form of heat by the molecular viscosity of the fluid. Generally the largest eddies are characterized by characteristic length scale l_0, velocity scale $u_{0\ and}$ with the turbulent intensity u'. The rate of dissipation ε of turbulent energy is determined by transfer of energy from the largest eddies. The kinetic energy contained in theses eddies are of the magnitude of $K \sim u_0^2$ and the time scale is of the order of l_0/u_0.

$$\varepsilon = \frac{{u_o}^3}{l_0}$$

The smallest length scale in the turbulent flows is kolmogorov length scale denoted by η given by an equation

$$\eta = \left(\frac{\nu^3}{\varepsilon}\right)^{1/4}$$

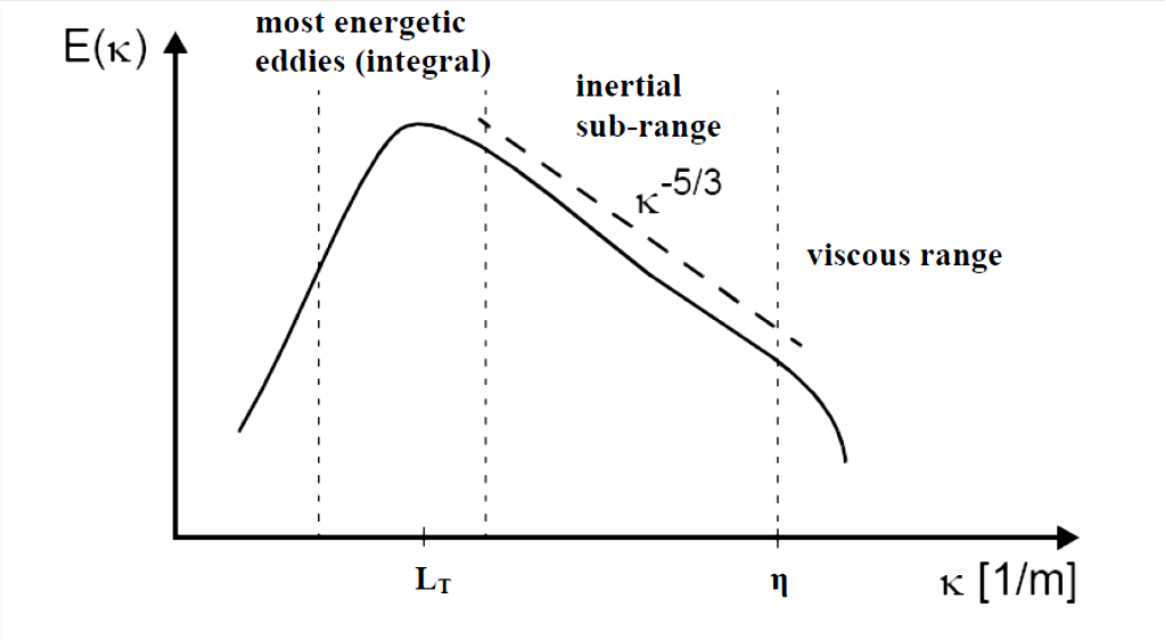

Figure 2.1.3 Energy Spectrum of turbulence E(K)

Figure shows the energy cascade process for the turbulent flows. The figure clearly states that the larger eddies are stronger when compared to smaller eddies and the rate of dissipation.

2.2 PREMIX COMBUSTION

In premix combustion fuel and oxidizer are mixed prior to the ignition. In order to start the combustion the air to fuel mixture ratio has to be within the flammability limits and the temperature of the local mixture has to be greater than the self-ignition temperature. The energy required to ignite the air fuel mixture is provided from an external ignition source such as a spark plug or a recirculation of hot combustion gases.

2.2.1 Laminar Premixed Flames

Laminar premixed flames gives a fundamental information regarding some of the important parameters of a given premixed mixtures, such as flame temperature, laminar flame speed, strain sensitivity, and extinction strain rates [Natarajan et al]. Moreover, in order to understand the behavior of turbulent premixed flames the knowledge of laminar flames is necessary.

2.2.1.1 Adiabatic Flame Temperature and Flame Propagation

Adiabatic flame temperature is defines as the temperature of burnt gas products at constant pressure with no heat transfer to and from its surroundings. Law and sung defined the adiabatic flame temperature as the maximum temperature of combustible mixture without the differential diffusion and strain effects. The adiabatic flame temperature gives the information regarding the NOx formation in a combustion process. According to thermal mechanism (zeldovich) NOx production is highly sensitive to flame temperature, and around 1800k NOx production substantially increases. Adiabatic flame temperature increases with increase in the reactant temperature.

Flame propagation or laminar burning velocity is fundamental to combustion processes. Many important flame characteristics such as stability, extinction, and flashback are generally dictated by the burning velocity of fuel-air mixtures. Laminar burning velocity depends on number of factors such as fuel composition, type of oxidizer, effect of inlet pressure and inlet temperatures and effect of diluents in the air fuel mixtures.

2.2.2 Turbulent Premixed flames

The flow is made turbulent by placing a grid within the burner, when the premixed gases encounter the grid and the flames that have been developed from such kind of flows are called premixed turbulent flames. Turbulent premixed flames display interesting facts than any other turbulent flows. One of them is they form a thin sheet of flame which is connected by highly wrinkled surface, which separates the reactants from the products [Damkohler, 1940].

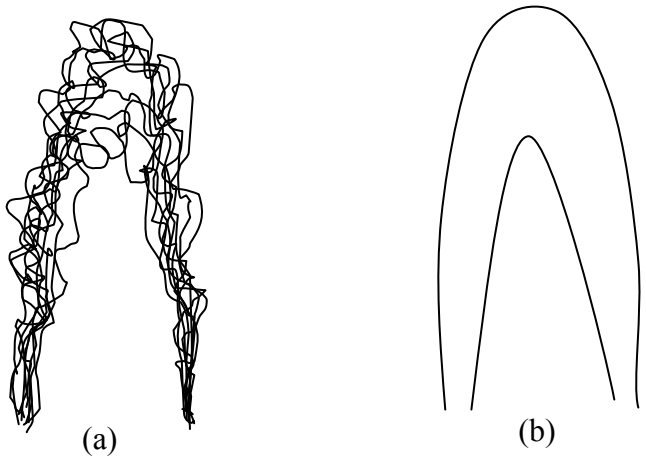

Figure 2.2.2: a) Superimposition of instantaneous flame fronts obtained at different times b) Turbulent flame brush associated with time averaged view of the same flame

Turbulent premixed flames are extensively used in several industrial devices for energy conversion of gaseous fuels. Gas turbine combustion chambers, afterburners of turbojet engines, and spark-ignited reciprocating engines are the main examples [Jozef et.al, 2009]. Since, turbulent premixed flames are highly efficient and produce

low emissions during the conversion of gaseous fuels; they have been extensively used in stationary gas turbines. The structure of turbulent premixed flames formed on the top of Bunsen burner using Schlieren photography technique at different intervals of time are shown in the Figure 2.2.2(Brandl et.al. 2006).From the figure it is noticeable that large folds appear on top of the flame. Since the location of reaction zone is subjected to change at a faster rate in space, producing a time averaged view, because of this the appearance of the flame tends to look like thick reaction zone often known as turbulent flame brush. But the instantaneous view shows that the reaction zone is relatively thin similar to the laminar flame and they are often referred as laminar flamelets.

2.2.2.1 Regimes of Premixed Turbulent Combustion

The mean volume occupied by premixed turbulent flames is same as that of the laminar premixed flames but the turbulent premixed flames tend to consume reactants at a much greater rate [Mallard and Le Chatelier, 1883].The substantial increase in the burn rate in turbulent premixed flames is due to the interaction of the turbulence flow with the flame. Hence there is a great need to understand the mechanisms and the effect of turbulence on the flame itself.

Generally turbulent premixed flames are described as flames that propagate as thin sheets, which are commonly known as flamelets. Such kind of phenomena occurs only when the chemical time scale is less than the turbulence integral time scale. The chemistry is supposed to be relatively fast enough for the flow to consist only two phase's, i.e. the burnt products and unburnt reactants. The reaction flamelets (which is

basically a reacting zone) separates the burnt products and unburnt reactants. Flamelets may be categorized further based on its turbulence and chemical length scales. If Kolmogorov scale is assumed to be the smallest turbulence length scale which is larger than the laminar flame thickness and the flamelets is assumed to be unsteady and stretched. Moreover, if the flame thickness is smaller than the length scale, the micro scale eddies may tend to enter and change the flame structure, thereby creating an impression of the thickened reaction zone. To differentiate between different regimes of premixed turbulent combustion, it is common practice to construct a regime diagram which is shown in the figure below. There has been a considerable variation in theoretical predicted regimes [Peters, 2000 and Pocheau, 1992], where Figure 2.2.2.1 below demonstrates one of the important features. The lower left corner of Figure 2.2.2.1 shows the regimes where the turbulence is weak and the time scale is small. If the turbulent Reynolds number is less than unity, the flame is said to be laminar and the turbulent Reynolds number is given by the Eq. (2.1)

$$Re_t = \frac{u'L}{\nu} \qquad (2.1)$$

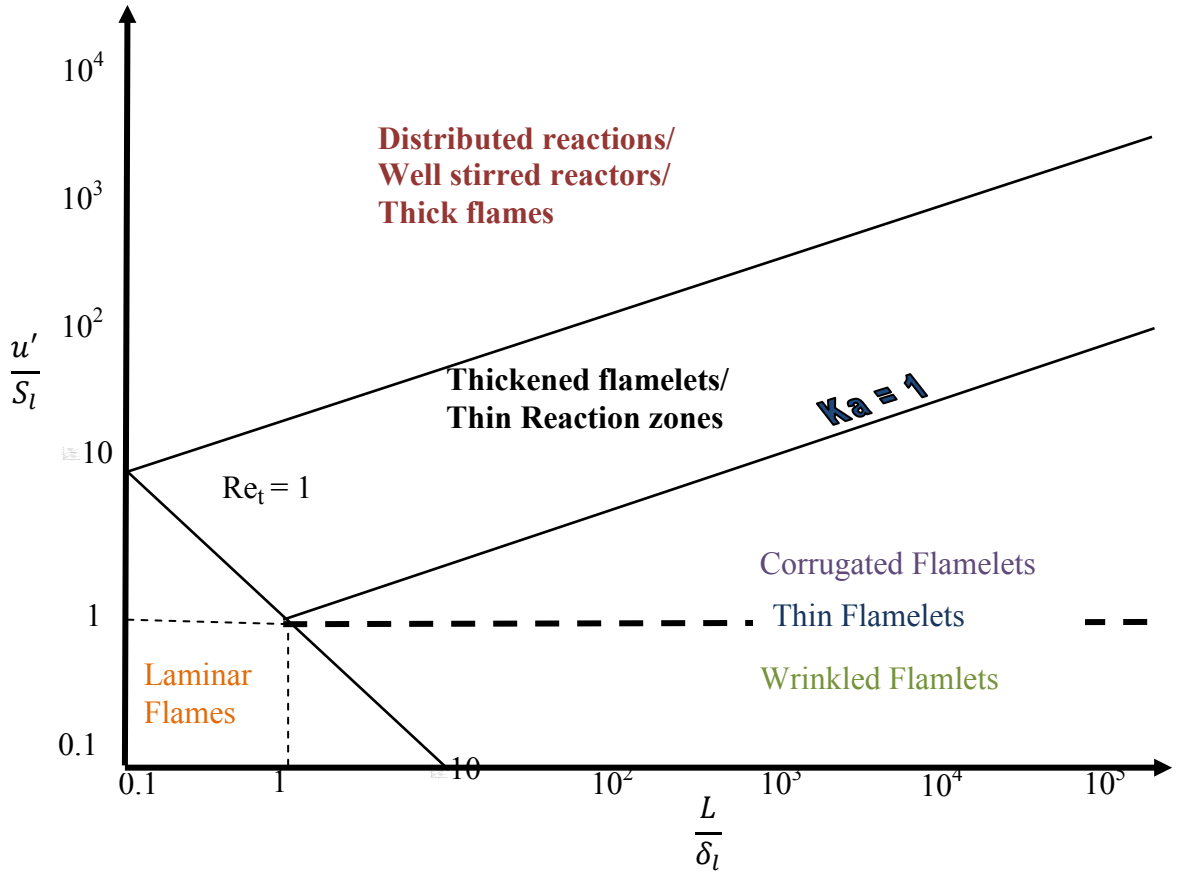

Figure 2.2.2.1: Regimes of turbulent premixed combustion (Borghis diagram)

The lower right corner of the figure shows the thin flamelet regime, which is further divided into wrinkled flamelets and corrugated flamelets. The basic difference between these is that in wrinkled flamelets regime no pocket formation is formed whereas the corrugated flamelets forms pockets of fresh and burnt gases at the convoluted flame front and the division is along the line at $\frac{u'}{s_l}$ =1. Above this exists the thickened flamelet regime along the line Ka = 1 where Ka is the Karlovitz number:

$$Ka = \frac{\tau_c}{\tau_k} \qquad (2.2)$$

Where τ_k is the Kolmogorov time scale. Above this there exists a regime which mainly comprises of thickened flames or distributed reactions. Of all the determining effects of turbulence on the flame front, the only importance of turbulence on the flame is it increases the flame front area is known with certainty (i.e. which has been proved by many researchers).It is highly uncertain to claim that the eddies have the ability to modify the flame surface since life time of the eddies is very short. Moreover the size of eddies are small when compared to the flame thickness. The existence of distributed reactions is generally only observed in cases of rapid compression ignition; the fast and uniform temperature rise due to compression caused homogenous reaction, not the turbulence [Driscoll]. However, the existence of the thin flamelet regime is well established and represents a wide range of conditions having practical importance [Eggenspieler and Menon, 2005]. Hence, the present research is primarily focused on turbulent premied combustion.

2.2.2.2 Thin Flamelet regime

Flamelets have the structure which is unsteady and stretched. This is the reason that these flamelets exit in thin sheets which separate them from fresh reactants with the burnt products. These two states are distinguishable by the reaction progress variable in Eq. (2.3):

$$c = \frac{T - T_u}{T_b - T_u} \qquad (2.3)$$

Where T is the temperature, u denotes unburnt reactants and b denotes burnt products. Thereby, when c=0 refers to the reactants and c=1 represents complete products side. At a particular value of c, i.e. c= c* represents the flame surface. The

flame surface shown in the figure clearly indicated that the flame is propagating at a rate which is faster when compared to the upstretched flame

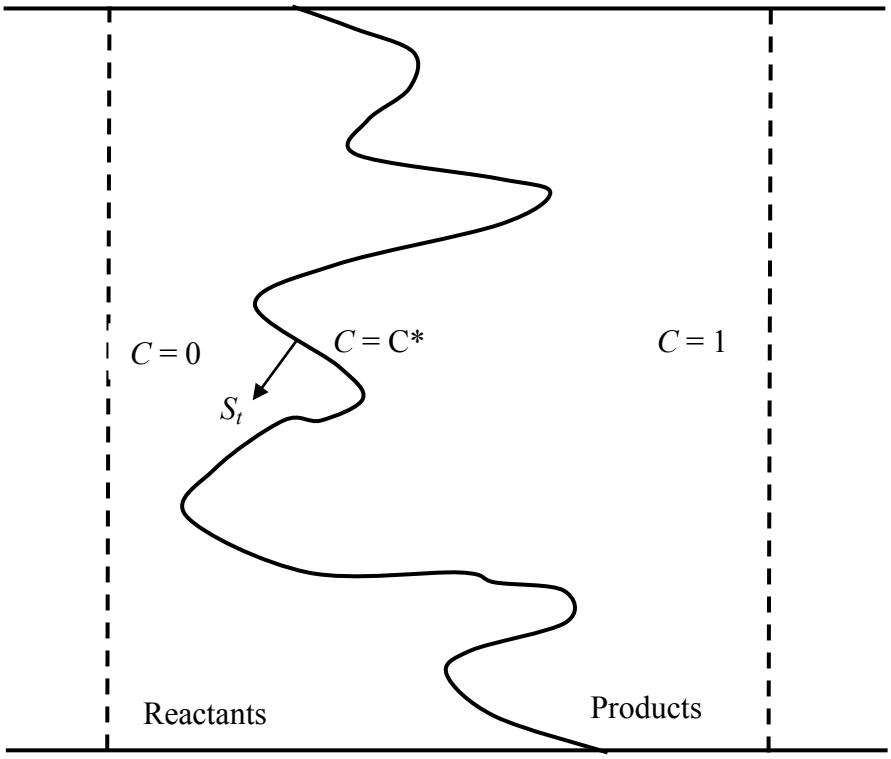

Figure 2.2.2.2: Turbulent Flame surface

Considering a control volume (V) through which the flame front is created as shown the mass flow rate of the reactants within this control volume along the flame is expressed in Eq. (2.4):

$$\frac{m_r}{V} = \rho_u s_t \frac{A_t}{V} = \rho_u s_t \sum \qquad (2.4)$$

Where m_r represents the mass flow of the reactants ρ_u is the density of the unburnt gas s_t is the flame speed, $\sum$ represents the flame surface density and A_t is the flame surface area.

The effect of turbulence triggers two important mechanisms:

- The f lame surface density is altered i.e. the turbulent flame is stretched due to the difference in the velocities between the reactants and the propagating flame front. This tends to increase in the surface area of the flame and the reaction rate of the flame.
- The local reaction rate is altered: The presence of turbulence causes the flame front to change dramatically thereby causing unequal diffusion of heat, which in turn results in the local reaction rate to change. The net effect alters the mean propagation speed[Law and Sung]

2.2.2.3 The Area of Turbulent Flame

Since we are evaluating turbulent burning velocities using flame angle method which is based on the conservation of mass principle (Method is based on the continuity equation). The formulae to evaluate the turbulent burning velocity is given by the expression shown below

$$S_T = \frac{\dot{m}}{\rho \bar{A}} \qquad (2.5)$$

Where $\dot{m}$ is the mass flow rate of air/fuel mixture, ρ is the density of the unburnt air fuel mixture and $\bar{A}$ is the turbulent flame area. Generally the value of mean progress variable is taken as 0.5 (i.e.c=.5) to evaluate the flame surface area.

2.2.2.4 Geometric Descriptions

The change in the flame surface area due to the turbulence has been explained by Schelkin, who believed that the relation between the propagating flame and a rotating vortex is identical, since both of them have maximum and minimum velocity

regions about the mean value (which has been illustrated by the Figure 2.2.2.4). In addition, Schelkin assumed that turbulence can create conical wrinkles, the shape and geometry of the wrinkles mainly depends on the vortex strength relative to the laminar flame speed. Depending upon the size and shape of the wrinkles, Schelkin came up with mathematical formulae for turbulent burning velocity which has been expressed as:

$$\frac{S_t}{S_l} = [1 + (\frac{2u'_{rms}}{S_l})^2]^{1/2} \qquad (2.6)$$

Where S_t is the turbulent burning velocity, $S_L$is the laminar burning velocity and u'_{rms} is the root mean square velocity.

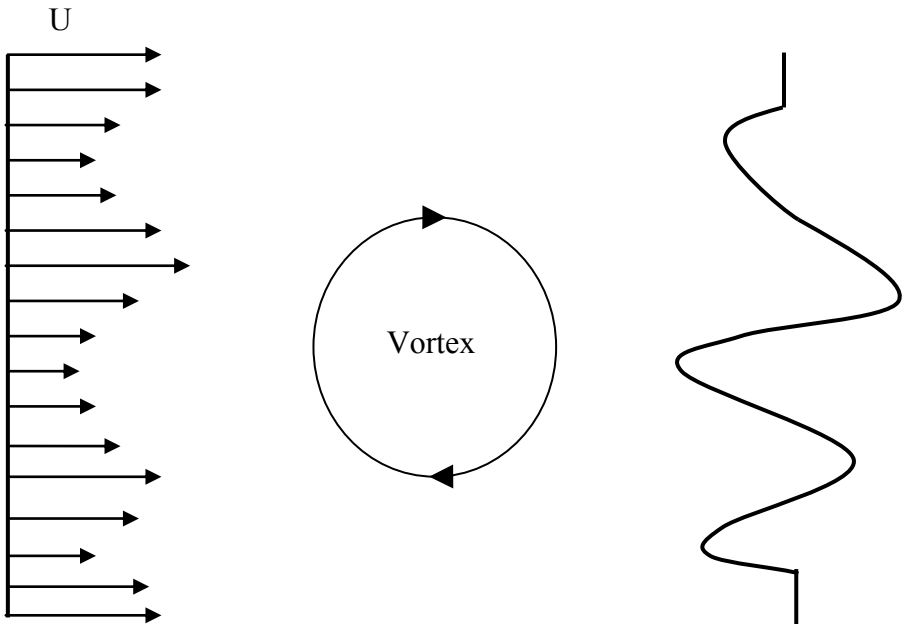

Figure 2.2.2.4 :Schelkin's concept of flame wrinling by vortex

The above expression was able to reproduce the values of experimental data only at moderate turbulence levels, which denotes that the turbulent burning velocity tends to increase with the increase in the value of the ratio between the fluctuating velocities to laminar burning velocities. However, there has been a significant difference in the experimental and mathematical evaluated values of the ratio of turbulent to laminar burning velocities. In order to minimize the differences between the computational and experimental values Driscoll (2008) and Peters (2000) developed a generalized expression to determine the turbulent burning velocity which has been expressed as:

$$\frac{S_t}{S_l} = [1 + b_1 \frac{u'_{rms}}{S_l})]^{b_2} \qquad (2.7)$$

Here b1 and b2 are the constants that depend on the intensity of turbulence [Driscoll, 2008]. The generalized form, however, does not seem to reproduce the experimental values [Driscoll(2008) and Poinsot et.al,2005] , which concludes that the turbulent flame velocity and intensity of turbulence are variables that depend mainly on the type of the flow and the geometry of the flow[Peters, 2000]. Moreover the turbulent flame velocity does not tend to increase with the increase in the turbulent intensity, but displays a sharp decline at higher fluctuating velocities [Poinsot, 2000 and Veynante, 2005]. This is mainly because of flamelet quenching and flamelet merging, and is highly influenced by the shape of the flame, which makes the turbulent burning velocity difficult to predict using the simple mathematical expressions.

Currently there has been extensive research going on in order to establish a relation between turbulent burning velocity and the other parameters of turbulence.

2.2.2.5 Flame Stretch

Turbulent flame interactions cannot be evaluated just by knowing the terms such as turbulent burning velocity or flame surface area. The accuracy of the flame area method mainly depends upon understanding the mechanisms of turbulence which has a significant impact on the area of the flamelet. The expression that represents the change in area is defined as Stretch rate and is expressed as: [Matalon, 1983 and Candel et al., 1990]

$$\kappa = \pi \frac{1}{\delta A} \frac{D(\delta A)}{Dt} \qquad (2.8)$$

The expression which is defined above is related to turbulent by several methods. In order to relate the above expression with turbulence, one must consider a plane A(x) and distance perpendicular to the plane with a distance of unity is denoted by n which has been shown in the Figure 2.2.2.5.

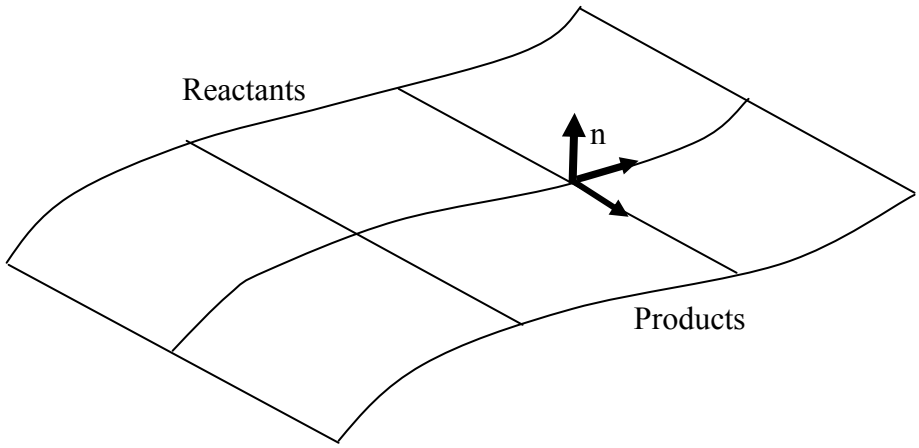

Figure 2.2.2.5: Material surface subjected to strain rates

Chapter 3: Experimental Setup

3.1 Nozzle Burner Assembly

The burner used in the present investigation consists of five distinctive parts each – namely, the perforated plate, the manifold, the stem, the connector and the burner nozzle exit. The burner nozzles are fabricated with brass, selected for its better thermal properties over aluminum. The perforated plate is fitted in between the connecter and burner nozzle. Different levels of turbulence are generated by changing the blockage ratio of the perforated plate. The fuel and air enter into the inlet manifold through four alternate injection holes. The fuel-air mixture then passes through honeycomb structure in order to eliminate the flow irregularities and ensure the laminar flow. The schematic of the burner used is shown in Figure 3.1.1.The burner top has a smoothly contoured nozzle at about 3 cm downstream and then straightened to the top of the burner. The burner produces a pipe flow velocity profile at the exit of the burner. The burner is provided with an adaptor which can accommodate burner top with varying diameter ranging from 6 mm to 25 mm. The burner top with a 18 mm exit diameter has been for the present investigation, i.e., to determine the turbulent burning velocities of syngas fuels.

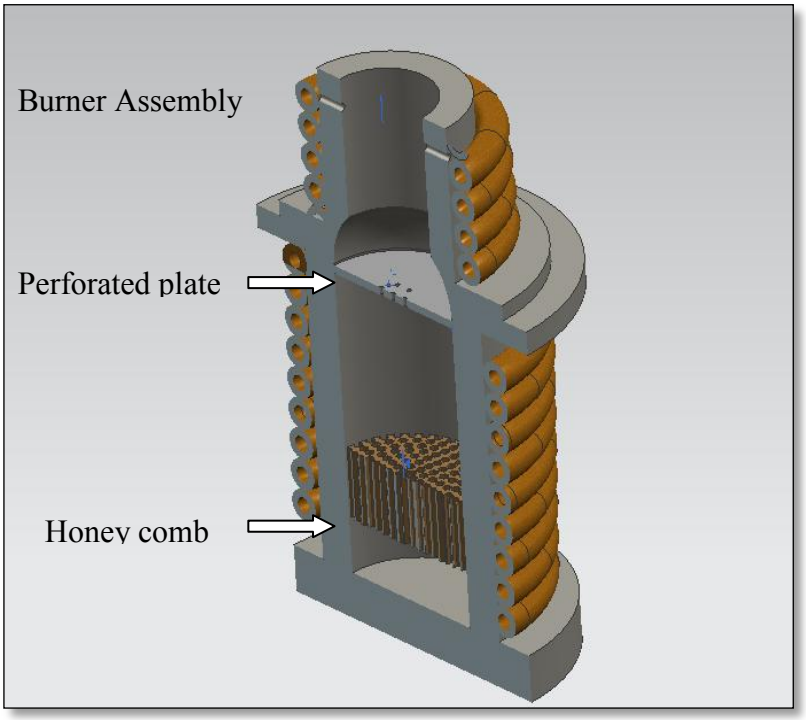

Figure 3.1.1: Burner Assembly

3.2 BOILER SETUP:

Boiler system (figure 3.2.2) has been integrated into the current burner setup to ensure that high quality steam is provided during combustion process. The boiler consists of the heating unit, the storage tank and a pump. The storage tank is filled with the distilled water to eliminate the scaling issues. The boiler upper pressure limit was set to 70 psi and the lower limit to 40 psi. A supply pressure of 40 psi is maintained constant by the use of the steam regulated value. The burner surface, inlet fuel and oxidizer supply lines are wrapped with the heating tape. The preheat temperature is controlled by the temperature controller which was set to 180 degrees C, so that the incoming air/fuel stream does not condense the steam. The outlet temperature of the air fuel stream is recorded to evaluate the properties of the mixtures. The complete experimental setup

is shown in the figure .One parameter will be varied to study their effects on recirculation ratios ($RR_{CO_2} = \frac{m_{CO_2}}{m_{O_2}+m_{CO_2}+m_{H_2O}}$ and$RR_{H_2O} = \frac{m_{H_2O}}{m_{O_2}+m_{CO_2}+m_{H_2O}}$), at constant Reynolds number and constant firing rate or fuel energy input (q_{in}).

Figure3.2.1 Boiler System

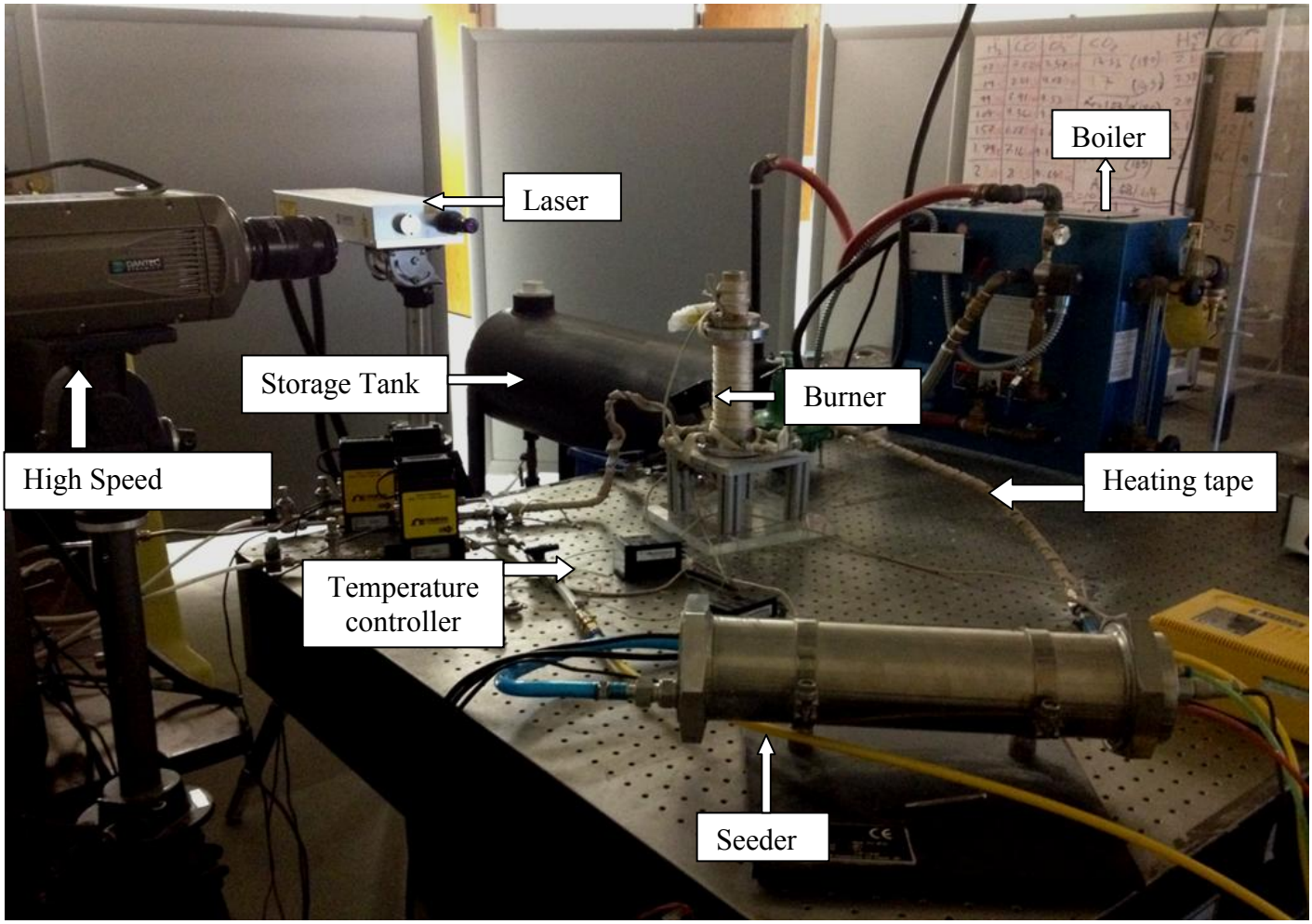

Figure 3.1.2 Nozzle burner setup with mounted high speed PIV and boiler

3.3 COMBUSTOR ASSEMBLY:

For this study a laboratory scale gas turbine combustor was used in order to study the effects of recirculation ratio ($RR_{CO_2} = \frac{m_{CO_2}}{m_{O_2}+m_{CO_2}+m_{H_2O}}$ and $RR_{H_2O} = \frac{m_{H_2O}}{m_{O_2}+m_{CO_2}+m_{H_2O}}$), firing input and fuel composition on flame flashback as well as to analyze the flow-field/flame interaction dynamics at the moment of flashback. The combustor rig has three configurable modules: (i) inlet manifold with static mixture, (ii) swirl burner with mixing tube, and (iii) optically accessible combustion chamber. Figure 3.3.1 shows a

schematic diagram of the gas turbine combustor. The combustion chamber integrates a pilot flame with a mixture of methane and air. The swirl burner module is fitted with a quartz mixing tube. The quartz glass tube is needed for the high speed imaging of flashback inside the premixer. The fuel and air enter the inlet manifold through five alternate injection holes. The fuel-air mixture then passes through the static mixture section to eliminate any injection induced flow irregularities and to ensure proper mixing of air and fuel. The burner module can accommodate both centerbody and hubless swirlers. For the present study, experiments were carried out using a twelve vane centerbody swirler, as shown in figure 3.3.2. As part of the experiments, a circular sleeve, as shown in figure 3.3.1, was fitted inside the inlet of the combustion chamber; this allows the air-fuel mixture to enter the combustion chamber through the passage between the sleeve and the centerbody of the swirler without experiencing any pressure drops due to the divergence at the inlet of the combustion chamber below.

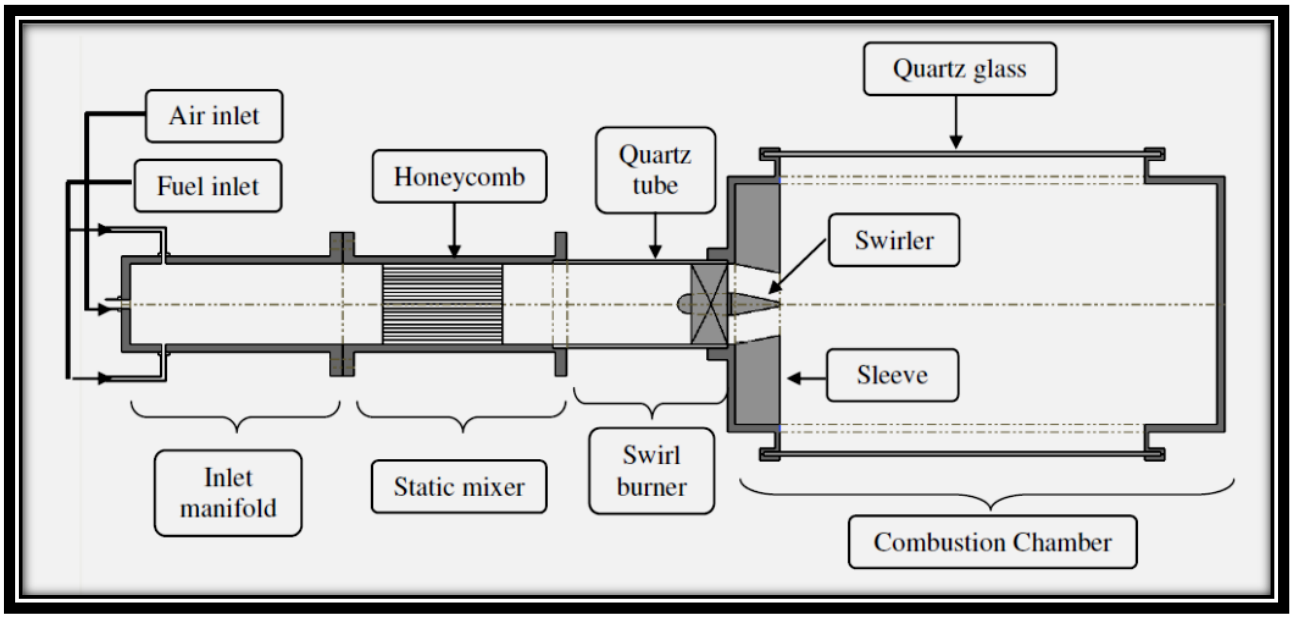

Figure 3.3.1 : Schematic of Combustor Assembly

Figure 3.3.2 : Swirler

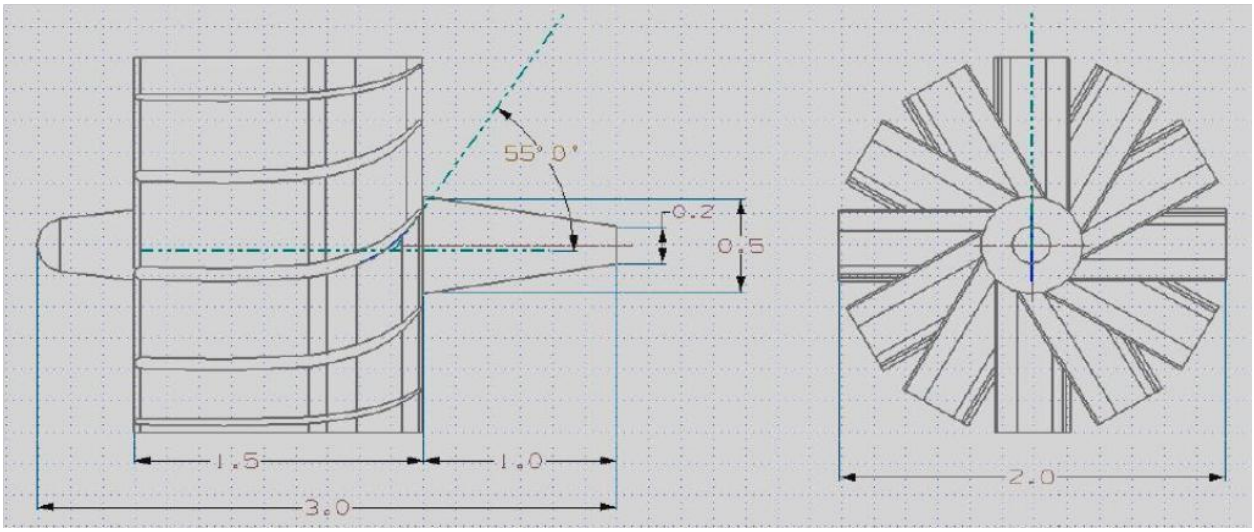

Figure 3.3.3 Cross sectional view of swirler

3.4 FLOW MEASUREMENT DEVICES AND DATA ACQUISITION

3.4.1 Flow Meter

Digital mass flow meters (Omega FMA 1700/1800 series in Figure 3.4.1(a)) were used to measure the mass flow rate of air and fuel. The mass flow meters are designed

to withstand temperatures ranging from 0° C to 50° C, pressures up to 500 psig and relative humidity of 70%. The mass flow meters used in the present study varied in full scale 0-5L/min to 0-1000 L/min. For all cases the accuracy is ±1.5% of full scale. The mass flow meter is shown in Figure 3.4.1(a). These flow meters are calibrated by Dry Cal Meter Calibrates as shown in Figure 3.4.1(b).

(a) (b)

Figure 3.4.1 (a) Digital Mass Flow Meter (b) Dry Cal Calibrator

3.4.2 Metering and Shutoff Valves

Precision metering values (SS-SS4VH in Figure 3.4.2(a)) were used to regulate the air and fuel mixtures. The shutoff values (SS-4P4T4 in Figure 3.4.2(b)) were used to shut off the fuel flow from the pressurized gas cylinders.

(a) (b)

Figure 3.4.2 (a) Swagelok SS-SS4 Metering Value (b) Swagelok SS-4P Shutoff Value

3.4.3 Data Acquisition

For temperature measurement a National Instruments Lab View data acquisition system was constructed to attain signals from the individual sources. The input module is shown in Figure 3.3.3,

Figure 3.4.3.1 NI USB 9263

The NI USB 9263 is a four channel, 16 bit analog voltage output module and ranges from -10 volts to +10 volts. Two s-type thermocouples are connected to the two channels by means of long connecting wires. The s-type thermocouple is generally comprises of platinum and platinum-10% rhenium.

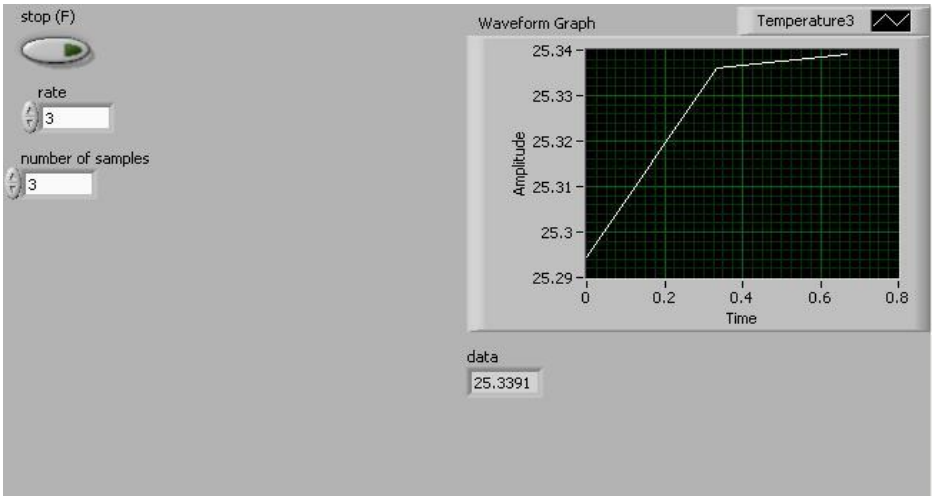

Figure 3.4.3.2 Front Panel for Data Acquisition

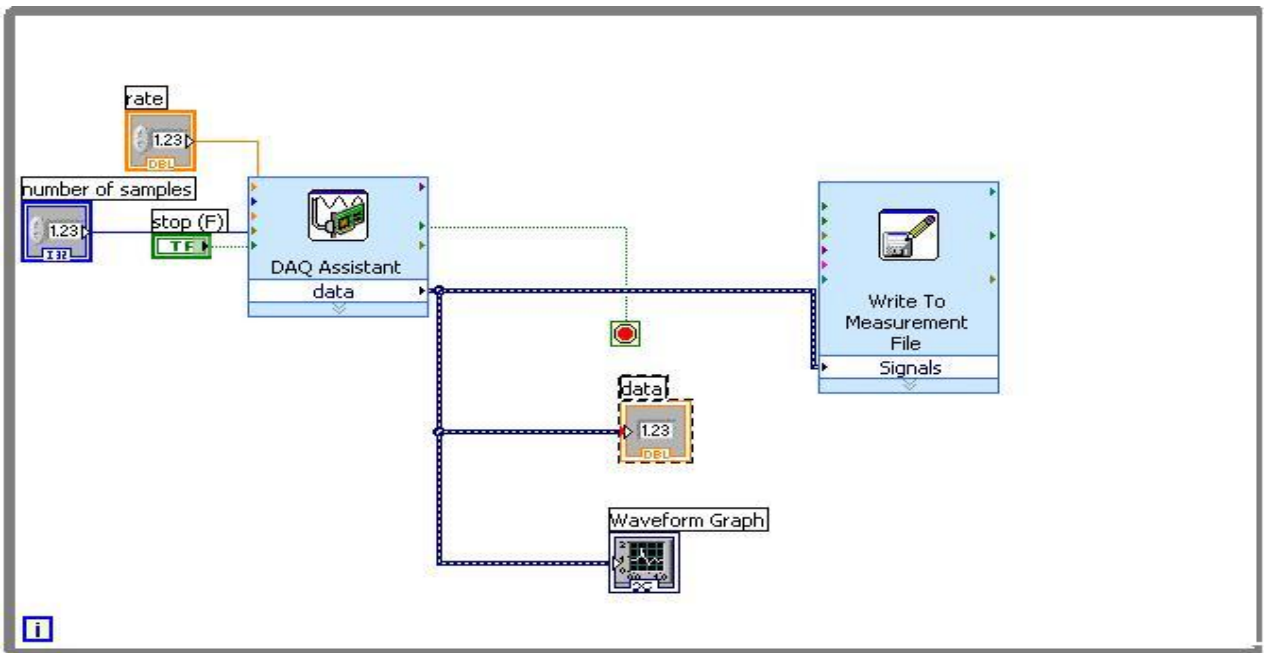

Figure 3.4.3.3 Block Diagram for Data Acquisition

Chapter 4: Measuring Techniques:

4.1 Thermal Anemometry

A constant temperature anemometry system, as shown in Figure, is used to characterize the cold flow at burner exit. The thermal anemometer measures velocity of the flow-field by sensing the changes in heat transfer from its sensor to its surrounding air, which is a small. An electrically-heated wire of diameter four to six microns is exposed to the air passage exiting the burner. Reduction in sensor temperature due to the air stream is balanced by current to maintain a constant temperature, and the magnitude of this current is calibrated to measure the velocity of the stream.

Figure4.1: Hot-wire Anemometry System

4.2 LASER DOPPLER VELOCIMETRY (LDV).

LDA (Figure 4.2.1) is a non-intrusive and well-established technique for measuring local instantaneous velocities in single phase transparent flows [12]. . It offers high spatial and temporal resolution and no prior calibration is needed when compared to the hot wire anemometry. It is ideal for applications, where the physical sensors are difficult to use. Flow characterization can be done in reacting flow, reversing flow and multiphase flows as long as optical access is possible and the system is dilute enough to allow transmission of the laser beam and scatter light [13].It requires seeding particles in the flow. Depending on how the probe is positioned the LDA would allows us to measure the velocity of the particles in the axial and tangential directions. This is accomplished by turning the probe so that the laser beams are either vertically or horizontally. These intersecting beams create a fringe pattern (Figure 4.2.2) and as the particle passes through this point the light pulsates due to the reflection. The pulsating light is measured by a photodetector and the frequency along with the fringe spacing is used to compute the velocity [14]. The downstream flow field for 12.7 mm burner tube diameter was characterized by using Laser Doppler Velocimetry (LDV) system at a sampling rate of 100Hz. A Particle Image Velocimetry (PIV) system also recorded the flow field at a rate of 100 frames per second to characterize the turbulence flow field and used for comparison to the LDV results.The results were shown in the data quantification section.

Figure 4.2.1: Dantec Dynamics LDA 2 Beam Red Wavelength System.

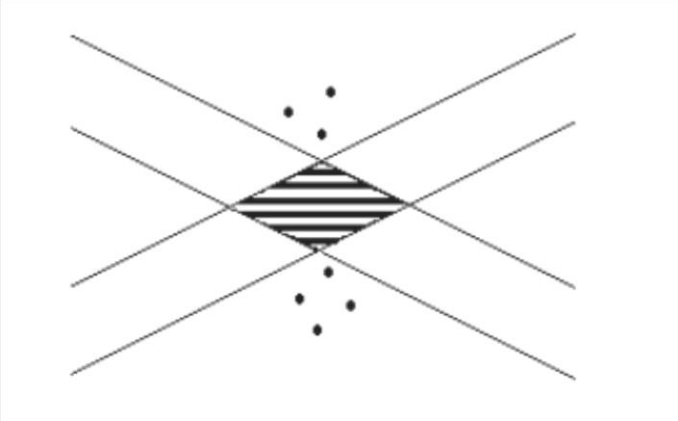

Figure 4.2.2: LDA Beams Fringe Pattern

4.3 PIV Technique

Particle Imaging Velocimetry (PIV) is a non-intrusive, optical method to obtain the velocity information from so called seeding particles in fluids which are in motion.

Seeding particles are illuminated by a laser sheet. The illuminated particles are tracked down by the CCD camera which is positioned at right angle to the sheet of laser. Further, the laser and the CCD camera are synchronized such a way that particles that are illuminated by the laser at the first instance of time is captured on camera frame 1, and particles from the second laser pulse is captured on the frame 2. The vectors are obtained by correlating the distance travelled by seeding particles of frame 1 to that of frame 2. This is how the flow visualization is accomplished using the PIV technique. This technique is used to characterize the flow field at the exit of burner. One of the major advantages of PIV is that it can be extensively used in both isotropic and hot flow conditions.

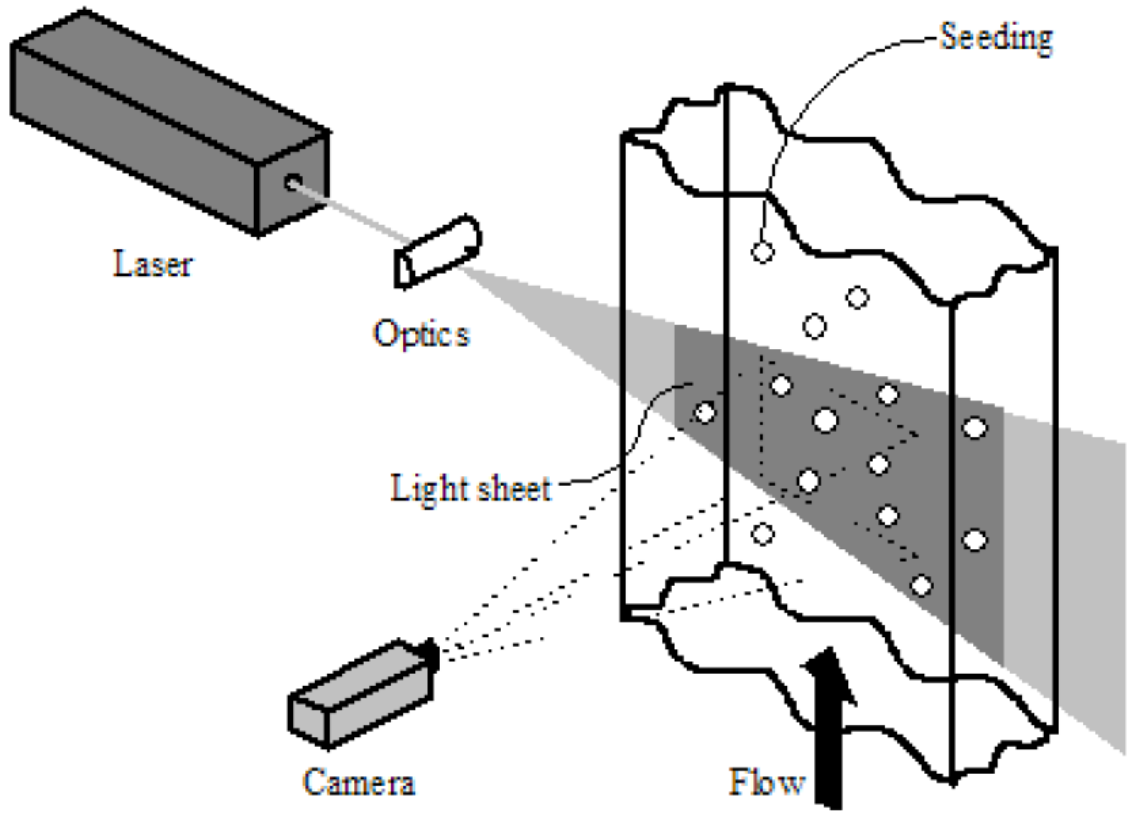

Figure 4.3.1: Components needed for PIV measurement (Picture taken from 2D-PIV Reference manual)

The system used for the current study consists of a high resolution direct imaging system (Phantom v310 camera) shown in figure 4.2.2(a), with a resolution of 1280 x 800 at 3250 fps and a maximum frame rate of 500,000 fps and a high speed ND: YLFLDY 300 Laser system shown in figure 4.2.2(b) with a maximum firing rate of 20 kHz and a maximum energy output of 15 MJ. All the equipments were synchronized with Dantec Dynamics software. In PIV experiments, Aluminum particles were used as seeding elements. A schematic of the PIV setup with the burner is shown in figure 4.2.3 and a schematic and experimental setup of the combustor assembly is shown in figures 4.2.4 and 4.2.5 respectively.

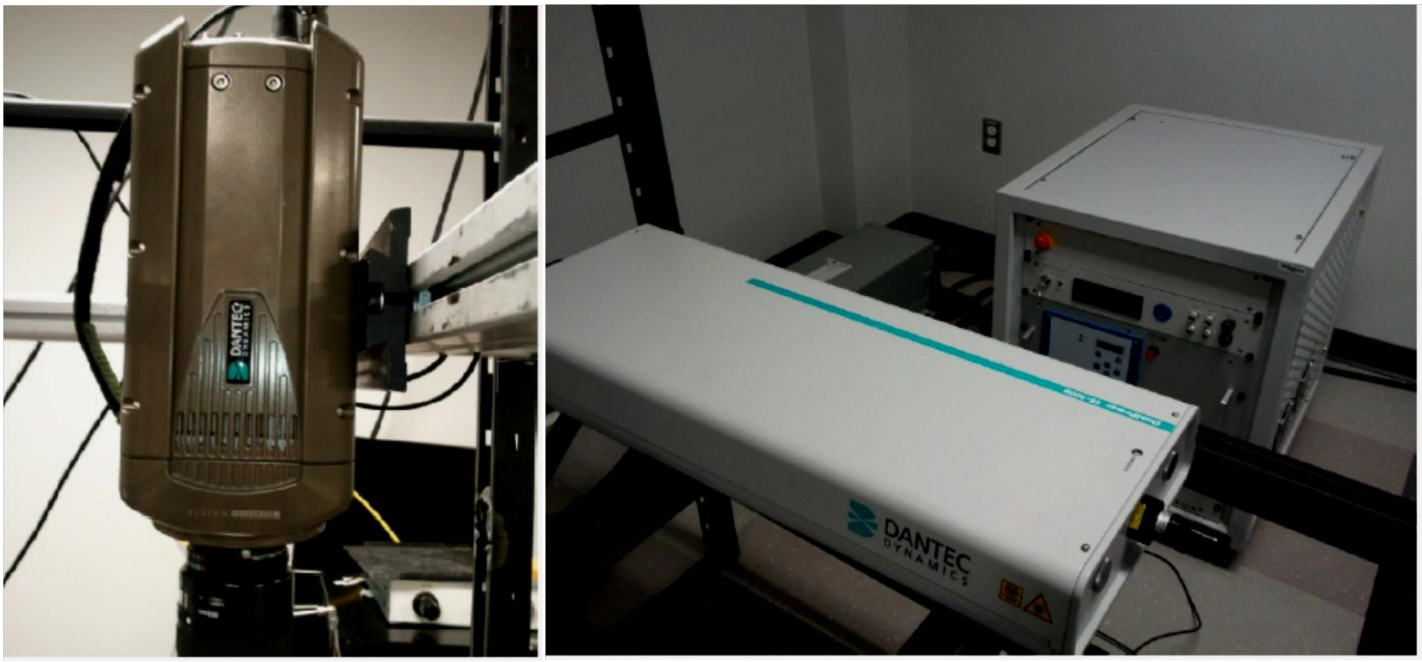

(a) (b)

Figure 4.2.2 (a) Phantom v310 camera, (b) LDY300 series high speed laser

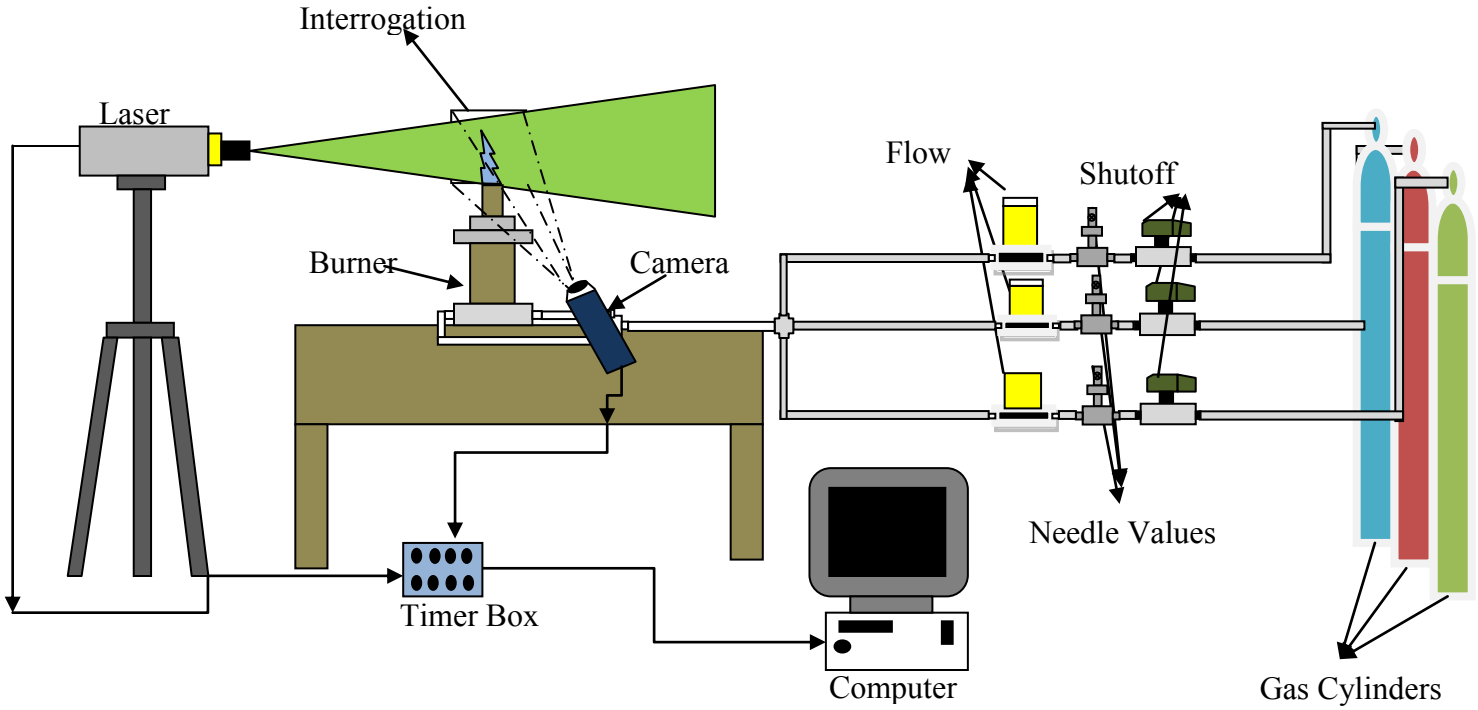

Figure 4.2.3 Schematic diagram of the Nozzle Burner setup

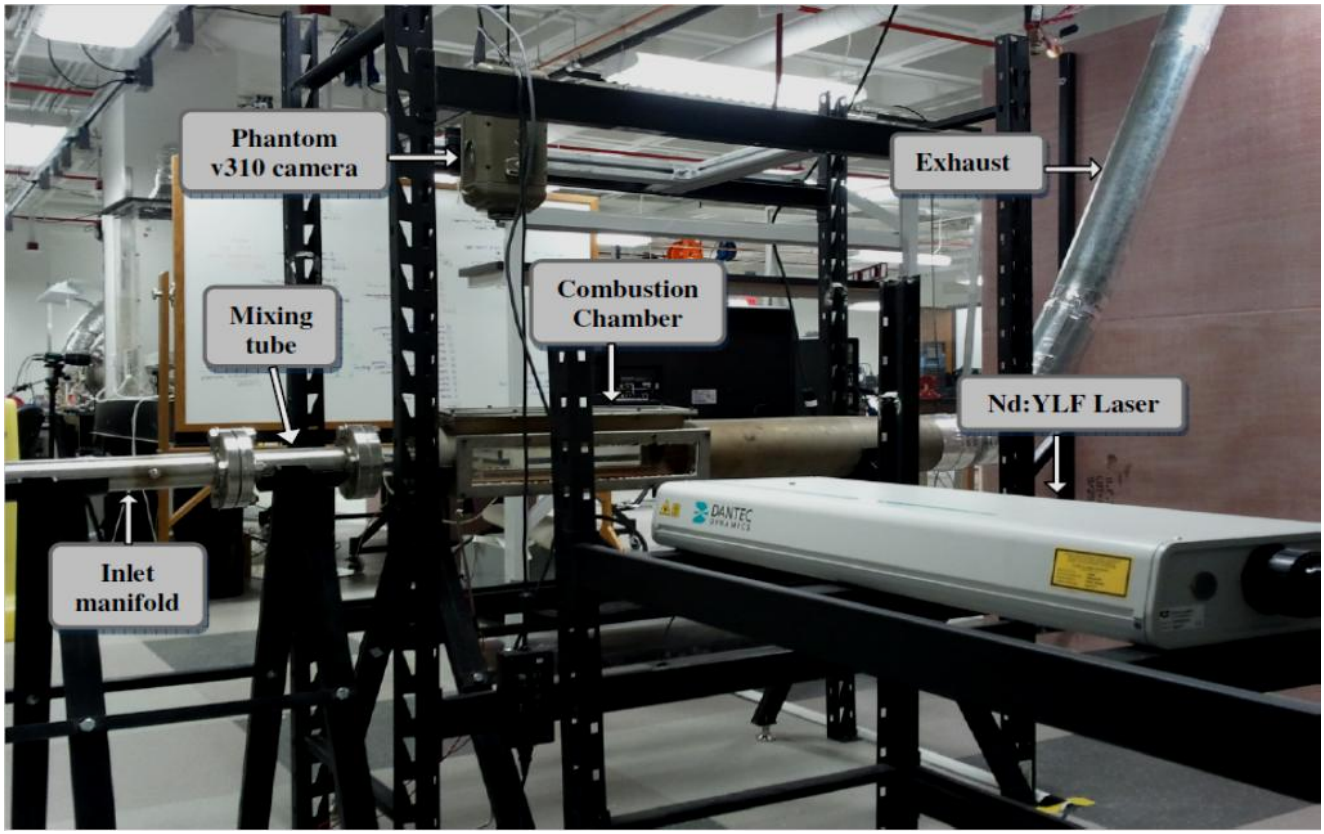

Figure 4.2.4 Gas turbine combustor setup with mounted high speed PIV

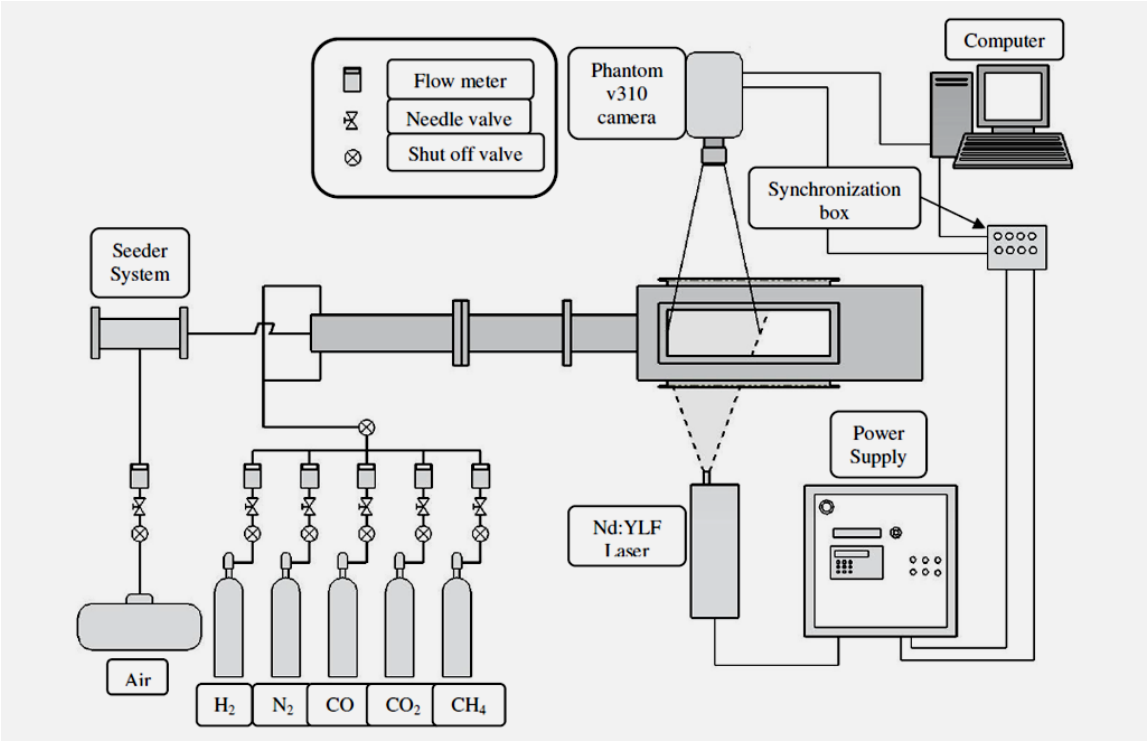

Figure 4.2.5 Schematic diagram of the combustor setup

4.4 Flow Seeding

Selection of seeding particles is very important when one is doing the experimentation with PIV. With PIV, the velocity of particles coming out of the burner exit with a predefined interrogation area (flow of interest) will be measured - i.e. seeding particle is just like a probe used in hot-wires anemometry. The seeding particles act like velocity probes in determining the velocity of the flow. However, in order to evaluate the exact velocity of the flow the particles must be small enough to track the flow accurately and yet big enough to scatter sufficient light for the camera to be able to detect them. Ideally, the particles should be neutrally buoyant in the fluid/flow, so their density should be approximately the same as the fluid itself. According to Durstet al. (1981)

the flow of the particles can be corresponded to the flow fluid if and only if the particle that has been used is

- Able to follow the flow
- Good light Scatter
- Non-Toxic, Non-Corrosive and NON-Abrasive
- Non Volatile and can withstand high temperatures
- Chemically inactive

The seeding particles that have been used in the present investigation are 1 micron alumina particles. A PS-10 Seeder system from SCITEK Consultants Ltd. was used to introduce the particles in the flow, see Figure 4.4.1 The seeder has a maximum working back pressure of 10 bar and can operate with temperatures in the range of 0 to 60°C.

Figure 4.4.1 PS-10 Seeder systems from SCITEK

4.5 Intensifier

The ICCD camera consists of a Image intensifier unit, relay lens , a CCD camera and UV lens and an OH filter fitted to the UV lens (see Figure4.5.1) Digital images of the fluctuating flame surface are taken with a 12-bit intensified CCD (2048 x 2048 pixels). The built in first image intensifier is available with a multialkali photocathode having a wide range of spectral response range from ultra-violet (UV) through near infrared, and hence capable of identifying the OH* chemiluminescence from the flame region zone. The ICCD system operates with a minimum gate time of 10 nanoseconds and a maximum gate repetition frequency up to 200 KHZ and also allows multi-exposure. The determination of the conical flame surface is done by tracking the high intensity regions along the flame surface area.

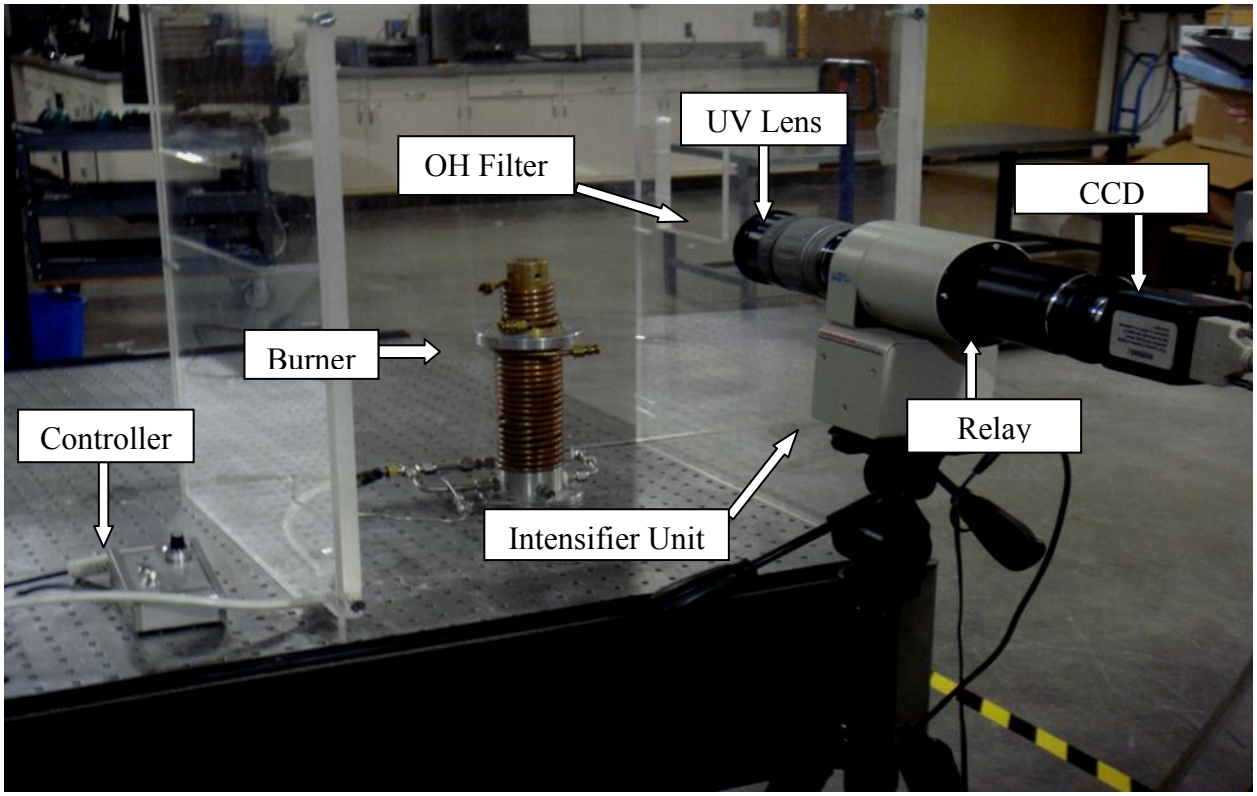

Figure 4.5.1 Intensifier Unit

4.6 Schlieren Technique

In this approach, the light is emitted from Dolan-Jenner (900W) through a fiber optic wire and then passes through the slit of 1000 microns. The diverging light emanating from the slit is assumed as a point source for the first achromatic lens. The burner tip is placed in the middle of the test region defined by the collimated rays that are formed between two achromatic lenses. A knife edge is placed on the focal point of the second lens that blocks the deflected light to reach the focusing screen of the camera. The resulting images called Schlieren images are captured on the CCD camera. The camera records the video onto the onboard memory at the desired frame rate. The conceptual Schlieren system is shown in the Figure 4.6.1.

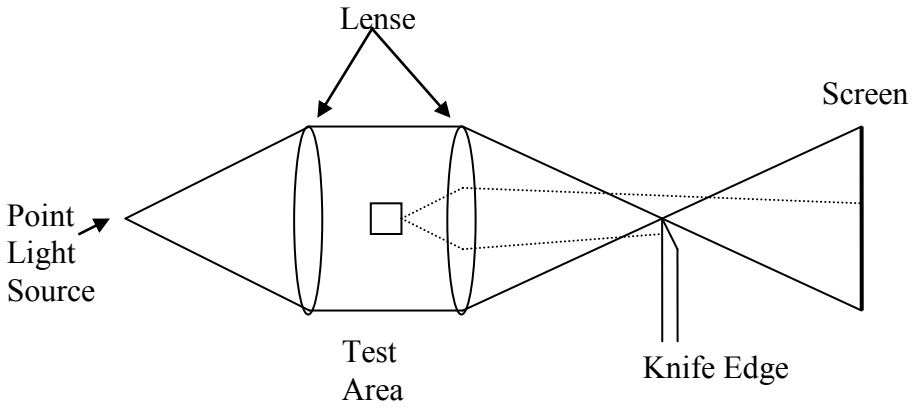

Figure 4.6.1: Conceptual Schlieren System

4.7 PROPER ORTHOGONAL DECOMPOSITION (POD):

It is powerful method for system identification aiming at obtaining low-dimensional approximate descriptions for multi-dimensional systems. The POD provides basis for the modal decomposition of a system of functions, as in the case of data acquired

through experiments. It provides an efficient way of capturing dominant components of a multi-dimensional system and representing it to a desired precision by using a relevant set of modes, thus reducing the order of the system.POD consists of two parts, taking the "snapshot" of a series of data, and then "projecting" the data through a selection of modes. POD, is closely related to Principal Component Analysis, PCA, from linear algebra and was first introduced in the context of Fluid Mechanics by Lumley [Lumley, 1986]. This implementation of POD applies the so-called "Snapshot POD" proposed by Sirovich [Sirovich, 2007].

4.8 REYNOLDS NUMBER CALCULATIONS:

Fuels ranging from methane to synags fuel compositions were tested at constant equivalence ratio (ϕ=1), constant firing input (1700 W) and constant reynolds number (2500). Viscosities for the fuel and air mixture were calculated with data from Maxwell (1968) and the Eqs. (2.9-10) from Kanury (1975).

$$\mu_{mixture} = \sum_{i=1}^{n} \frac{\chi_i \mu_i}{\sum_{j=1}^{n} \chi_j \Omega_{ij}}$$

$$\Omega_{ij} = \frac{1}{\sqrt{8}} \left(1 + \frac{MW_i}{MW_j}\right)^{-1/2} \left[1 + \left(\frac{\mu_i}{\mu_j}\right)^{-1/2} \left(\frac{MW_j}{MW_i}\right)^{1/4}\right]^2$$

$$\rho_{mixture} = \sum_{i}^{n} \chi_i \rho_i$$

$$\nu_{mixture} = \frac{\mu_{mixture}}{\rho_{mixture}}$$

$$Re = \frac{velocity_{burner\ exit}.\ exit\ diameter}{\nu_{mixture}}$$

Where $\chi_i$is mole fraction of the species i, n is total number of species in the mixture, μ_i is the viscosity of the species i, ρ_i is the density of the species i and MW_i is the molecular weight of species i. Table 2.3 lists the nominal experimental conditions and range of Re for the fuels.

4.9 Blockage ratio (BR):

The term blockage ratio for a perforated plate is defined as the solid area of perforated plate (A_{Perf}) to the exposed area (A_{Exp}), as shown by Eq. (4.9.1). Increasing of the blockage ratio can be achieved either by decreasing the number of holes in the perforated plate or by decreasing the size of the holes of perforated plate. When BR = 0, there is no blockage and BR = 1 is the condition for a solid plate.

$$BR = \frac{A_{Perf}}{A_{Exp}} = \frac{A_{Exp} - A_{Hole}}{A_{Exp}} = 1 - \frac{Nd_0^2}{D^2} \quad (4.9.1)$$

Where N is the total number of holes, d_o is the hole diameter and D is the overall disc diameter.

Chapter 4: Results and Discussions

4.1 Burner Characterization:

Two distinctive measurement techniques (Particle Imaging Velocimetry (PIV) and Laser Doppler Velocimetry (LDV)) were implemented to draw burner exit velocity profile at a distance of 3mm from the burner top. Fig. 4.1.1 shows the fully developed parabolic profile at the burner exit plane. There is a slight deviation between the two techniques but the deviations are within 5% of the mean value. The downstream flow field for 12.7 mm burner tube diameter was characterized by using Laser Doppler Velocimetry (LDV) system with the rate of 100 samples per second and averaging 1000 samples for each point. Particle Image Velocimetry (PIV) system with the facility of 100 frames per second was also implemented to characterize turbulence flow field for both the reactive and isothermal flow field. The PIV images were averaged over time period of 10 seconds. The RMS velocities were selected from the average of 2000 images for each location.

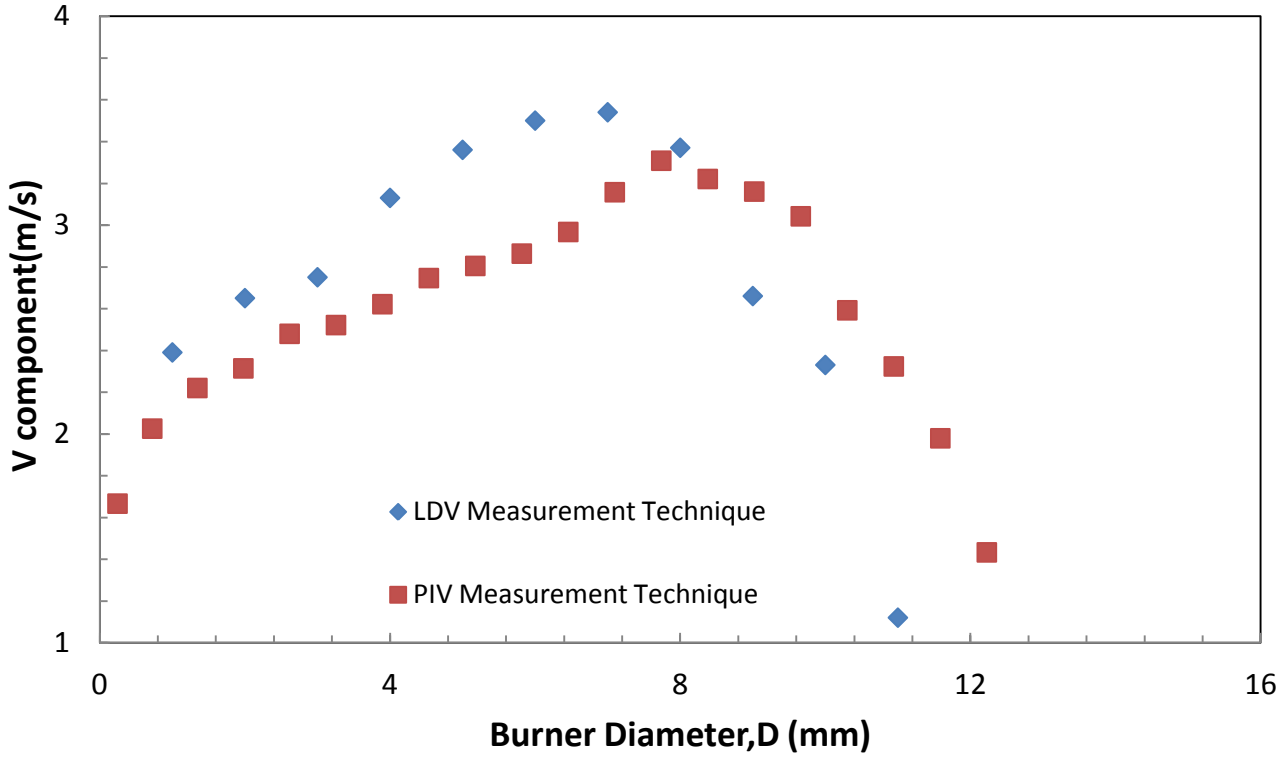

Figure 4.1.1: Burner exit velocity profile in isothermal flow field

4.2 DETERMINATION OF LAMINAR BURNING VELOCITIES OF AIR/FUEL MIXTURES

Figure 4.2.1 shows the images of flame measured at 30%H_2+70%CO using different measurement techniques. Figure 4.2.2 shows burning velocity of syngas fuels (30%H_2+70%CO) . Similar to the burner exit velocity effects the different imaging techniques produced slightly different burning velocity values only at very rich conditions.

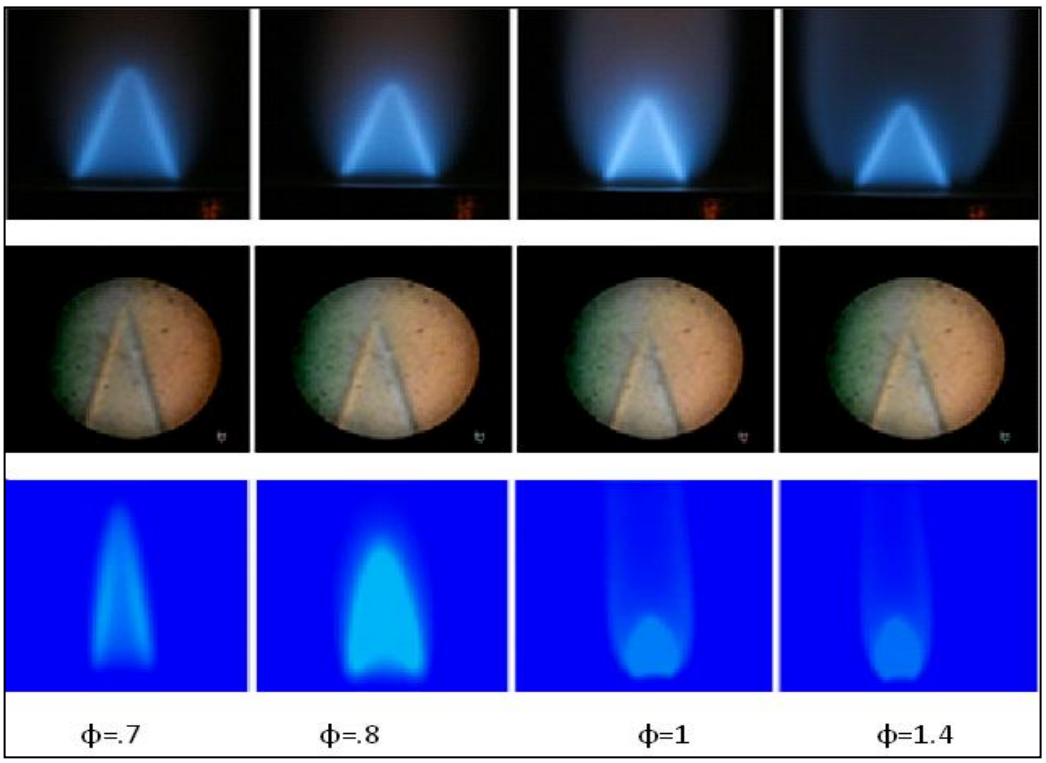

Fig. 4.2.1 Flame images with different techniques (Top—Direct Imaging, Middle—Schlieren Technique, Bottom—Intensified Imaging technique)

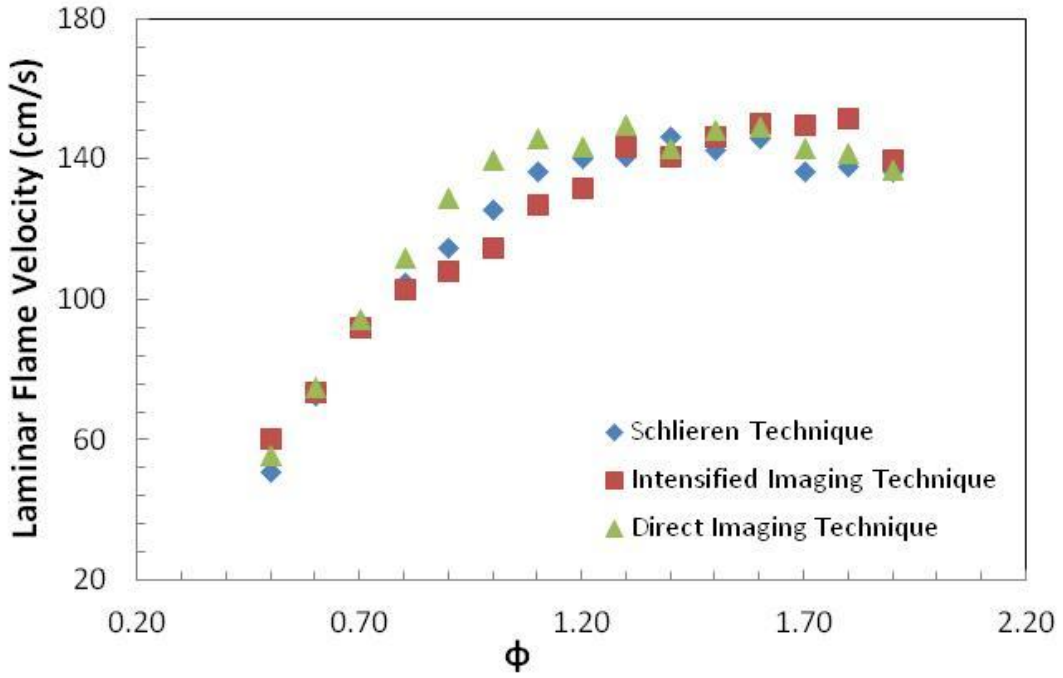

Fig. 4.2.2 Comparison with other measurements (30% H_2 +70% CO) for the nozzle burner using the direct digital imaging technique

Burning velocity measurements of H_2-CO mixtures at different H_2 concentrations and mixture equivalence ratios are presented in Fig. 4.2.3. It is found that the burning velocity of H_2-CO increases nonlinearly with the increase in H_2 content in the mixture. The effect of hydrogen addition is especially significant at lean conditions. The presence of hydrogen in fuel mixtures creates the necessary branched chain reactions to accelerate the flame propagations. The H_2 in the mixtures supplies the necessary active radicals and atoms such as OH, O and H and their diffusion rates into the unburned gas determines the magnitude of flame burning velocity. However, it is interesting to note that the maximum burning velocity of H_2-CO mixtures shifted back to lean condition with the increase of H_2 concentration in mixtures. This is due to the shift in mixture stoichiometry with the increase in H_2 in mixture compositions.

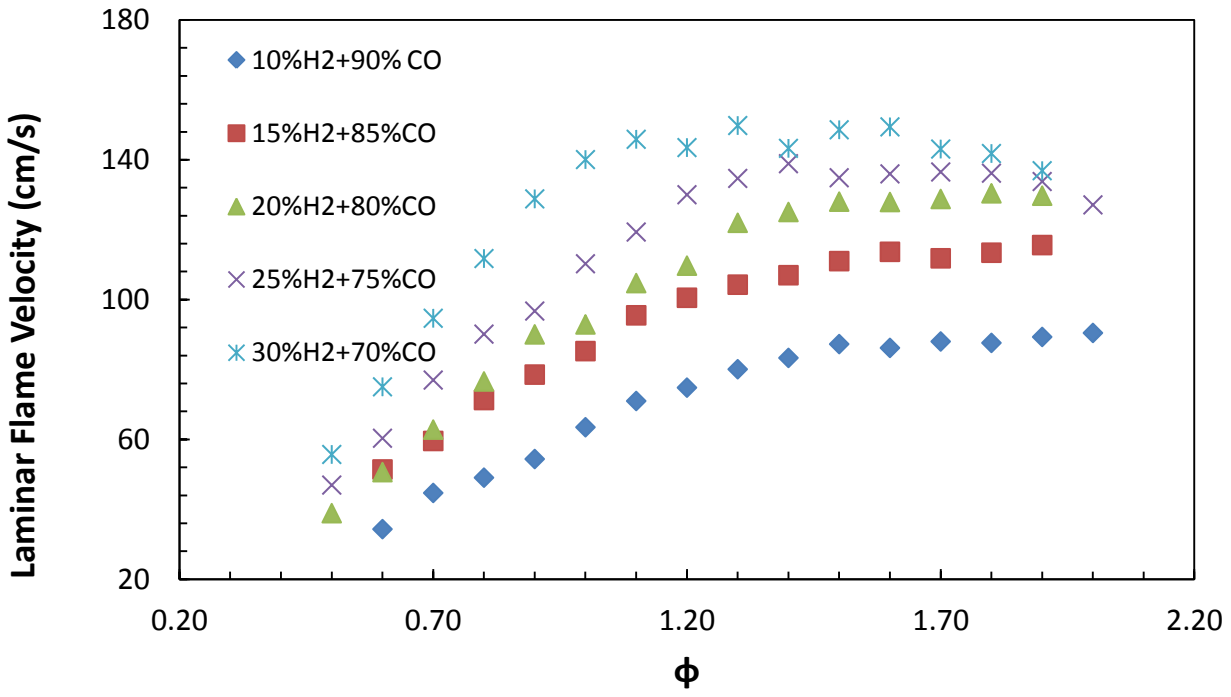

Fig. 4.2.3 Burning velocities at different mixture compositions measured for nozzle burner using the direct imaging technique

To quantify the effects of diluents (N_2 and CO_2 in the case syngas mixtures), burning velocity H_2-CO-N_2 and H_2-CO-CO_2 mixtures with same mixture adiabatic flame temperature (t_{ad}=1900K) are measured (Fig 4.2.4). It is observed that the effects of N_2 and CO_2 on the mixture burning velocity are significantly different. H_2-CO and H_2-CO-N_2 mixtures with similar adiabatic flame temperature have a similar flame propagation velocity. In contrast the flame propagation is significantly slower in H_2-CO-CO_2 mixtures. It appears that the more kinetically active CO_2 strongly chain branching and acts as a strong chain termination source.

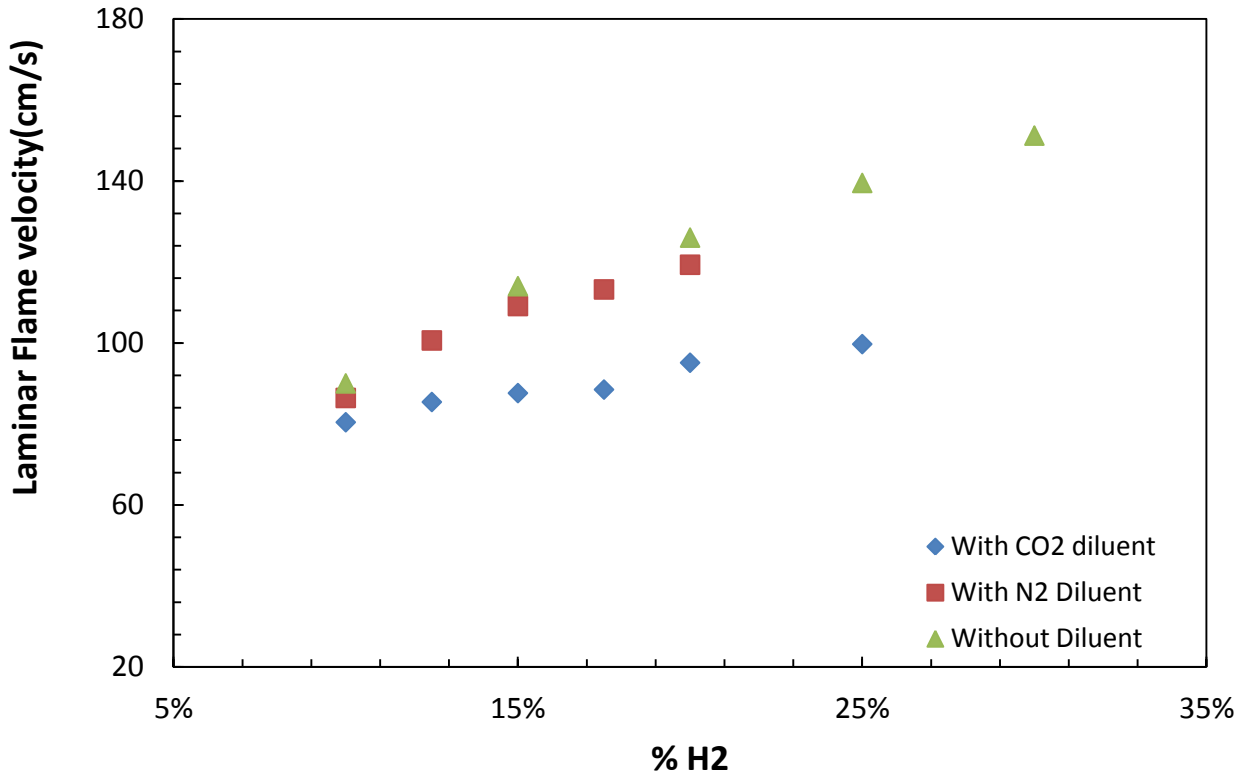

Fig. 4.2.4 Effect of diluents on burning velocity measured for nozzle burner using the direct imaging technique

Different compositions of syngas mixture (based on different coal types) and corresponding burning velocity measurements are presented in Fig. 4.2.5, respectively. In compared to Lignite and Coke derived syngas, equivalence ratio at the maximum mixture burning velocity shift toward leaner condition for brown and bituminous syngas mixtures. This is due to the presence of higher hydrogen contents in brown and bituminous syngas mixtures. Additionally despite similar H_2 and CO contents, Bituminous coal derived syngas has higher burning velocity due to a less CO_2 concentration in the mixture. As discussed earlier kinetically active CO_2 strongly affects the flame propagation velocity. Similar effects of CO_2 are also observed in the burning velocity of Lignite and Coke syngas mixtures.

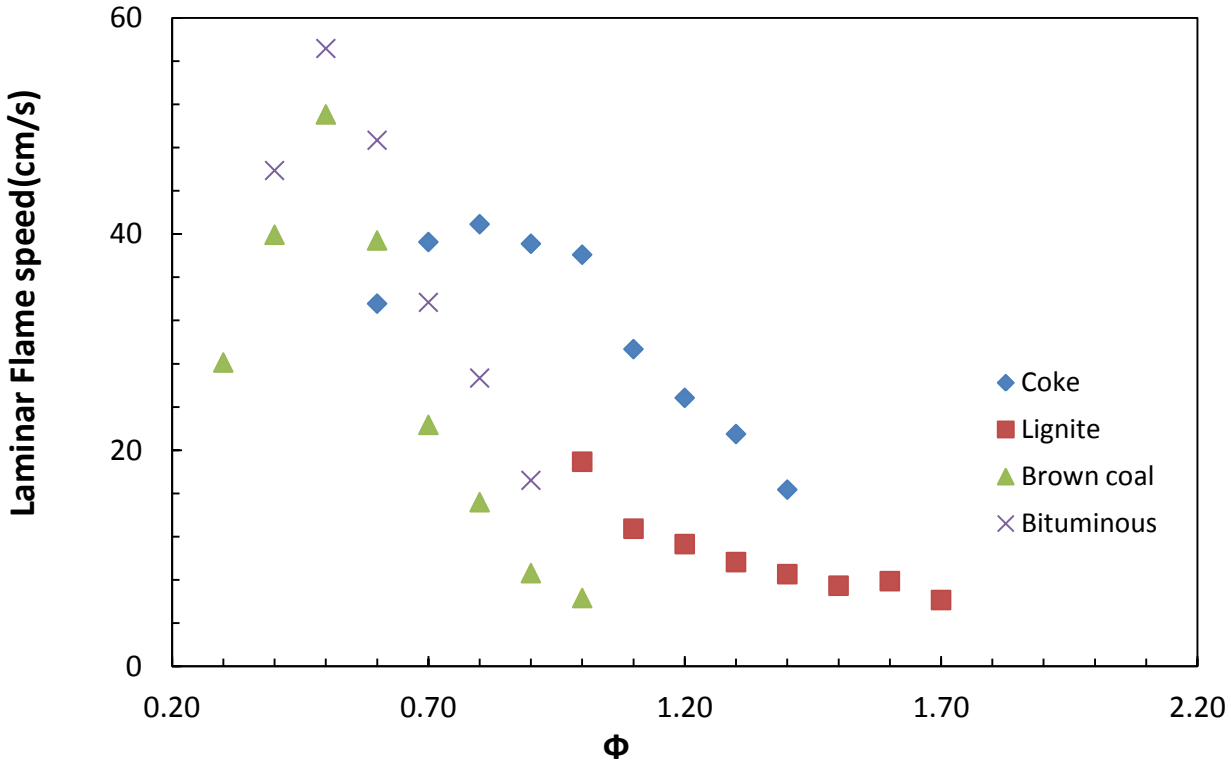

Fig. 4.2.5 Burning velocity of actual syngas compositions measured using the nozzle burner the direct imaging technique

4.3 MEASUREMENT OF TURBULENT BURNING VELOCITIES OF SYNGAS FUELS:

4.3.1 Quantitative Measurement of Turbulent Flame Speed:

There are two different approaches to determine the turbulent burning velocity, one of them is to calculate the flame area/flame angle or by using quantitative measurement approach. In flame area method , flame images obtained using the high speed intensifier are averaged over 1000 samples and then mean flame area is calculated using equation 4.3.1 .

$$S_T = \frac{\dot{m}_r}{\rho_r A_C} \quad (4.3.1)$$

where $\dot{m}_r$ ρ_r $A_C$denote reactant mass flow rate, reactant density and mean flame area which is related to some given variable named as <c> contour or progress variable. Thus, the value of S_T is itself a function of the progress variable surface used to define the mean flame front area. The present study uses this approach to determine the ST a as this method was used extensively by Gouldin and Cheng, Kobayashi et al and Prabhakaran[9] et al. Calculated flame speed are higher when compared to laminar flame speed due to the turbulence for same initial conditions. Flame speeds measured in a gas turbine combustor significantly increase due to the presence of turbulence.

The extent of turbulence influence on the flame speed is not fully resolved, however. Lefebvre and Ballal described the visualization of a turbulent flame and explained how the turbulence caused a wrinkling the flame front which increased its specific

surface area thus increasing burning rate[4]. The authors show the following equation which can be used to determine turbulent flame speed:

$$S_T = S_L + u' \qquad (4.3.2)$$

Where S_T is the turbulent flame speed, S_L is the laminar burning velocity and u' is the RMS value of fluctuating velocity or the turbulent intensity which is obtained from the PIV vector averaged data.

4.3.2 Image Analysis

The turbulent flame speed is calculated by flame area method as shown in equation 2. The determination of flame surface is explained in this section.

Digital images of the flame are taken with a 12 bit intensified CCD (2048x2048 pixels). The built in first image intensifier is available with a multialkali photocathode having a wide range of spectral response range from UV through near infrared, and hence capable of identifying the OH* chemiluminescence from the flame region zone. The ICCD system operates with a minimum gate time of 10 nanoseconds and a maximum gate repetition frequency up to 200 KHZ. It allows multi-exposure. The system is integrated with a OH* filter.

Images obtained from the ICCD camera are averaged over thousand samples. The mean image is symmetric along the burner axis. The brightest pixels images are tracked using a flow visualization software(Dantech Dynamics) and the straight lines are drawn through those points to the flame anchoring points on the burner the resulting image looks like the image shown in the Figure 4.3.1(a) . Figure 4.3.2(b) shows the two peaks which are basically the brightest pixels when measures along the

burner radius at an axial distance of 5 mm from burner top.

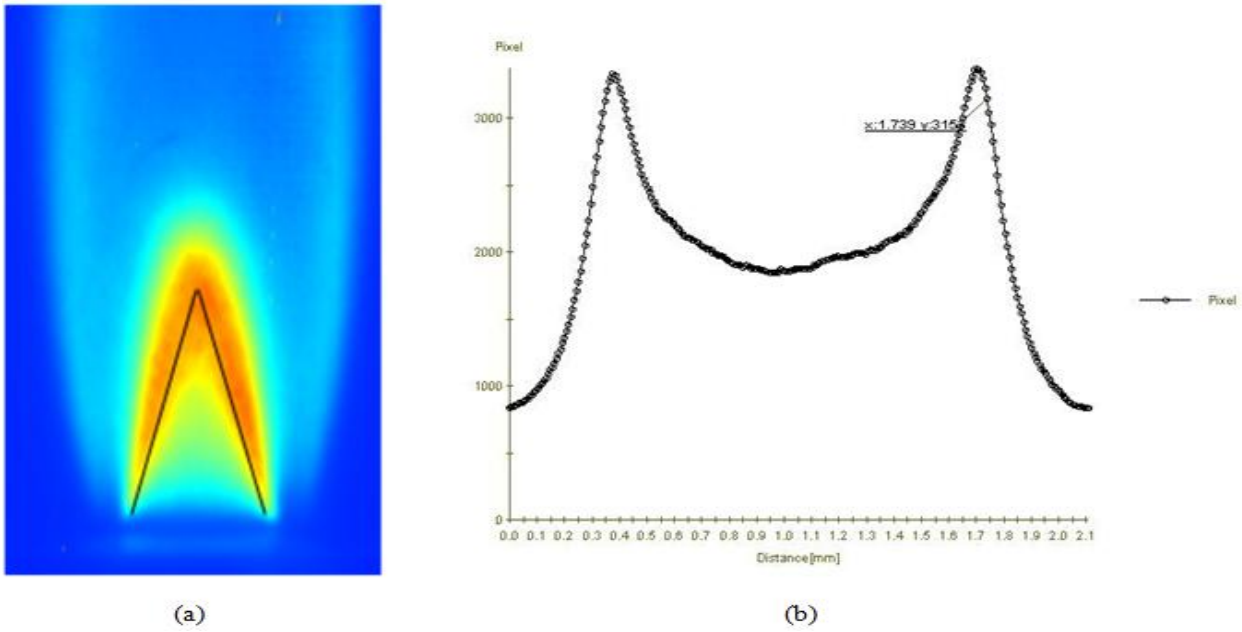

Figure 4.3.2 (a) Time averaged Flame image showing a mean intensified image (b) Pixel intensity along the radial axis of burner at an axial distance of 5 mm from burner top

4.3.3. Reacting Flow Field with H2-CO/Air Combustion

Figure 4.3.3.1 shows flow-field fluctuations for H2-CO/Air combustion. The height of the premixed cone is increased as the hydrogen content reduced as shown in the figure (sequence from (a) to (c)), which clearly shows the effect of hydrogen on the effective flame surface area resulting in increase in the local propagation velocity for high hydrogen content fuels. For the Bunsen type and rod-stabilized flames, the turbulence decays as the flow approaches the flame[5].The velocity fluctuations were observed to be highest at the burner top gradually reducing and at the inner cone or reaction zone tip. The fluctuations tended to increase up to certain distance due to the expansion of gases and then gradually decreased further downstream of the

burner. This effect is observed predominantly at higher blockage ratios since the fluctuations were larger.

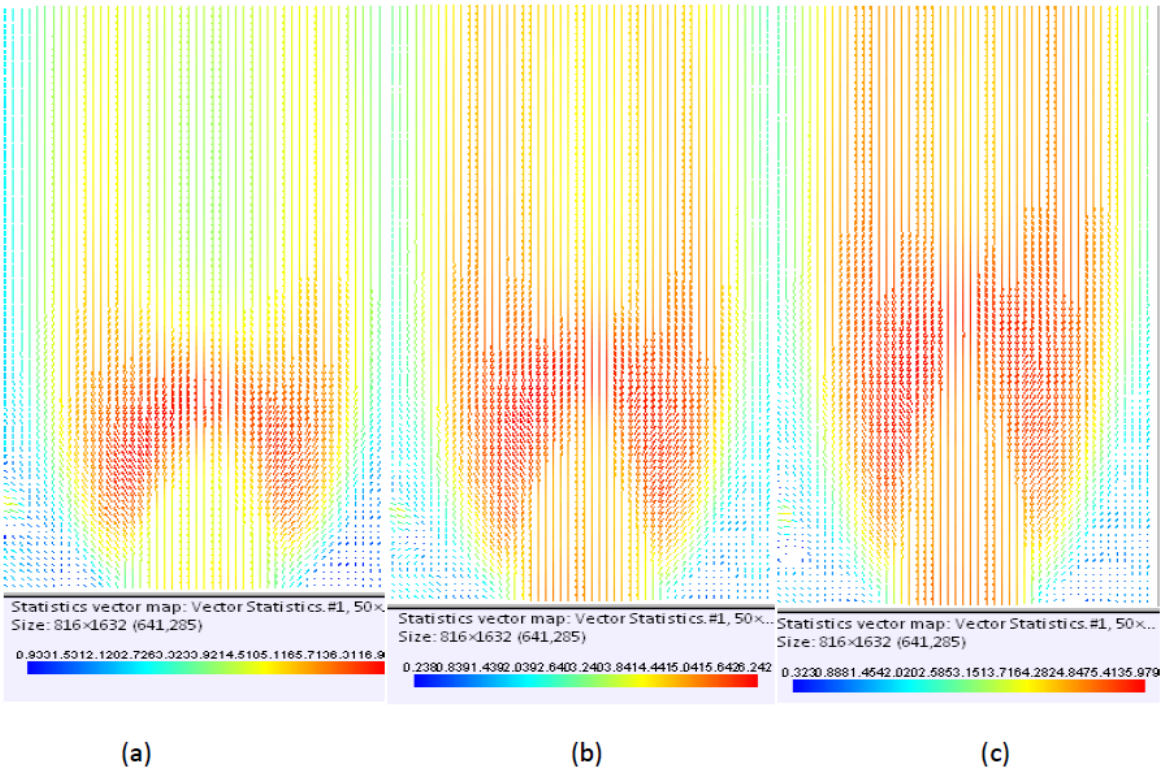

Figure 4.3.3.1 (a) Flow Field of 20%H2 80% CO at RE=2000 and Φ=.9 at BR=.83 (b)) Flow Field of 15 %H2 75 % CO at RE=2000 and Φ=.9 at BR=.83 (c)) Flow Field of 20%H2 80% CO at RE=2000 and Φ=.9 at BR=.83

Figure 4.3.3.2 shows the plot of velocity fluctuations of H2-CO/air at a constant Reynolds number of 2000 and constant equivalence ratio of 1 and at the two different blockage ratios of 83%and 73%.As we can see the velocity fluctuations increase with increase in the BR. From the Figure 4.3.3.2 the data shows that flame brush thickness increases with the increase in the BR. Figure 4.3.3.3 shows the velocity fluctuation at different syngas compositions at constant blockage ratio. The velocity fluctuations tend to remain same as hydrogen content increased. On the contrary Figure 4.3.3.4 shows the effect of turbulence on turbulent propagation speed at a constant

equivalence ratio of .9 and a constant Reynolds number of 2000. The turbulent propagation speed increased not only with the increase in the hydrogen content in the syngas mixture but also with the increase in the blockage ratio. Velocity fluctuations tend to increase with increase in the blockage ratio resulting in increase in the effective flame area. The turbulent flame propagation velocities are obtained using the flame area method.

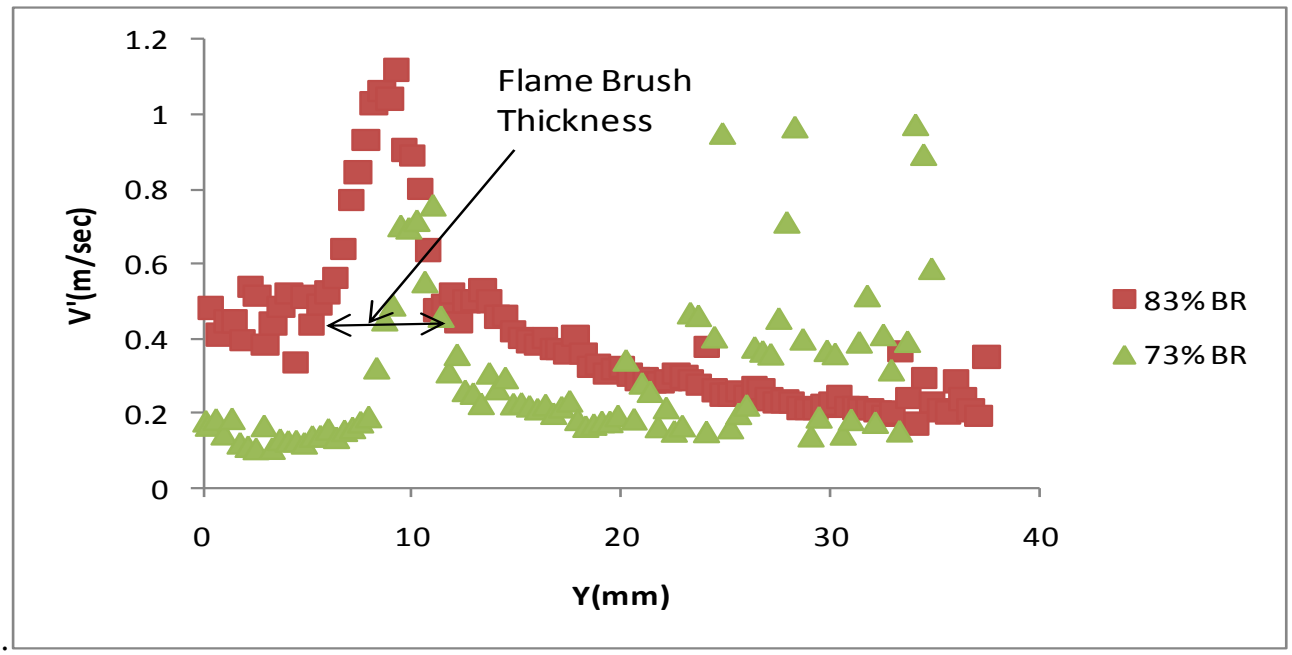

Figure 4.3.3.2: Turbulent intensity along the burner exit axially for 20% H2-80%CO at Re=2000 and Φ=.9

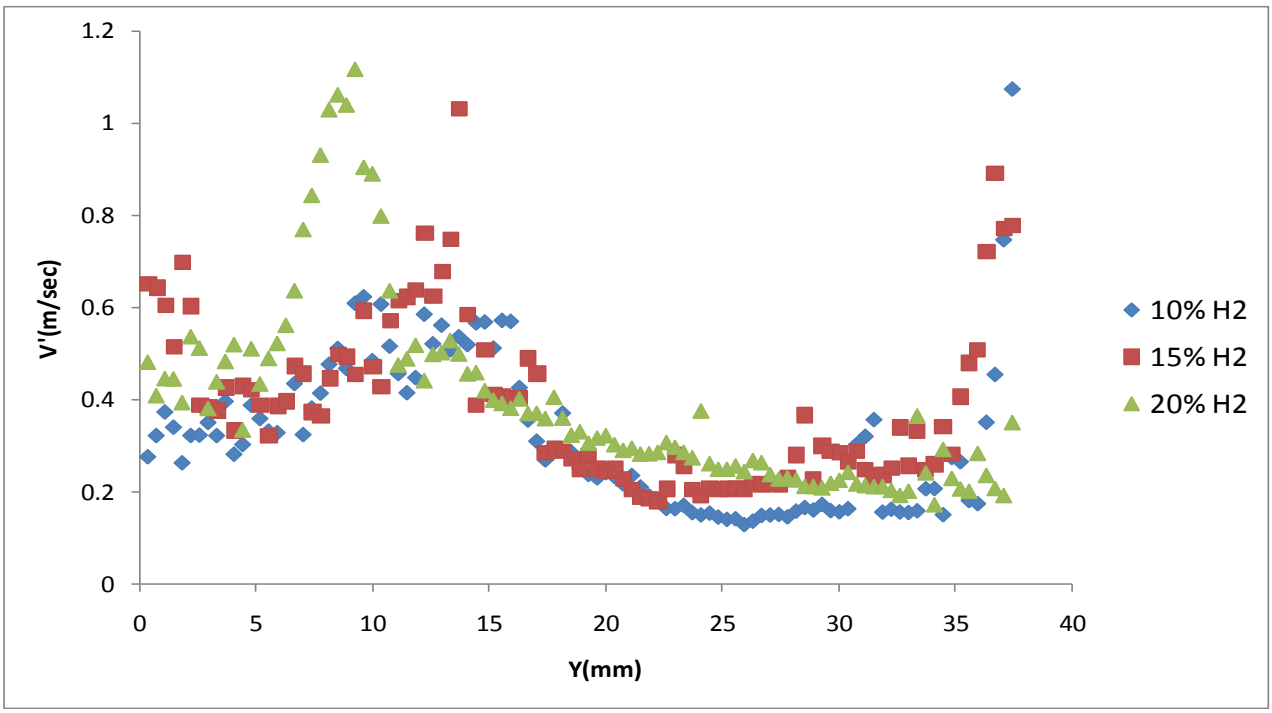

Figure 4.3.3.3: Turbulent intensity along the burner exit axially for 20% H2-80%CO at Re=2000 and Φ=.9

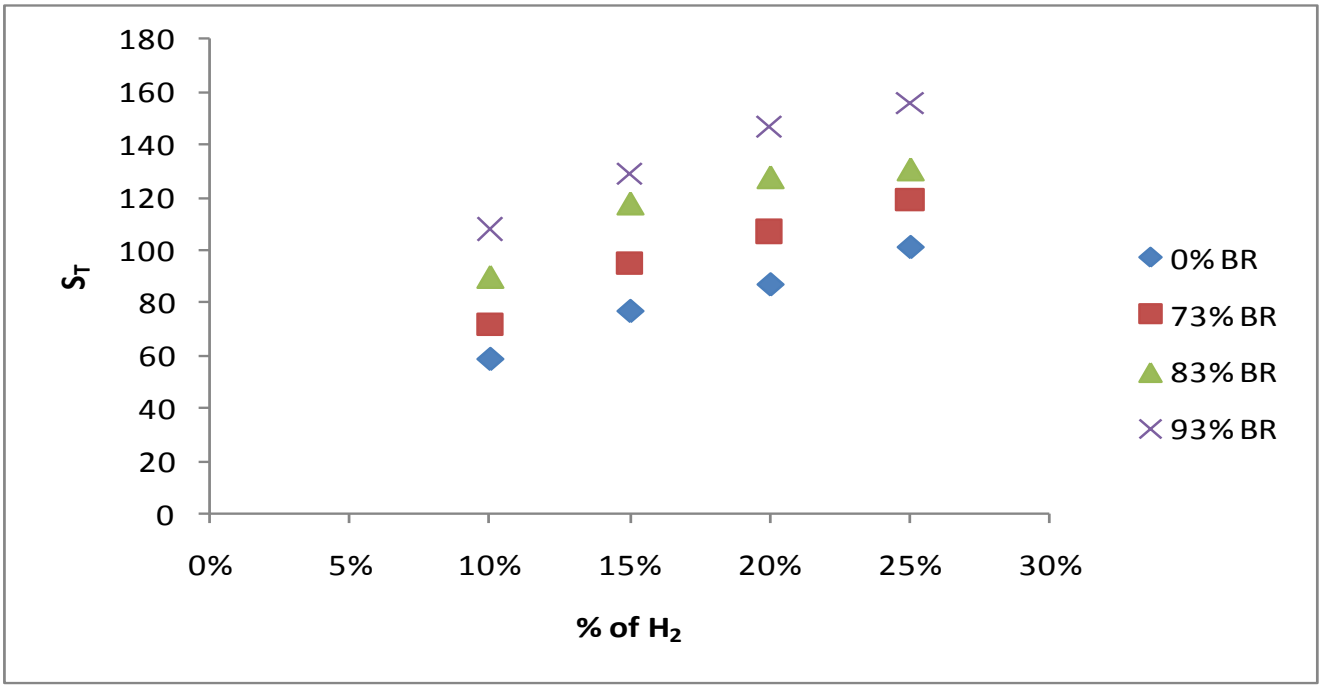

Figure 4.3.3.4: ST for different syngas compositions at constant RE=2000 and Φ=.9

4.3.4. Effect of turbulence on turbulent flame propagation at constant flame speed:

Figure 4.3.4.1 shows the plot of turbulent flame propagation velocity *ST,* for H2/CO mixtures of 10/90, 15/85, 20/80, 25/75, and 30/70 at a constant laminar burning velocity of 70 cm/sec and with a bulk velocity of 4 m/sec.

Table 4.3.4: Different syngas compositions at constant S_L=70 and at different equivalence ratios

Φ					U=4(m/sec)
1.2	0.9	0.8	0.7	0.6	SL=71
10%H2	15%H2	20%H2	25% H2	30%H2	

For a given fuel composition, S_T, increases monotonically with different blockage ratios (due to increase in level of turbulence intensity). One of the most important observations from the current data is the linear increase in S_T, with H2 levels. At 10%H2 the S_T is almost same for all the three different blockage ratios but it tend to increase with increase in the hydrogen content which indicate that there is an effect of hydrogen at higher blockage ratios which was noticed by kido et al.

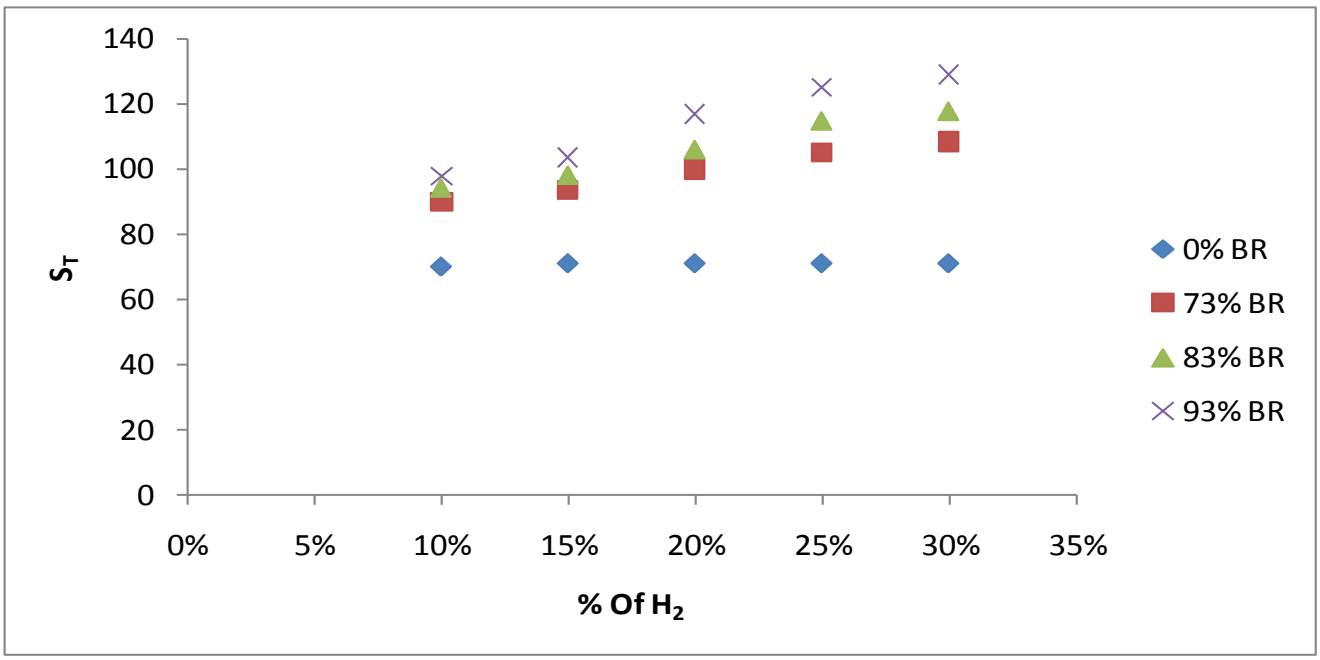

Figure 4.3.4.1: S_T for different syngas compositions at constant S_L=70 and at Different BR's

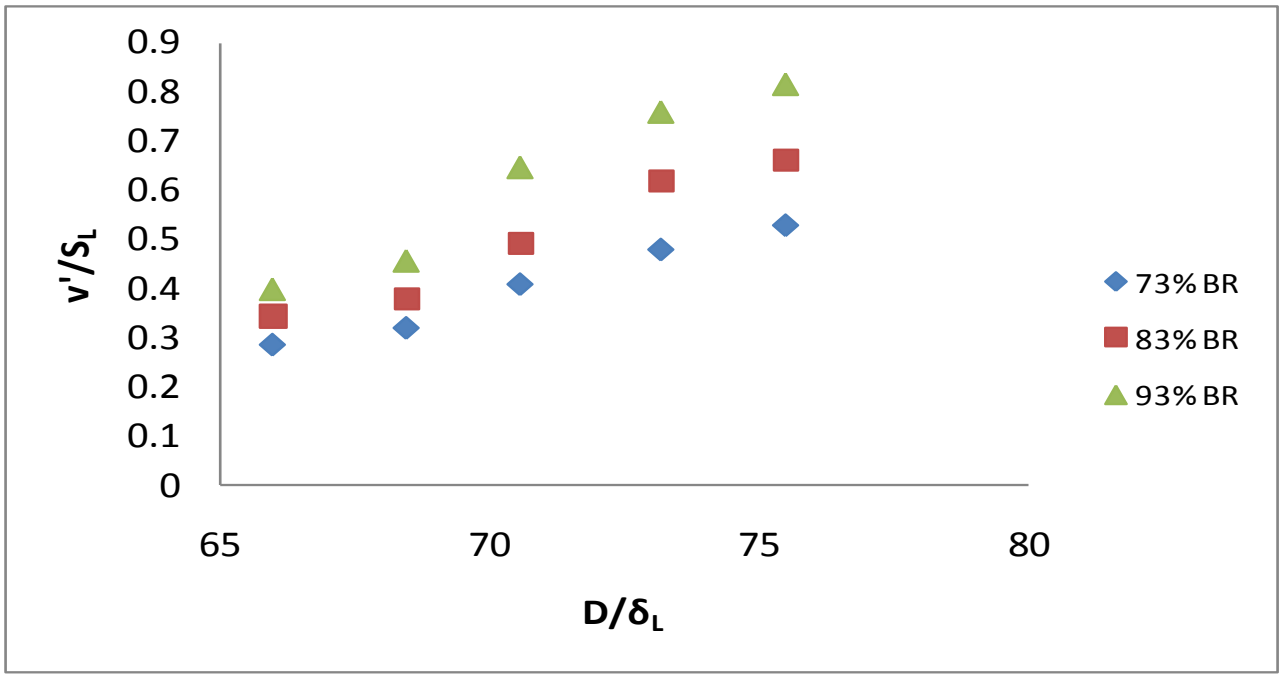

Figure 4.3.4.2: Borghi Diagram for constant flame speed with a burner diameter of 8 mm

Figure 4.3.4.2 summarizes where the measured data is located on a Borghi diagram for the 8 mm burner diameter. Since the magnitude of y axis is less than 1 it was difficult to scale the current diagram to the original Borghi diagram. The present set of data lie the region of wrinkled flamelets.

4.3.5. Effect of diluents on turbulent propagation velocity at constant adiabatic flame temperature at different blockage ratios

The effects of N_2 and CO_2 dilution (minor constituents of syngas fuels) on the turbulent flame propagation velocity of H2-CO mixtures were investigated at Tad =1900K temperature and at different blockage ratios .Experiments were performed with a simultaneous increase in H2, and Diluents (N2 and CO2) at different BR's, to understand the effect of N_2 and CO_2 concentrations at different blockage ratios. Bidhan et al investigated the effect of diluents on laminar burning velocity of syngas fuels and stated that CO_2 has a predominant effect when compared with N_2. Figure 4.3.5.1 shows that the turbulent propagation velocities for 0% BR and 73% BR with N_2 as a diluents in the mixture has lower S_T when compared with laminar burning velocity of syngas fuels at a similar composition. S_T for 83% BR and 93% BR with N_2 as diluents has higher velocities when compared with laminar burning velocity for a given mixture; this is mainly due to increase in the turbulent intensity within the flame. In case of CO_2 as a diluent (Figure 4.3.5.2), ST at 0% BR, 73% BR and 83% BR is much lower when compared with the laminar burning velocity for a wide range of syngas compositions. In addition to that Figure 4.3.5.3 compares the ST at 93% BR with simultaneous increase in H2 concentration along with N_2 and CO_2 as diluents for a wide range of syngas gas

compositions. From the Figure13, the data clearly states that CO_2 in H2-CO mixtures has a more dominating role in reducing the S_T when compared with N_2. The addition of more diluents to the mixtures, the recombination ($H+H+M \rightarrow H_2+M$) reaction is faster compare to the chain branching ($H+O_2 \rightarrow O+OH$) step. And also if the diluents (CO_2, N_2) of higher heat capacity are present in sufficient quantities, it will reduce temperature, thereby reducing the rate of energy release and eventually decrease the burning velocity.

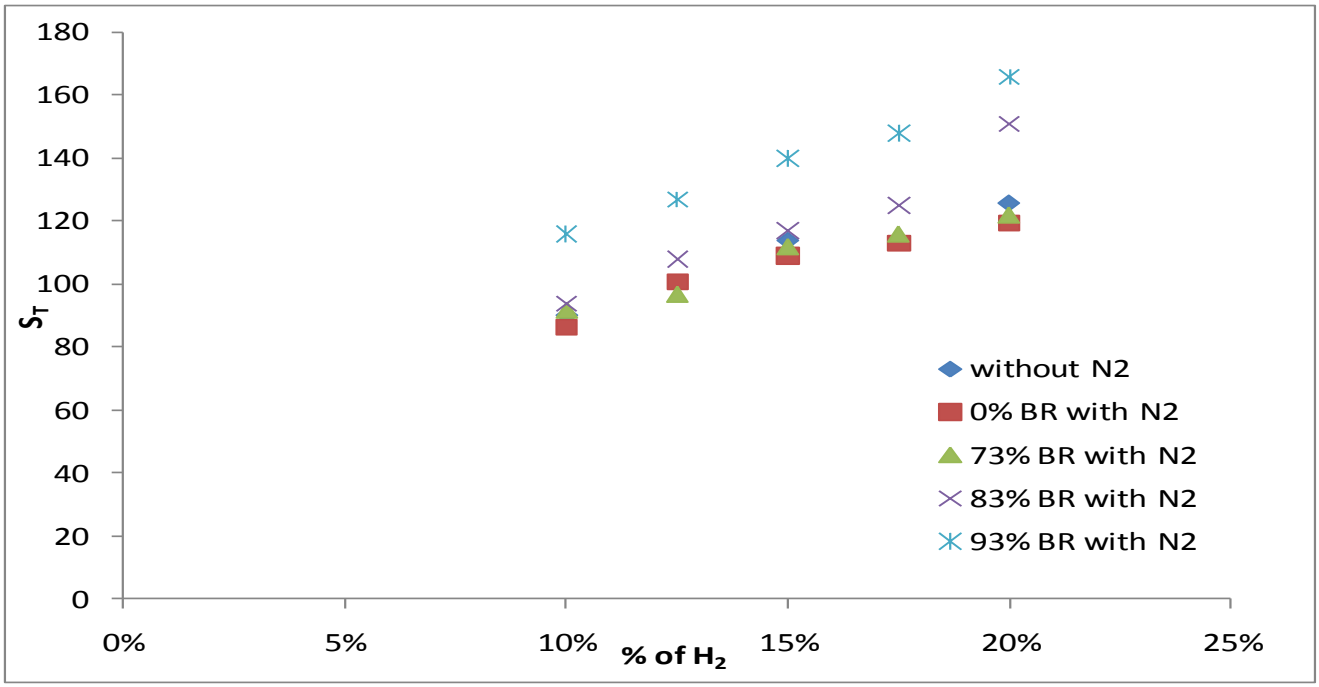

Figure 4.3.5.1: S_T for different H2-CO-N2 compositions at constant T_{ad}=1900K and at Different BR's

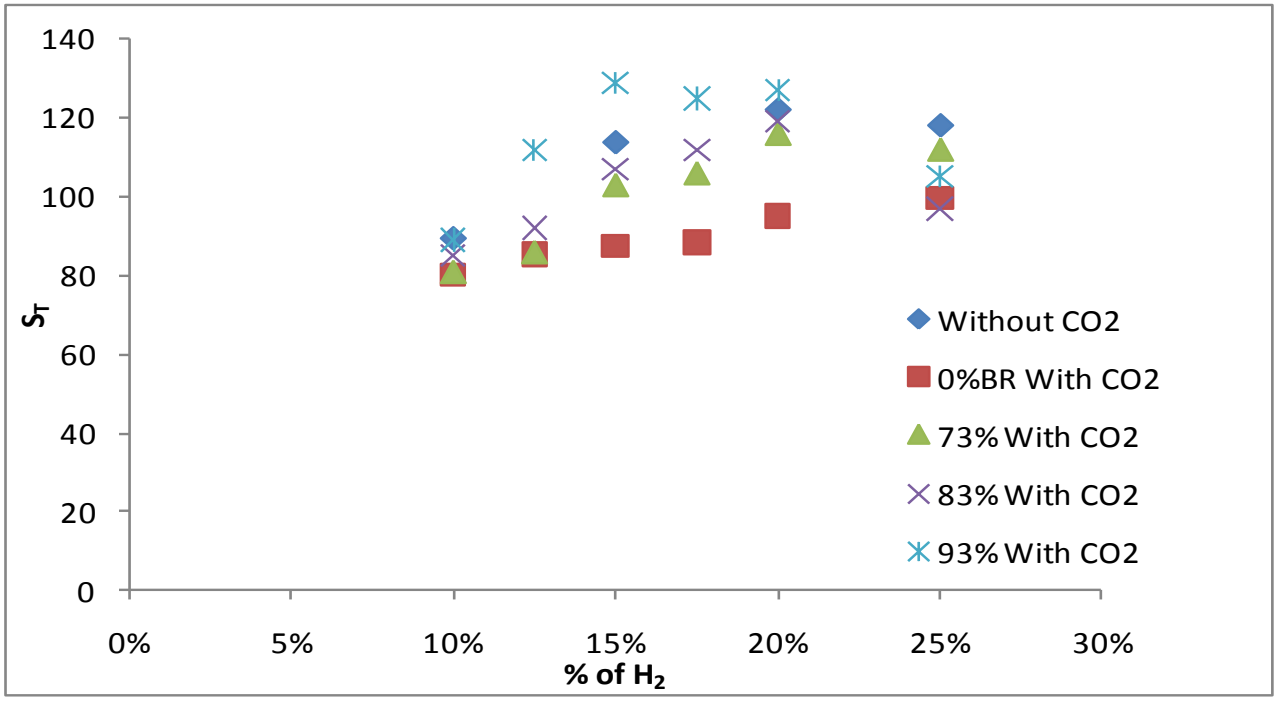

Figure 4.3.5.2: S_T for different H2-CO-CO2 compositions at constant T_{ad}=1900K and at Different BR's

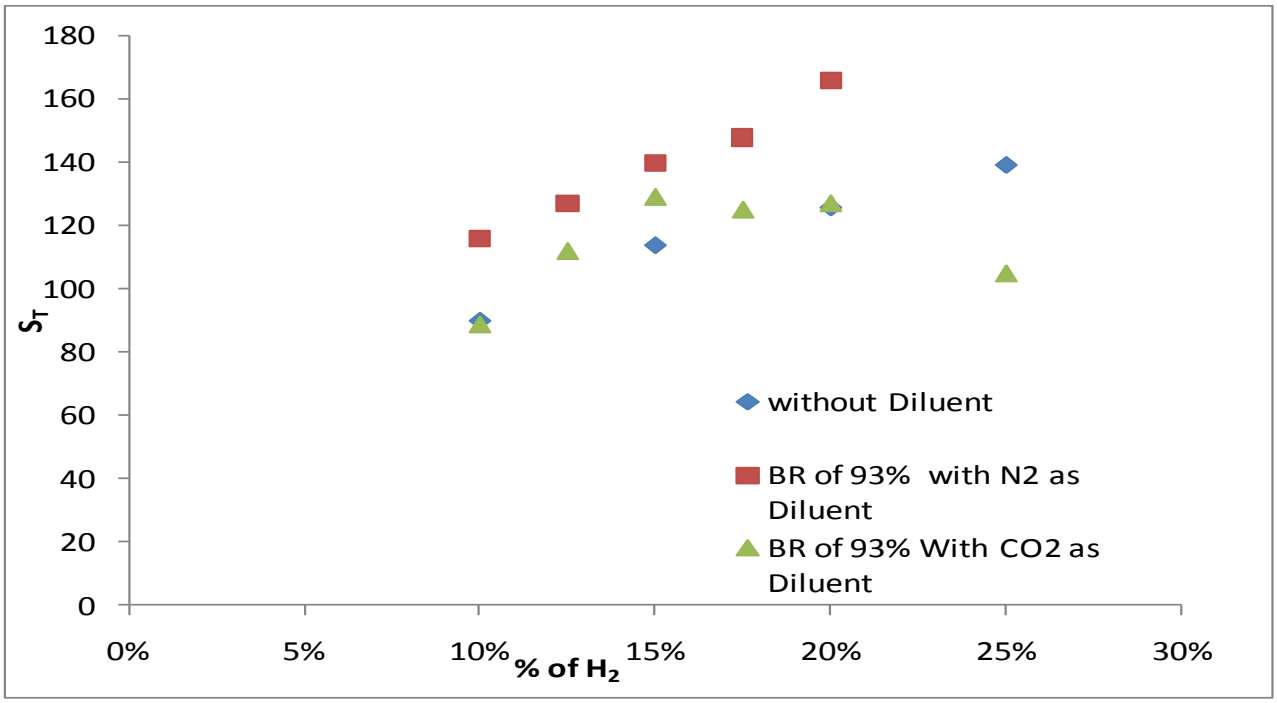

Figure 4.3.5.3: S_T for different H2-CO-CO2/H2-CO-N2 compositions at constant T_{ad}=1900K and at constant BR of 93%

4.4 LAMINAR BURNING VELOCITIES AND ADIABATIC FLAME TEMPERATURES OF OXY- FUEL FLAMES

The adiabatic flame temperatures and laminar burning velocities of CH4-O2-Diluent flames are evaluated using the GRI mechanism. Figure 4.4.1 shows the laminar burning velocities of CH4-O2-Diluent flames. The diluents used in the present case are N2, Ar and CO2. From the Figure 4.4.1, the data clearly states that CO_2 in CH4-O2 mixtures has a more dominating role in reducing the S_L when compared with N_2, and Ar. The addition of more diluents to the mixtures, the recombination ($H+H+M \rightarrow H_2+M$) reaction is faster compare to the chain branching ($H+O_2 \rightarrow O+OH$) step.

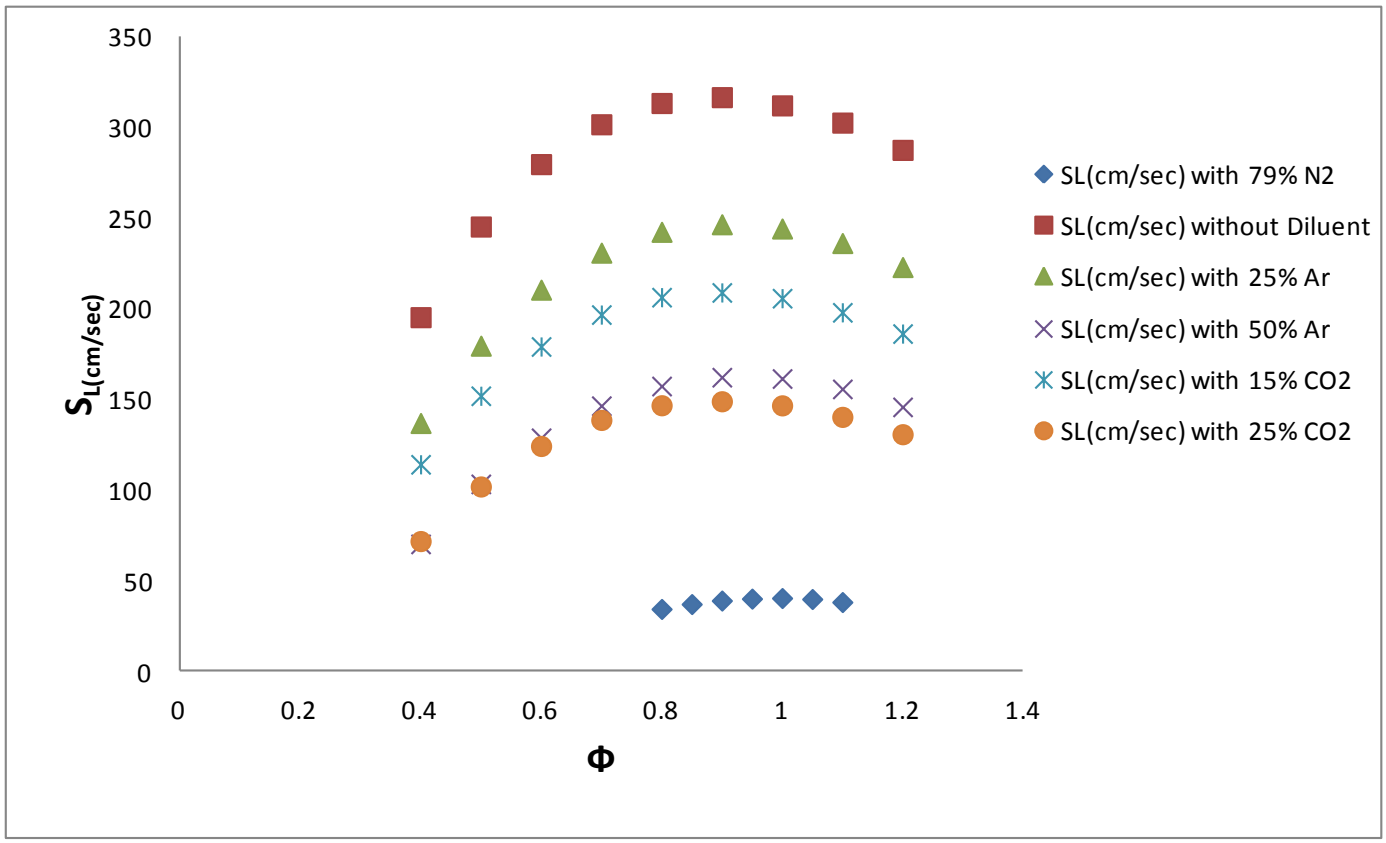

Figure 4.4.1: Laminar burning velocities of CH4-O2-Diluent mixtures

Figure 4.4.2 shows the adiabatic flame temperatures of the CH4-O2-Diluent mixtures. Due to the higher heat capacity of CO2, which present in sufficient quantities, it will reduce temperature, thereby reducing the rate of energy release causing reduction in the adiabatic flame temperatures when compared with N2 and Ar, which are chemically inert.

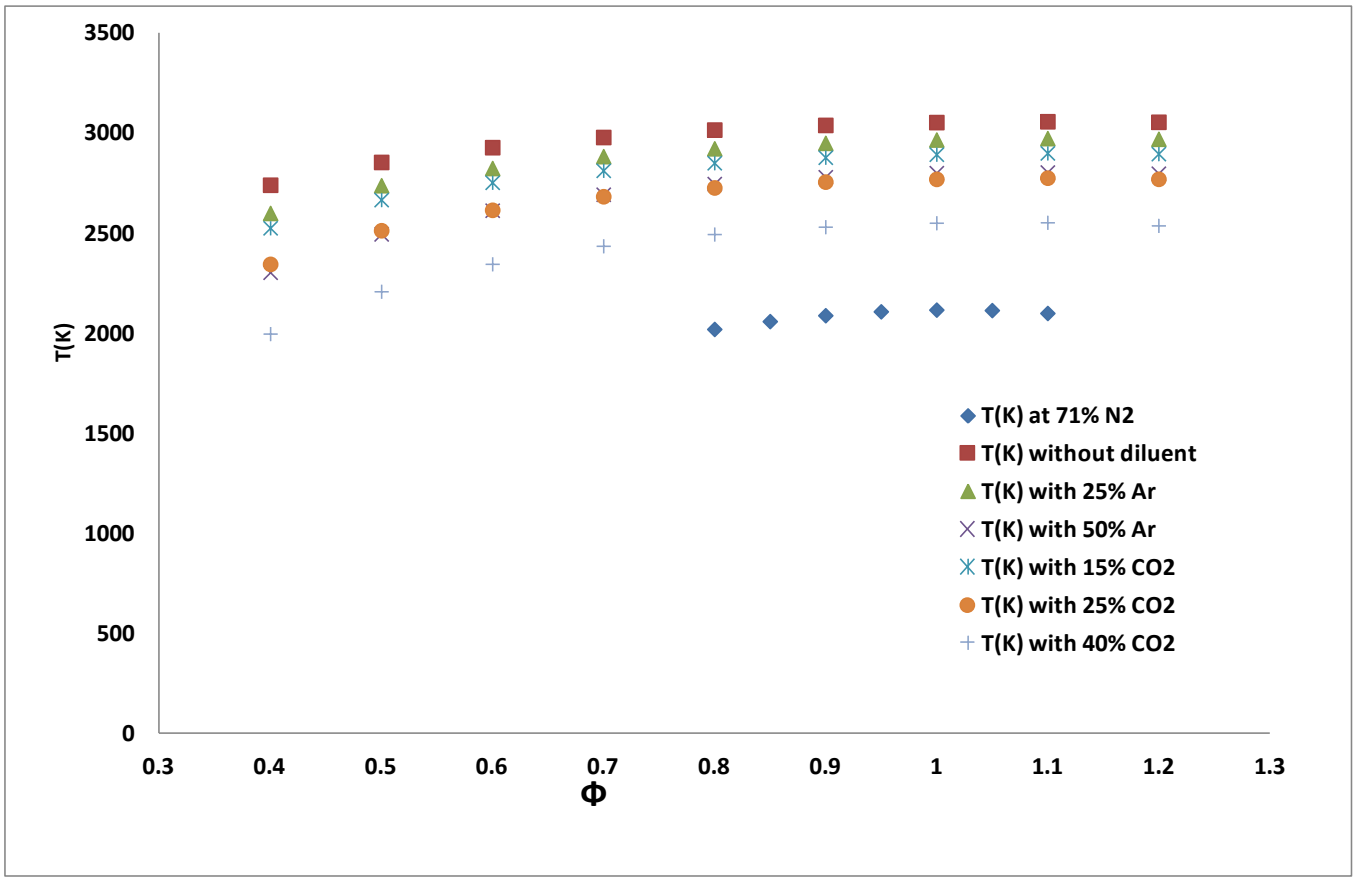

Figure 4.4.1: Adiabatic flame temperatures of CH4-O2-Diluent mixtures

4.5 Effect of blockage ratio on the local flow field fluctuations of CH4-O2-CO2 flames at constant Re (1000), firing input (1 KW) and constant stoichiometric ratio.

Figure 4.5.1 shows the axial plot of velocity fluctuations of CH4-O2-CO2 flames at a constant Re (1000), Firing input (1 KW) and constant stoichiometric ratio (Φ=1). As we can see the velocity fluctuations increase with increase in the BR.

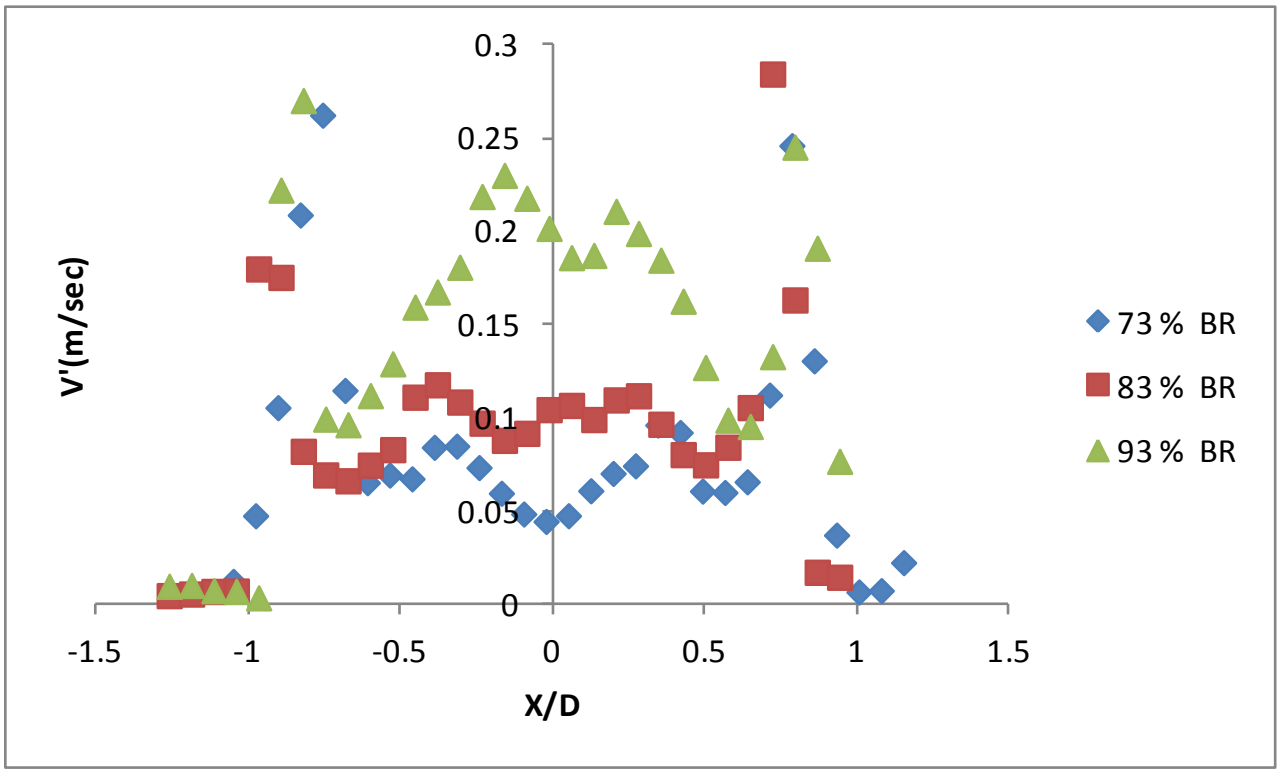

Figure 4.5.1 RMS fluctuating velocity profiles at X/D =0 for CH4-O2-CO2 flames

Figure 4.5.2 shows flow-field fluctuations for CH4-O2-CO2 flames. The height of the premixed cone is increased as the turbulent intensity reduced as shown in the figure (sequence from (a) to (c)), which clearly shows the effect of blockage ratio on the effective flame surface area resulting in decrease in the local propagation velocity.

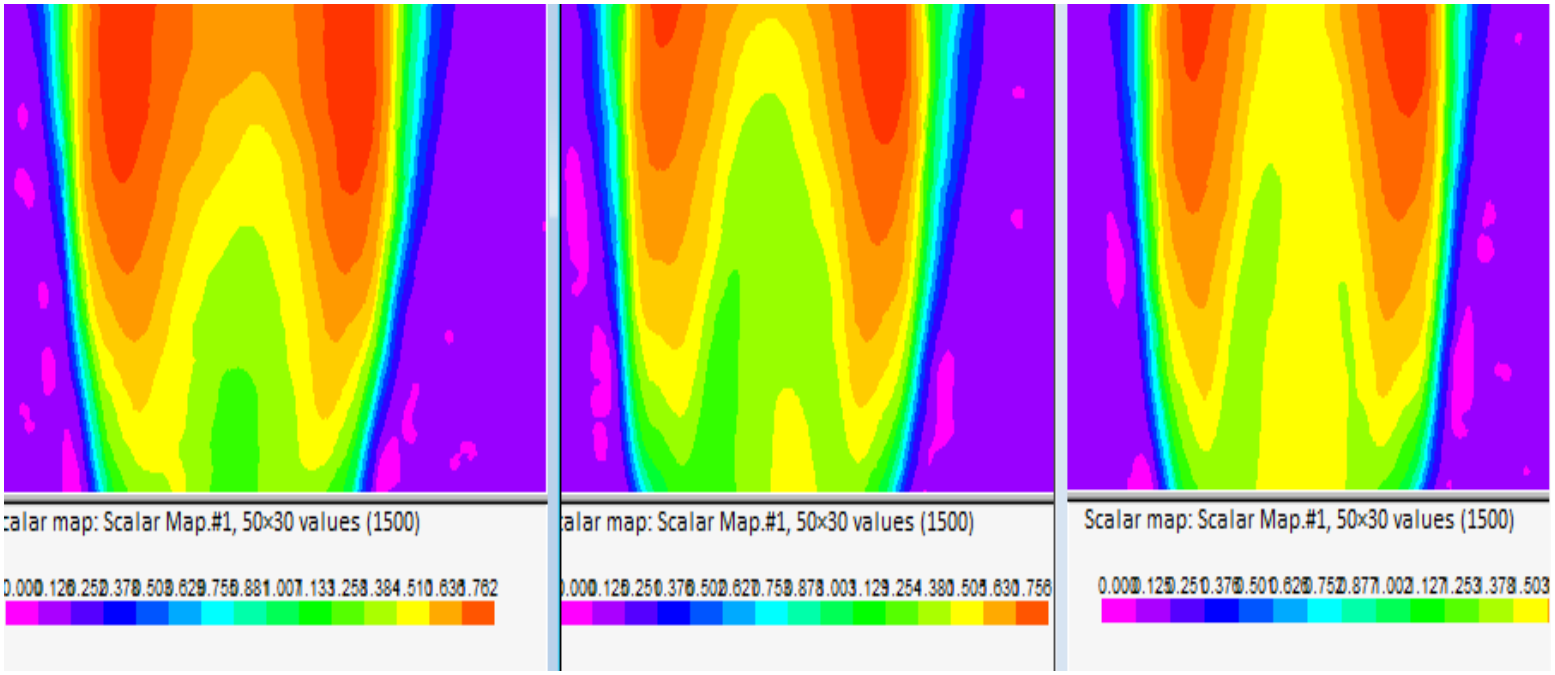

(a) (b) (c)

Figure 4.5.1 Scalar map of velocity for CH4-O2-CO2 flames (a) 93% BR (b)83% BR (c)73% BR

Figure 4.5.3 shows the radial plot of velocity fluctuations at an axial distance of 5 mm above the burner at different turbulent intensities (93% BR, 83% BR and 73% BR). The turbulent propagation speed increased with the increase in the blockage ratio. Velocity fluctuations tend to increase with increase in the blockage ratio resulting in increase in the effective flame area. Figure 4.5.4, 4.5.5 and 4.5.6 shows the plots of Radial RMS fluctuating velocity profiles at different axial distances for CH4-O2-CO2 flames at 93%, 83% and 73% blockage ratios.

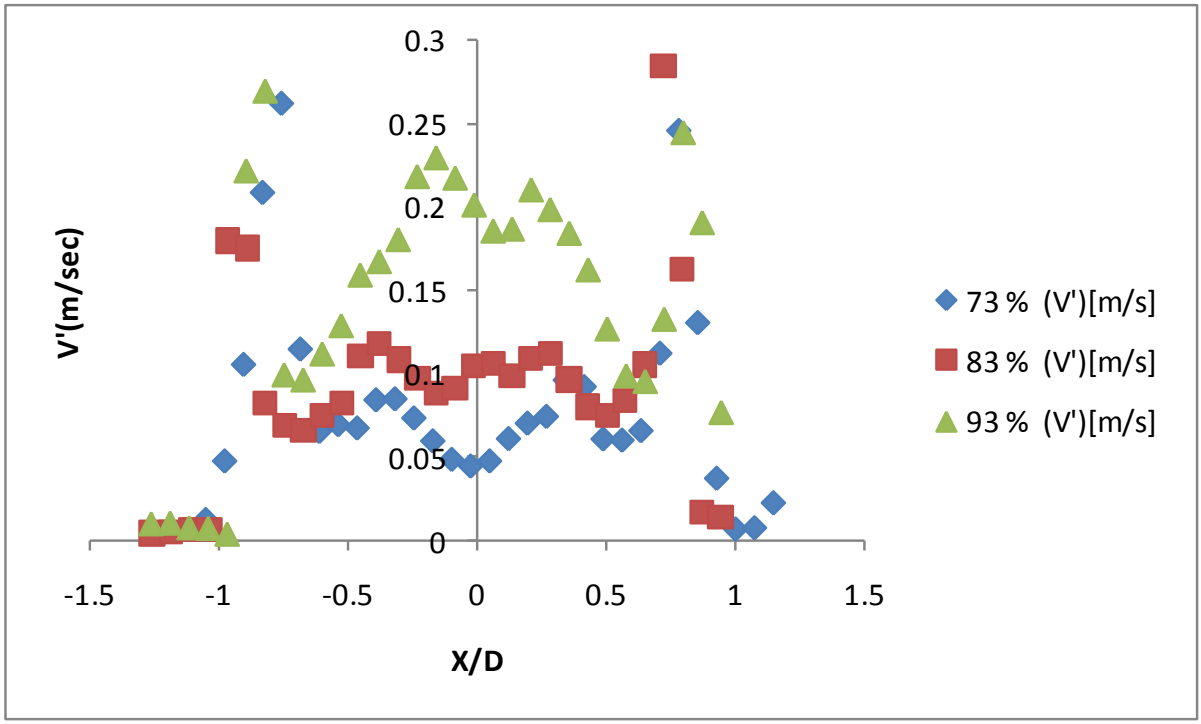

Figure 4.5.3 RMS fluctuating velocity profiles at Y/D =0.53 for CH4-O2-CO2 flames at different blockage ratios

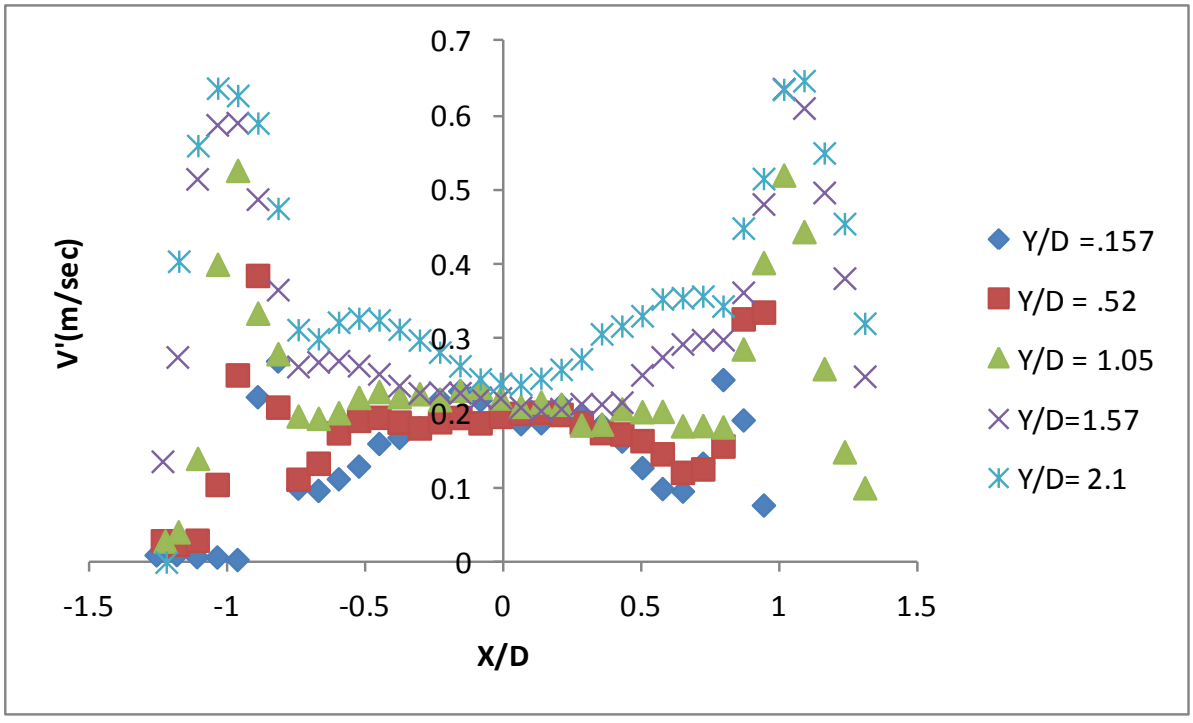

Figure 4.5.3 Radial RMS fluctuating velocity profiles at different axial distances for CH4-O2-CO2 flames at 93% blockage ratio,

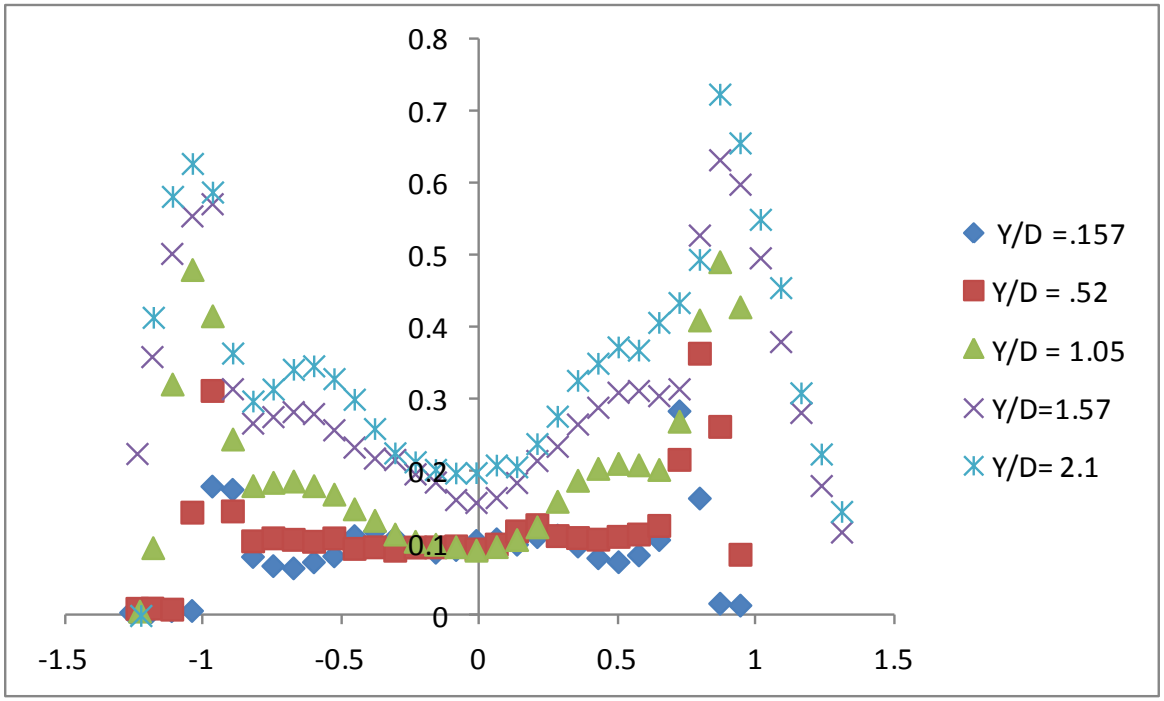

Figure 4.5.3 Radial RMS fluctuating velocity profiles at different axial distances for CH4-O2-CO2 flames at 83% blockage ratio.

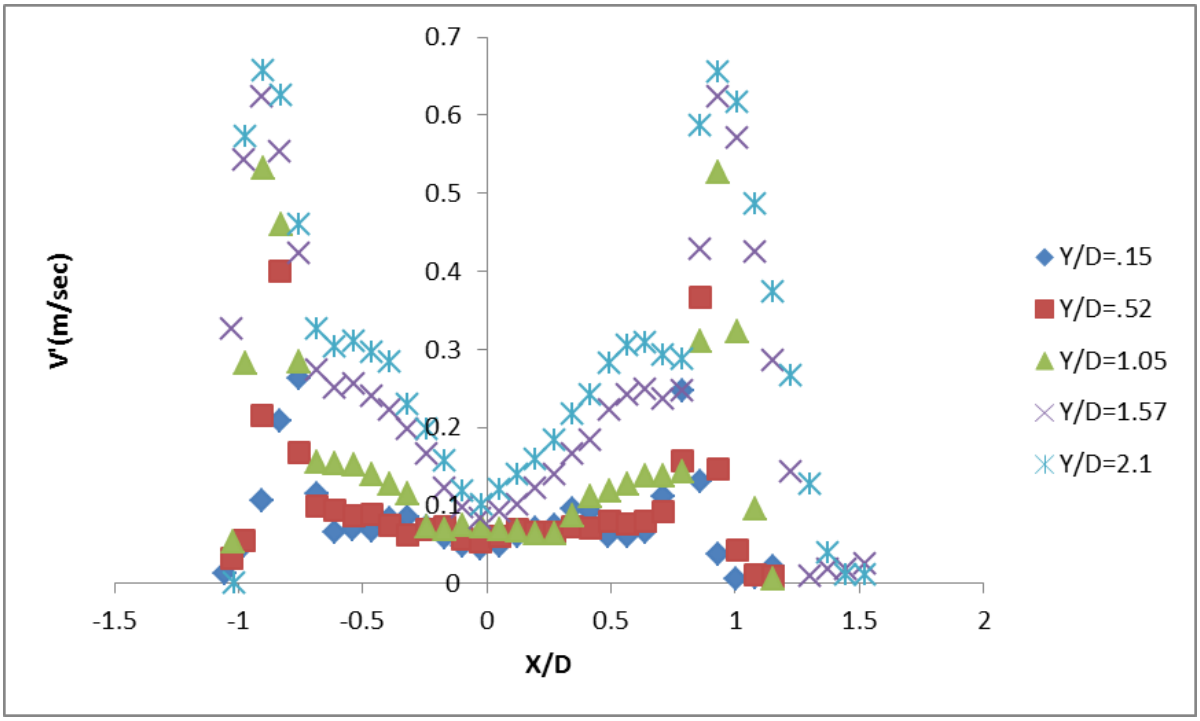

Figure 4.5.3 Radial RMS fluctuating velocity profiles at different axial distances for CH4-O2-CO2 flames at 73% blockage ratio

4.6 EFFECT OF FIRING INPUT ON THE LOCAL FLOW FIELD FLUCTUATIONS OF CH4-O2-CO2 FLAMES AT CONSTANT RE (2500), CONSTANT BLOCKAGE RATIO OF 83% AND CONSTANT STOICHIOMETRIC RATIO (Φ=1).

Three different firing inputs (1.5 KW, 1.7 KW and 1.9 KW) were chosen for the current study. Figure 4.6.1 shows flow-field fluctuations for CH4-O2-CO2 combustion. The height of the premixed cone is decreased as the firing input reduced as shown in the figure (sequence from (a) to (c)), which clearly shows the effect of firing input on the effective flame surface area resulting in increase in the local propagation velocity at higher firing input while maintain the constant Re (2500), constant blockage ratio of 83% and constant stoichiometric ratio (ϕ=1). At higher firing inputs the amount of heat released is higher, in addition to that by keeping the Reynolds number to be fixed at 2500 for all the three firing inputs , the recirculation ratio($RR_{CO_2} = \frac{m_{CO_2}}{m_{O_2}+m_{CO_2}}$)at higher firing input is lower when compared to the lower firing inputs, thereby increase in the local propagation velocity and increase in the effective flame surface area.

Figure 4.6.3 shows the comparison of radial velocity fluctuations at different axial distances for different firing inputs while maintain the constant Re (2500), constant blockage ratio of 83% and constant stoichiometric ratio (ϕ=1). Initially at the distance Y/D =.52 the velocity fluctuations for all the three firing inputs remained the same. As the axial distance increase (i.e Y/D=1.52 to 2.63) velocity fluctuations were highest for higher firing input , as the heat released is high at higher firing inputs.

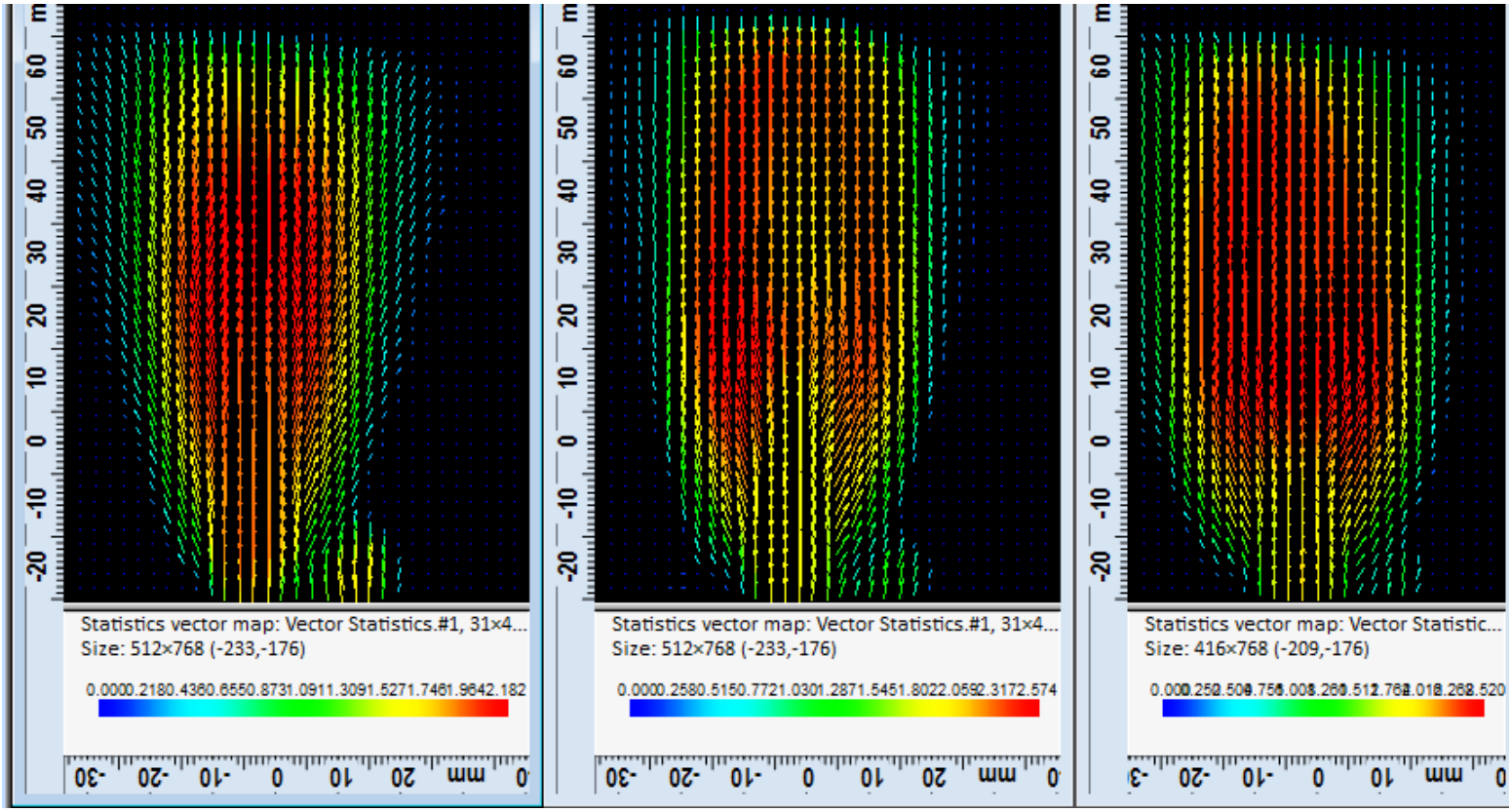

(a) (b) (c)

Figure 4.6.1 Flow-Field for CH4-O2-CO2 flames (a) 1700 W (b) 1800 W (c) 1900 W

Figure 4.6.2 shows the scalar velocity maps of CH4-O2-CO2 flames at different firing inputs (1.5 KW, 1.7 KW and 1.9 KW), constant Re (2500), constant blockage ratio of 83% and constant stoichiometric ratio(ϕ=1).

Figure 4.6.4, 4.6.5 and 4.6.6 shows the plots of Radial RMS fluctuating velocity profiles at different axial distances for CH4-O2-CO2 flames at firing input of 1500, 1700 and 1900 W respectively. Velocity fluctuations were recorded minimum at an axial distance X/D=.52 and then increased as we moved away from the burner exit, due to the high heat release rates and abrupt change in densities of the unburnt and burnt gas mixtures.

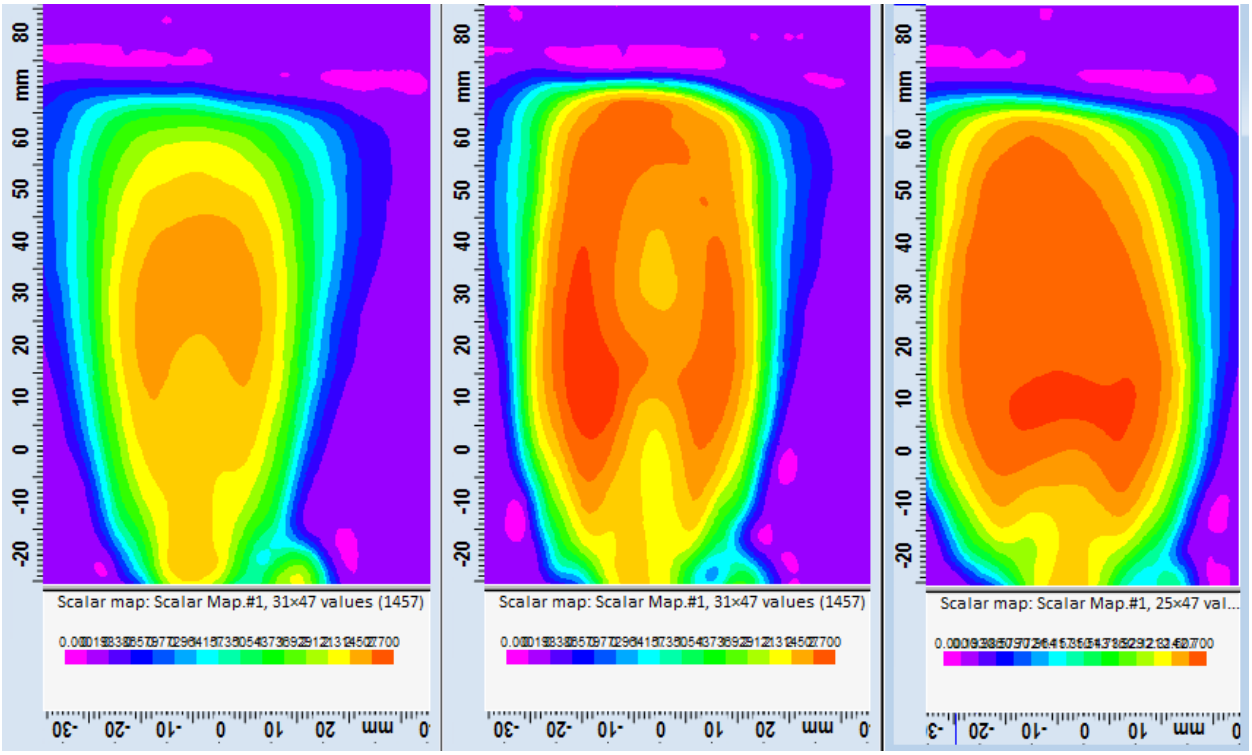

(a) (b) (c)

Figure 4.6.2 Scalar map of velocity for CH4-O2-CO2 flames (a) 1500 W (b) 1700 W (c) 1900 W.

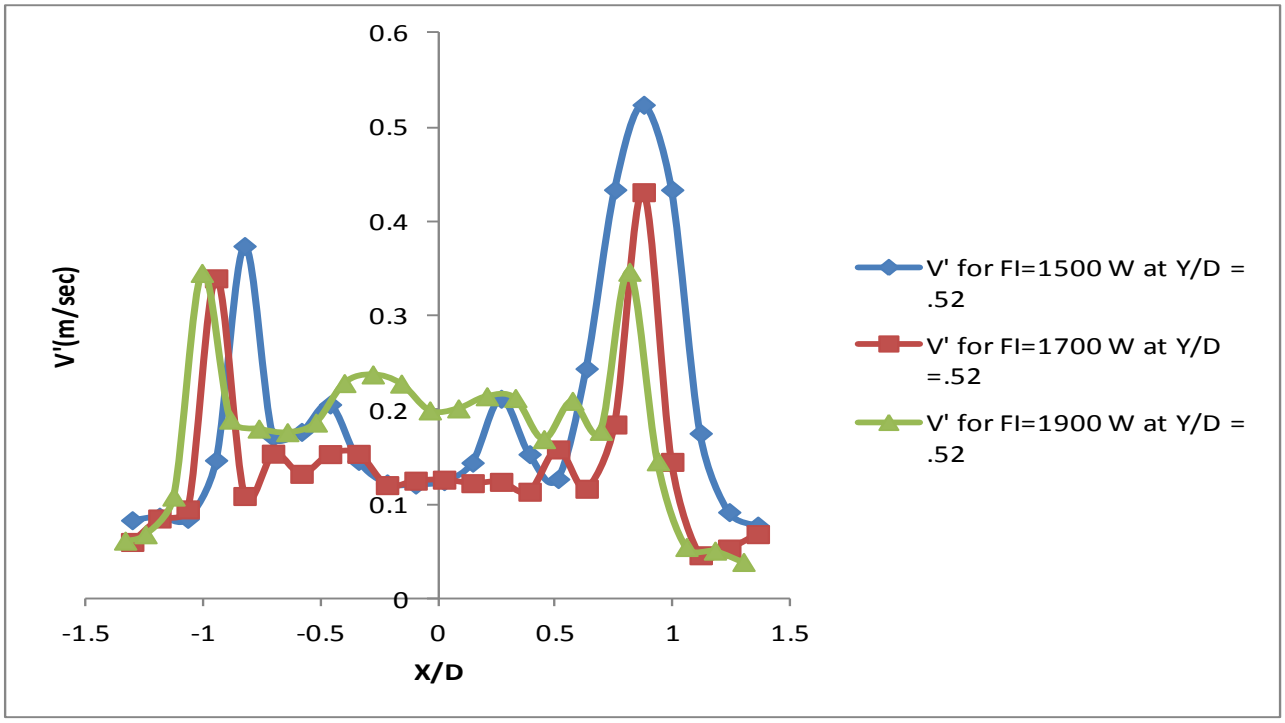

Figure 4.6.3 Comparison of 5 Radial RMS fluctuating velocity profiles at Y/D=.52 axial distances for CH4-O2-CO2 flames (a) 1500 W (b) 1700 W (c) 1900 W.

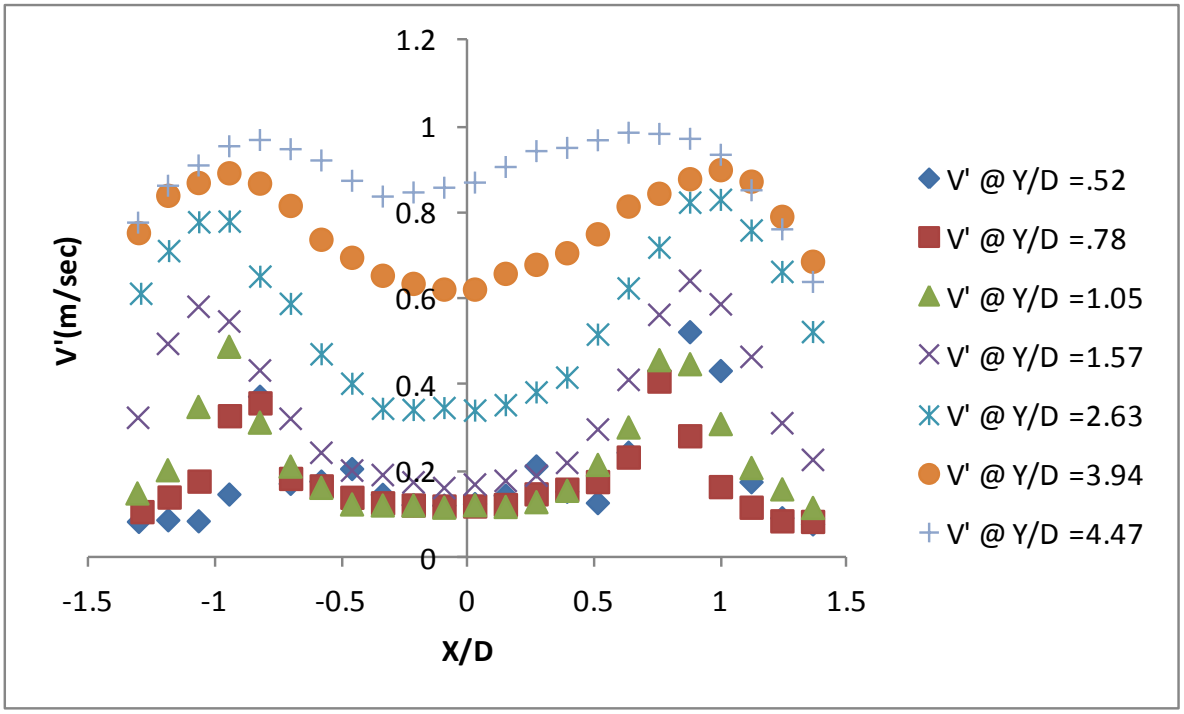

Figure 4.6.4 Radial RMS fluctuating velocity profiles at different axial distances for CH4-O2-CO2 flames at firing input of 1500 W.

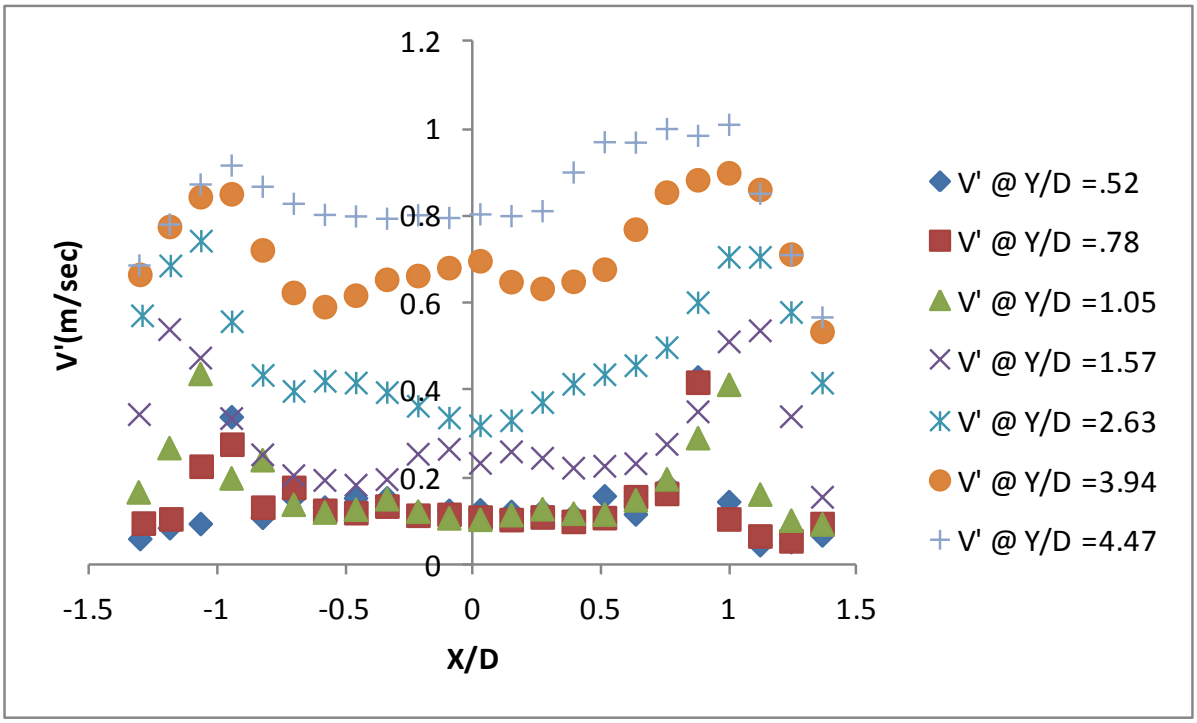

Figure 4.6.5 Radial RMS fluctuating velocity profiles at different axial distances for CH4-O2-CO2 flames at firing input of 1700 W.

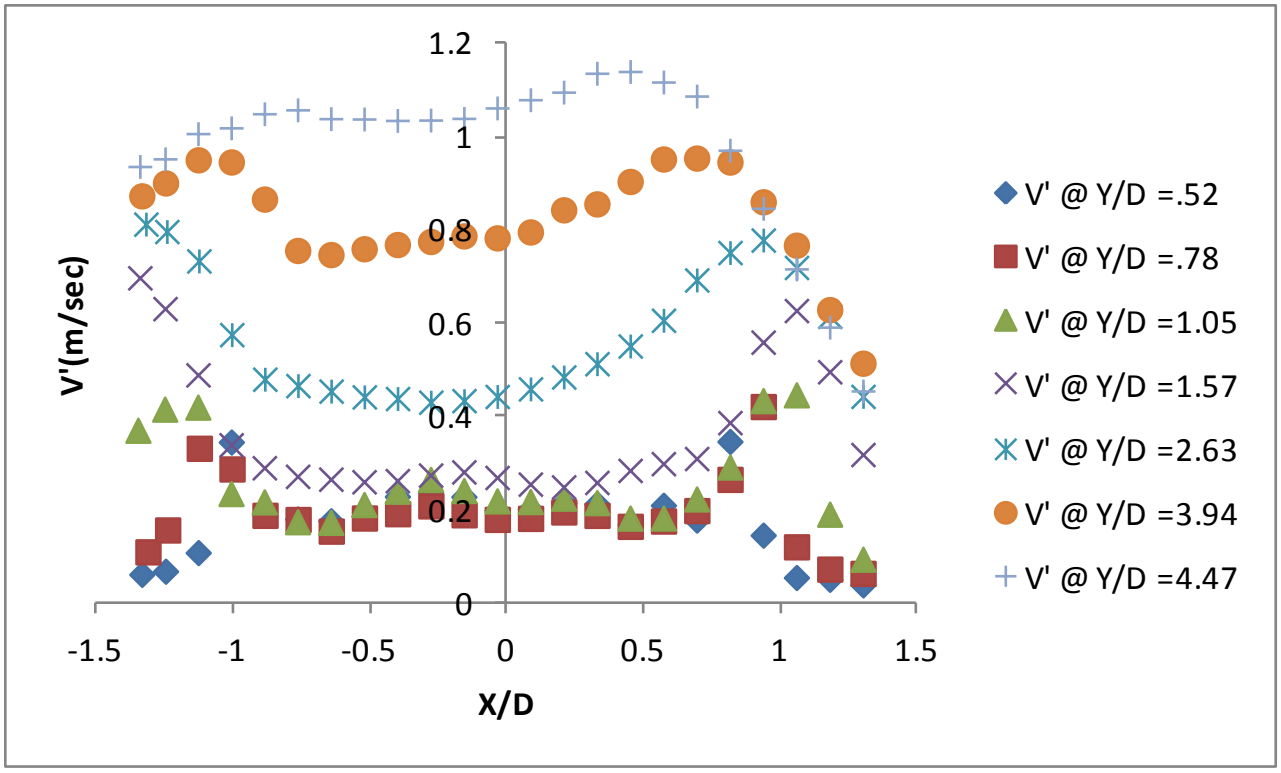

Figure 4.6.6 Radial RMS fluctuating velocity profiles at different axial distances for CH4-O2-CO2 flames at firing input of 1900 W.

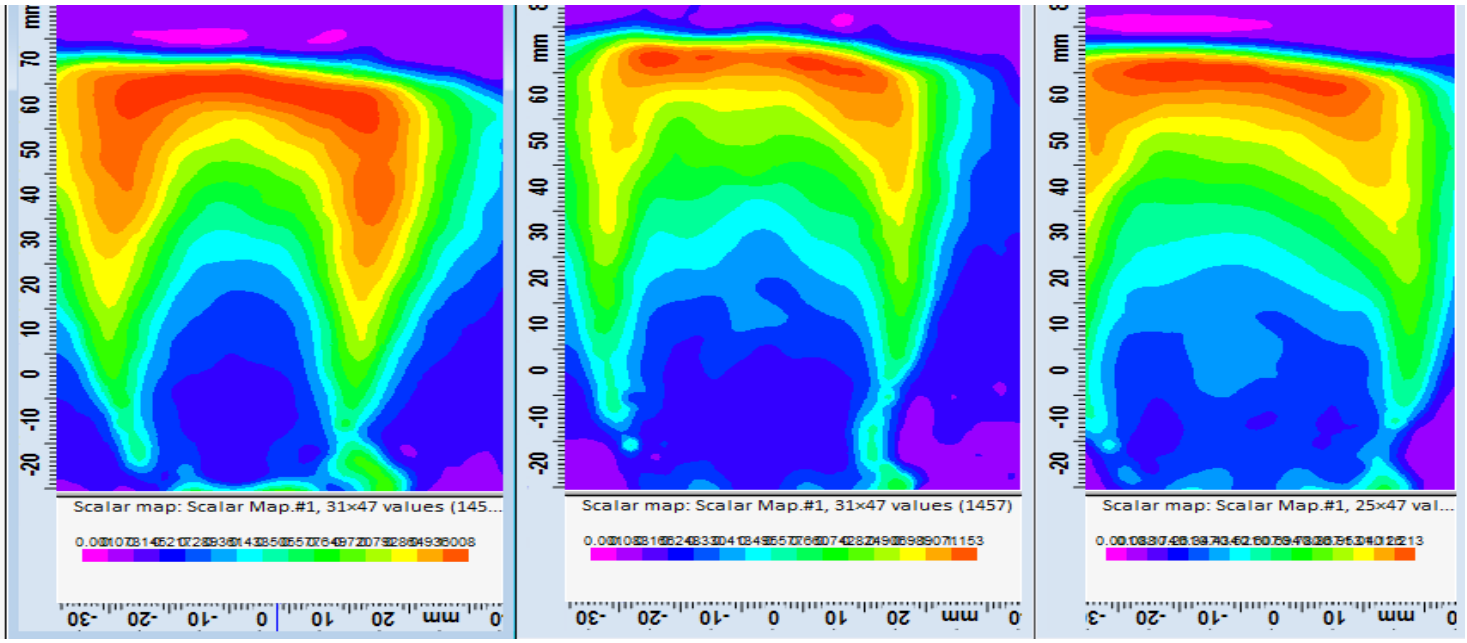

Figure 4.6.6 Scalar map of turbulent intensity for CH4-O2-CO2 flames at (a) 1500 W (b) 1700 W (c) 1900 W.

4.7 Effect of recirculation ratio on the local flow field fluctuations of CH4-O2-CO2 flames at constant RE (2500), constant firing input (1700 W), constant blockage ratio of 83% and constant stoichiometric ratio (Φ=1).

Two different recirculation ratios (RR_{CO_2}= 74% and RR_{CO_2} =70%) were chosen for the current study. In case of mixture with RR_{CO_2} of 70 percent, equal amounts of argon was replaced with CO2 (by mass) to maintain the Reynolds number to be 2500 for the mixture. Argon was chosen in this case, it is chemically inert and the density and viscosity of argon were close to CO2. Figure 4.6.1 shows flow-field fluctuations for CH4-O2-CO2 and CH4-O2-CO2-Ar combustion. The height of the premixed cone is decreased as the recirculation ratio is reduced 74 percent to 70 percent as shown in the figure (sequence from (a) to (b)), which clearly shows the effect of recirculation ratio on the effective flame surface area resulting in increase in the local propagation velocity at lower recirculation ratio while maintaining constant Re (2500), constant blockage ratio of 83% and constant stoichiometric ratio (ϕ=1). The result clearly states that CO2 is chemically active and reduces the flame temperature thereby reducing the local propagation velocity and decrease in the effective flame surface area.

Figure 4.6.5 shows the comparison of radial velocity fluctuations at different axial distances for different recirculation ratios while maintain the constant Re (2500), constant blockage ratio of 83% and constant stoichiometric ratio (ϕ=1). Initially at the distance Y/D =.52 the velocity fluctuations for RR_{CO_2}= 74% and RR_{CO_2} =70% remained the same. As the axial distance increase (i.e Y/D=.1.35 to 3.15) velocity fluctuations were highest for higher at RR_{CO_2} =70%, as the heat released is high for CH4-O2-CO2-Ar

flames, asCO2 is chemically active and reduces the flame temperature whereas Argon is chemically inert and does not participate in any reaction.

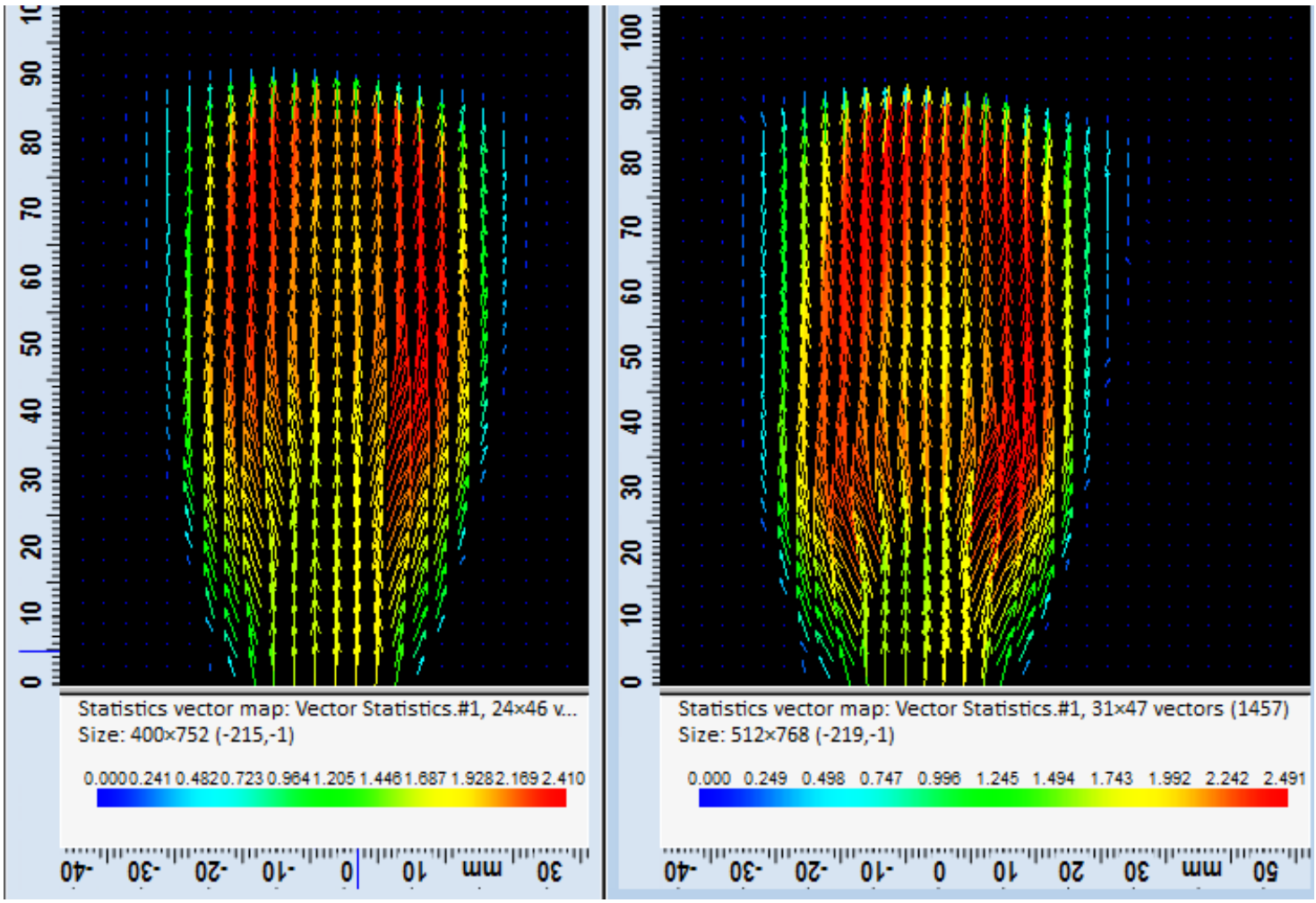

(a) (b)

Figure 4.7.1 Flow-Field for CH4-O2-CO2/ CH4-O2-CO2-Ar flames at (a) RR_{CO_2}= 74% (b) RR_{CO_2} =70%

Figure 4.7.2 shows the scalar velocity maps of CH4-O2-CO2/ CH4-O2-CO2-Ar flames at different recirculation ratios (RR_{CO_2}= 74% and RR_{CO_2} =70%), contant firing input (1700), constant Re (2500), constant blockage ratio of 83% and constant stoichiometric ratio(ϕ=1).

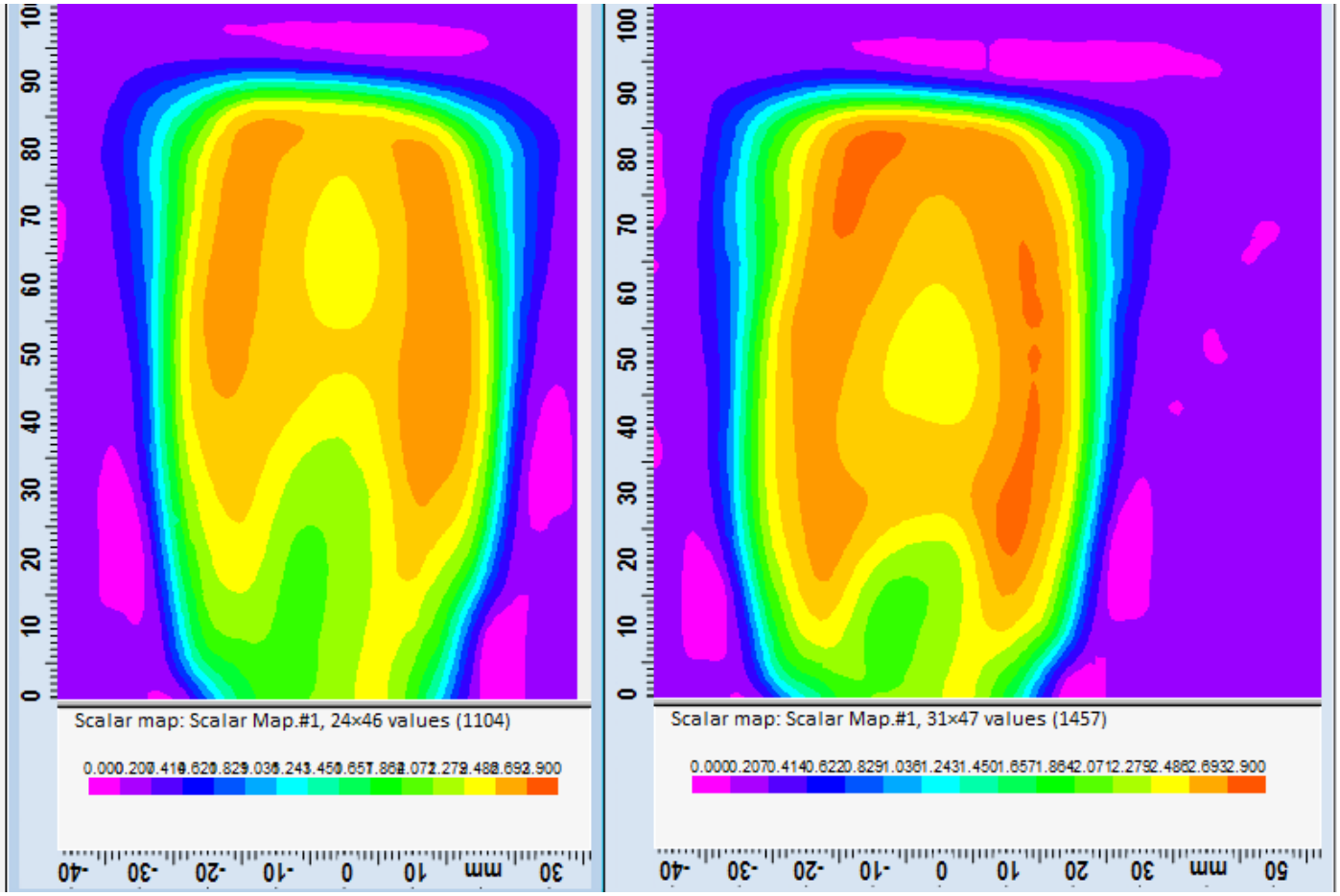

(a) (b)

Figure 4.7.2 Flow-Field for CH4-O2-CO2/ CH4-O2-CO2-Ar flames at (a) RR_{CO_2}= 74% (b) RR_{CO_2} =70%

Figure 4.7.3 and 4.7.4 shows the plots of Radial RMS fluctuating velocity profiles at different axial distances for CH4-O2-CO2/ CH4-O2-CO2-Ar flames at recirculation ratios (RR_{CO_2}= 74% and RR_{CO_2} =70%) respectively. Velocity fluctuations were recorded minimum at an axial distance X/D=.26 and then increased as we moved away from the burner exit.

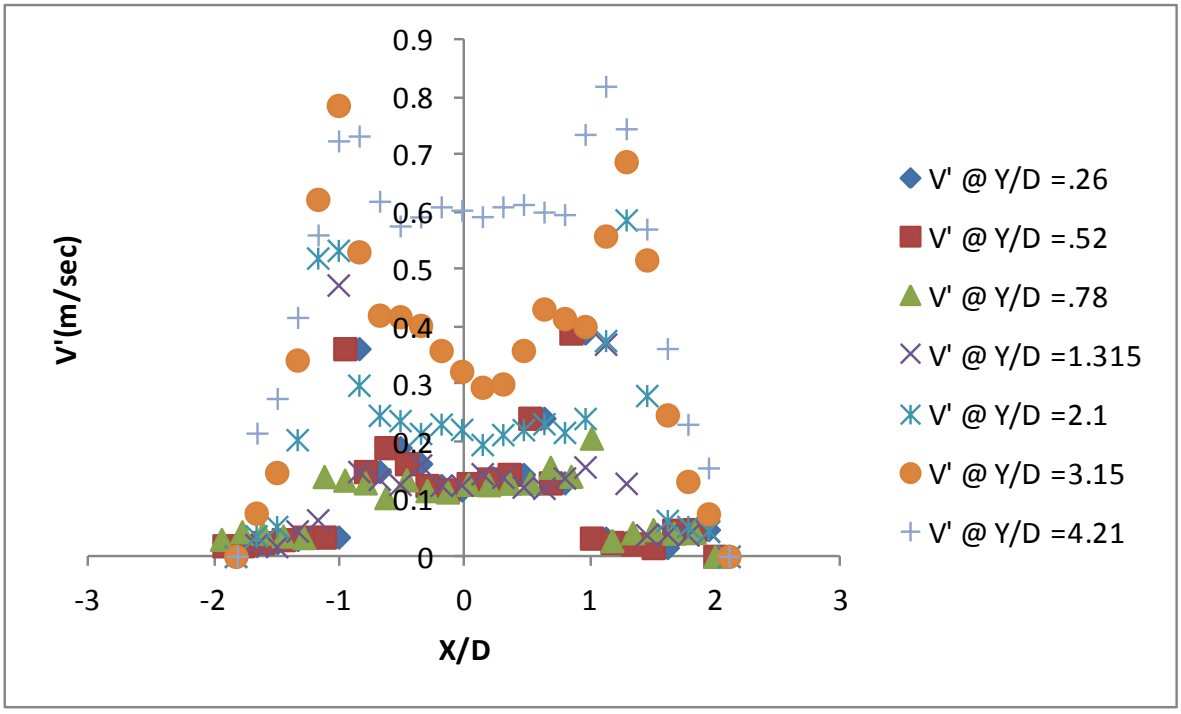

Figure 4.7.3 Radial RMS fluctuating velocity profiles at different axial distances for CH4-O2-CO2 flames at RR_{CO_2}= 74%

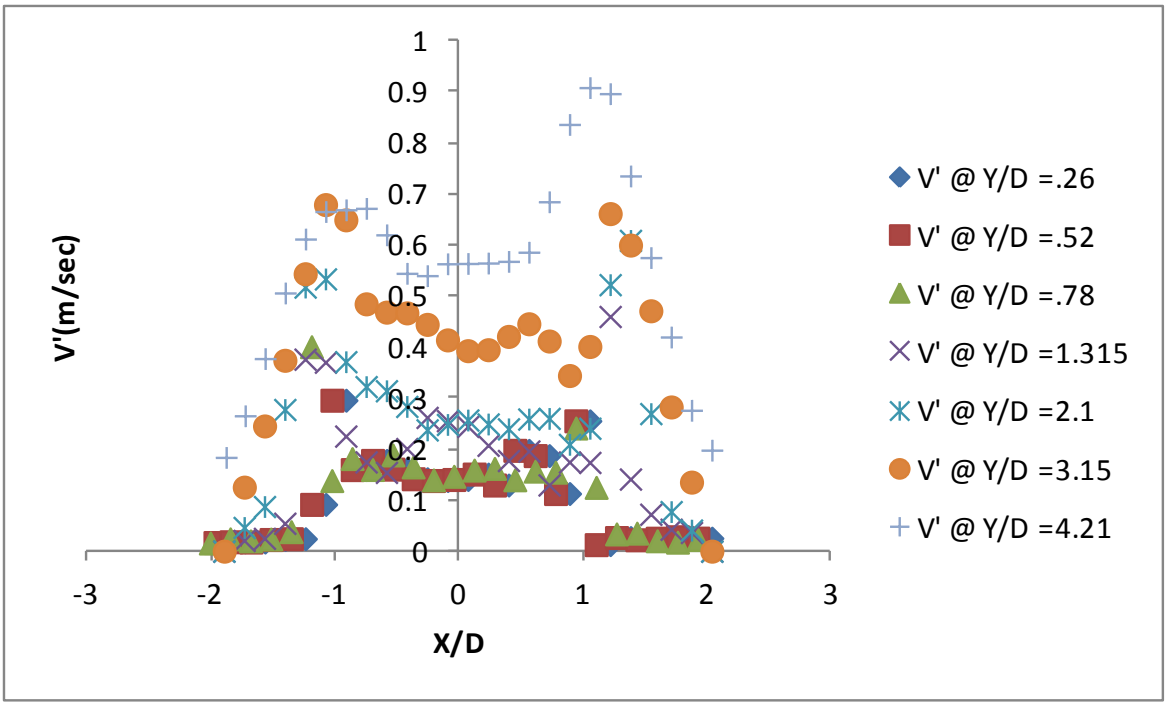

Figure 4.7.4 Radial RMS fluctuating velocity profiles at different axial distances for CH4-O2-CO2-Ar flames at RR_{CO_2}= 70%.

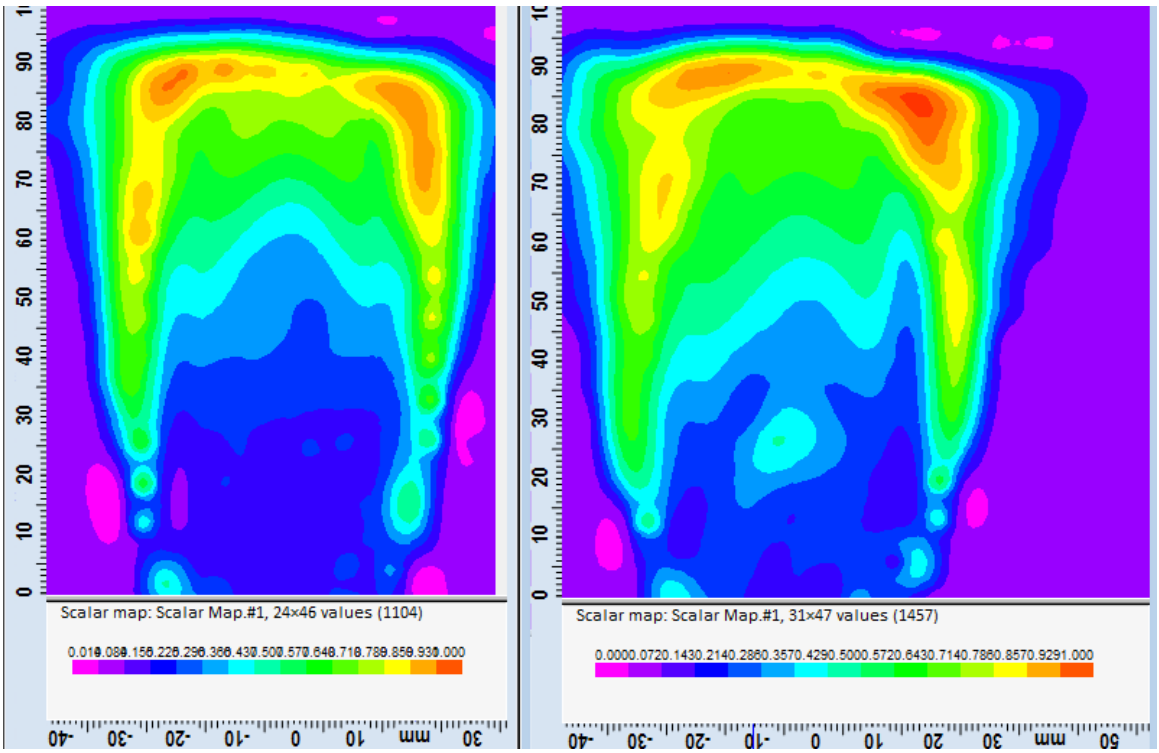

Figure 4.7.5 Scalar map of turbulent intensity for CH4-O2-CO2/ CH4-O2-CO2-Ar flames at (a) RR_{CO_2}= 74% (b) RR_{CO_2} =70%

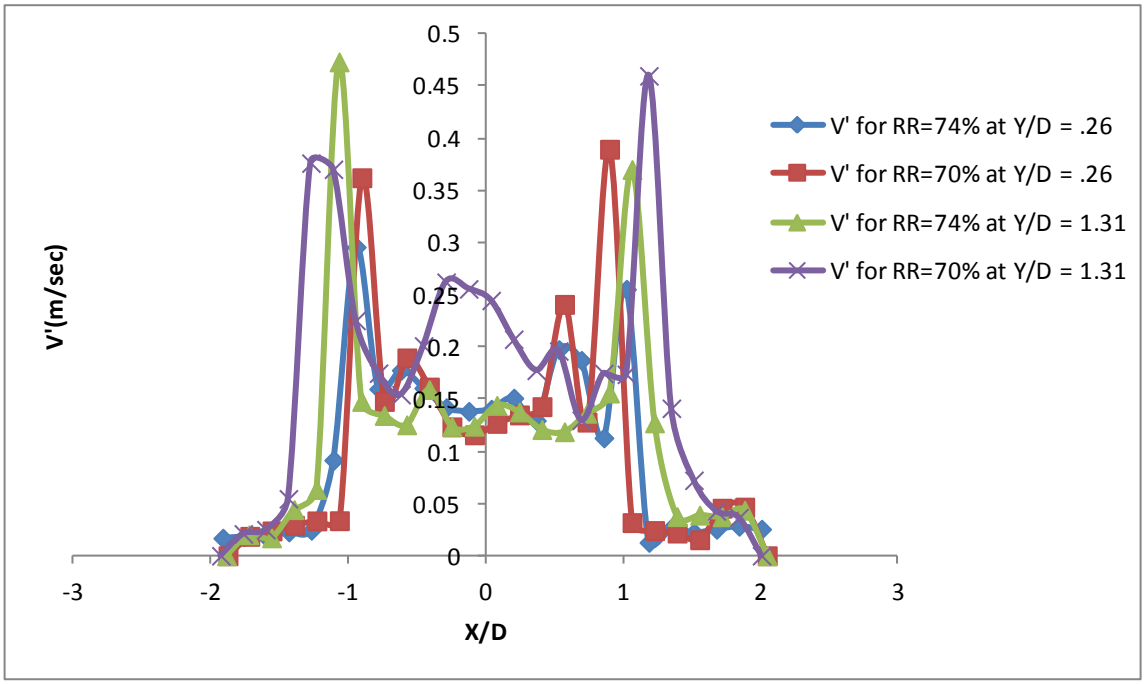

Figure 4.7.6: Comparison of Radial RMS fluctuating velocity profiles at different axial distances for CH4-O2-CO2 flames at (a) RR_{CO_2}= 74% (b) RR_{CO_2} =70%

4.8 Effect of blockage ratio on the local flow field fluctuations of CH4-O2-CO2 flames at constant Re(2500), Firing input (1700 W) and constant stoichiometric ratio.

Three different blockage ratios (78%, 83% and 93%) were chosen to vary the turbulent intensity level above the burner exit. Figure 4.8.1 shows flow-field fluctuations for CH4-O2-CO2 flames. The height of the premixed cone is decreases as the turbulent intensity increases as shown in the figure (sequence from (a) to (c)), which clearly shows the effect of blockage ratio on the effective flame surface area resulting in increase in the effective flame surface area thereby resulting in increase in the local propagation velocity. At higher blockage ratio, the turbulent intensity is higher which greatly enhances the fuel mixing and heat transport from burnt to unburnt gases thereby increasing the local flame propagation velocity. Figure 4.8.2 shows the scalar velocity maps of CH4-O2-CO2 flames at different blockage ratios (78%, 83% and 93%), constant firing input (1700), constant Re (2500) and constant stoichiometric ratio(ϕ=1).

Figure 4.8.3, 4.8.4 and 4.8.5 shows the plots of Radial RMS fluctuating velocity profiles at different axial distances for CH4-O2-CO2 flames at blockage ratios (73%, 83% and 93%) respectively. Velocity fluctuations were recorded minimum at an axial distance X/D=.05 and then increased as we moved away from the burner exit.

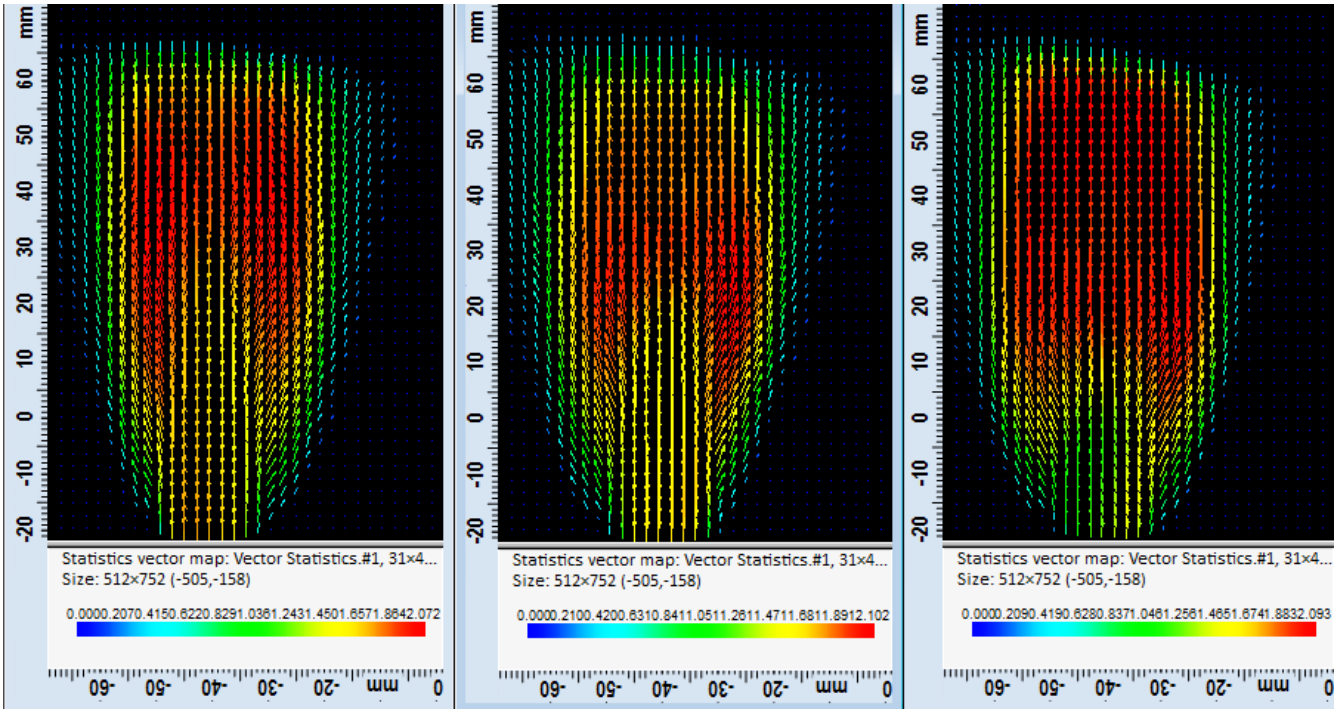

(a) (b) (c)

Figure 4.8.1 Flow-Field for CH4-O2-CO2 flames at (a) BR of 73% (b) BR of 83% (c) BR of 93%

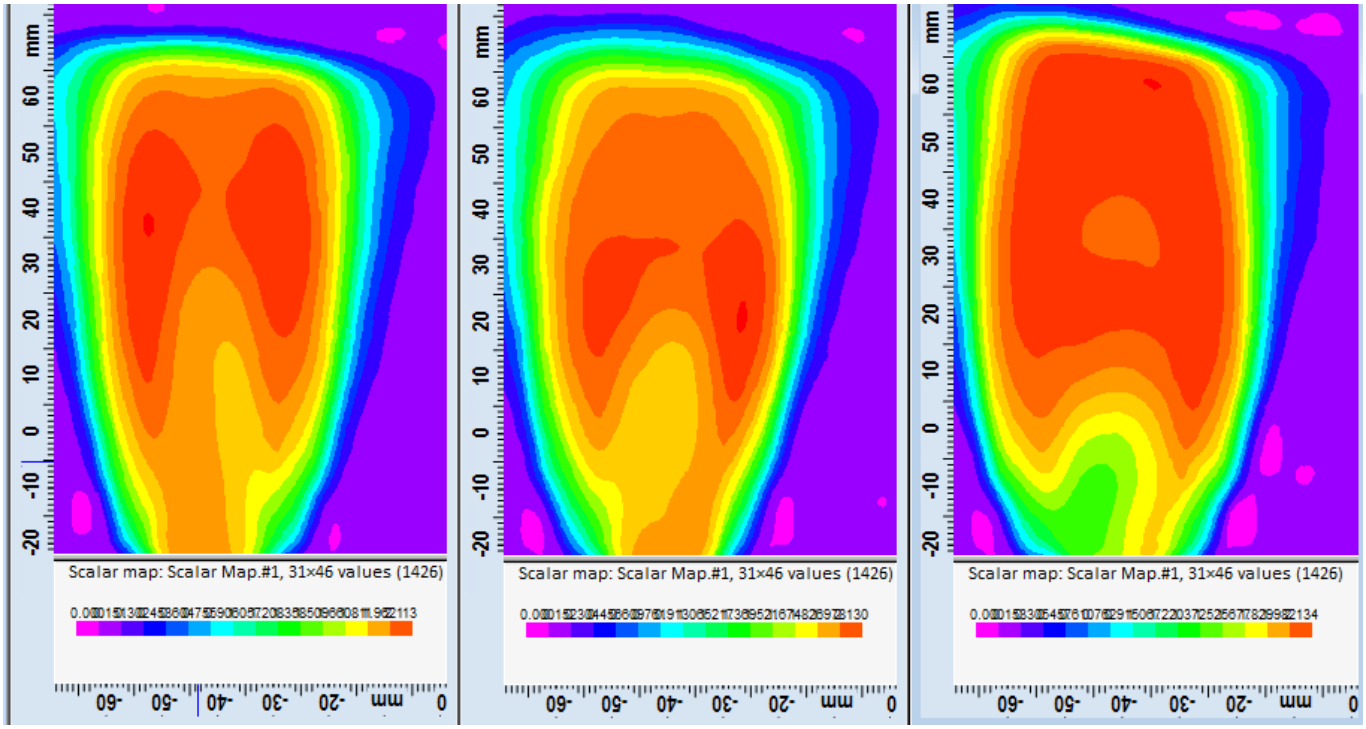

(a) (b) (c)

Figure 4.8.2 Scalar map of velocity for CH4-O2-CO2 flames at (a) BR of 73% (b) BR of 83% (c) BR of 93%

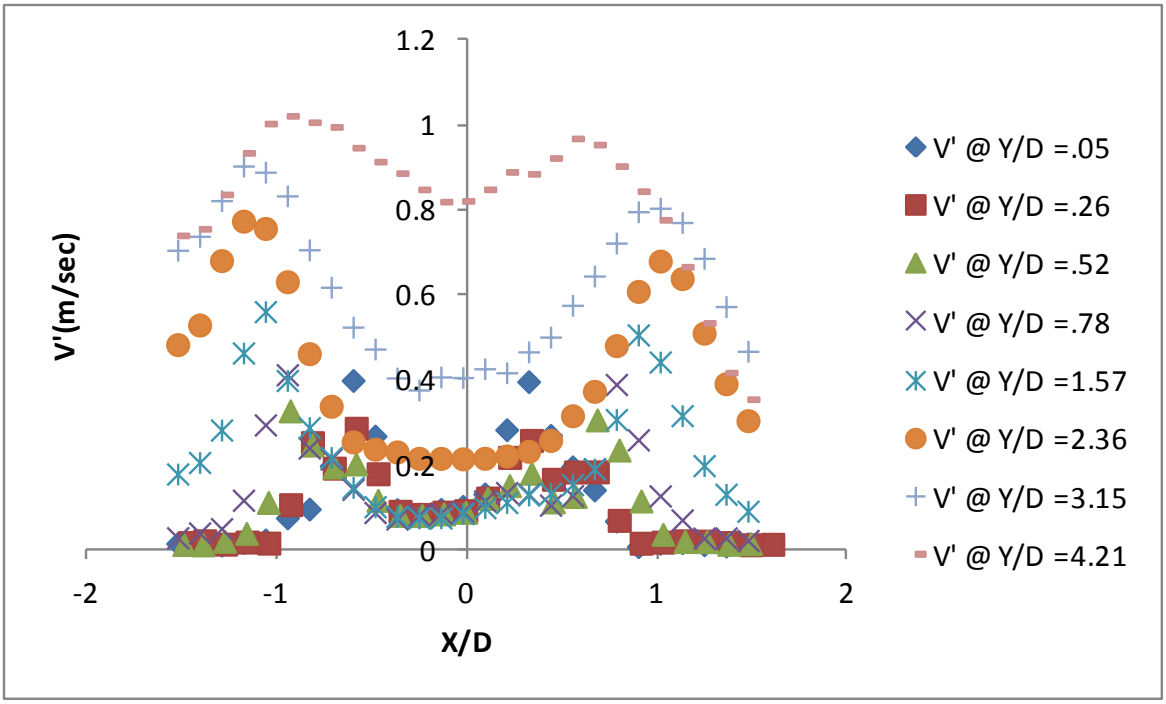

Figure 4.8.3 Radial RMS fluctuating velocity profiles at different axial distances for CH4-O2-CO2 flames at 73% BR

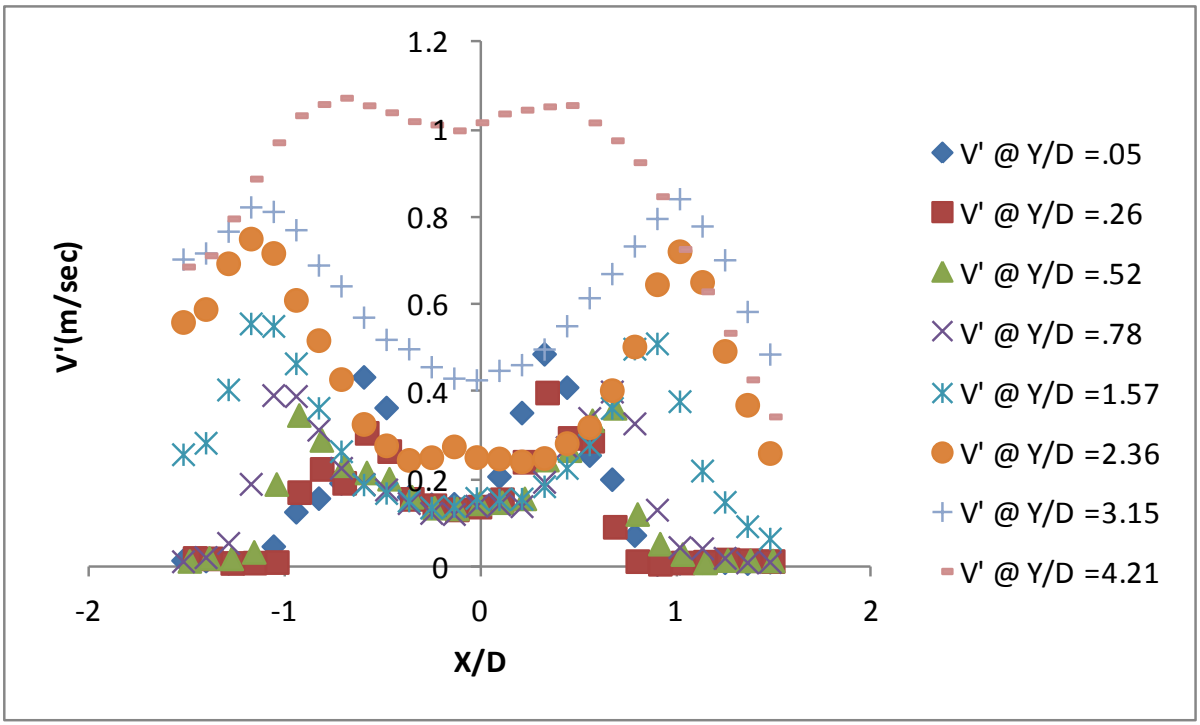

Figure 4.8.4 Radial RMS fluctuating velocity profiles at different axial distances for CH4-O2-CO2 flames at 83% BR

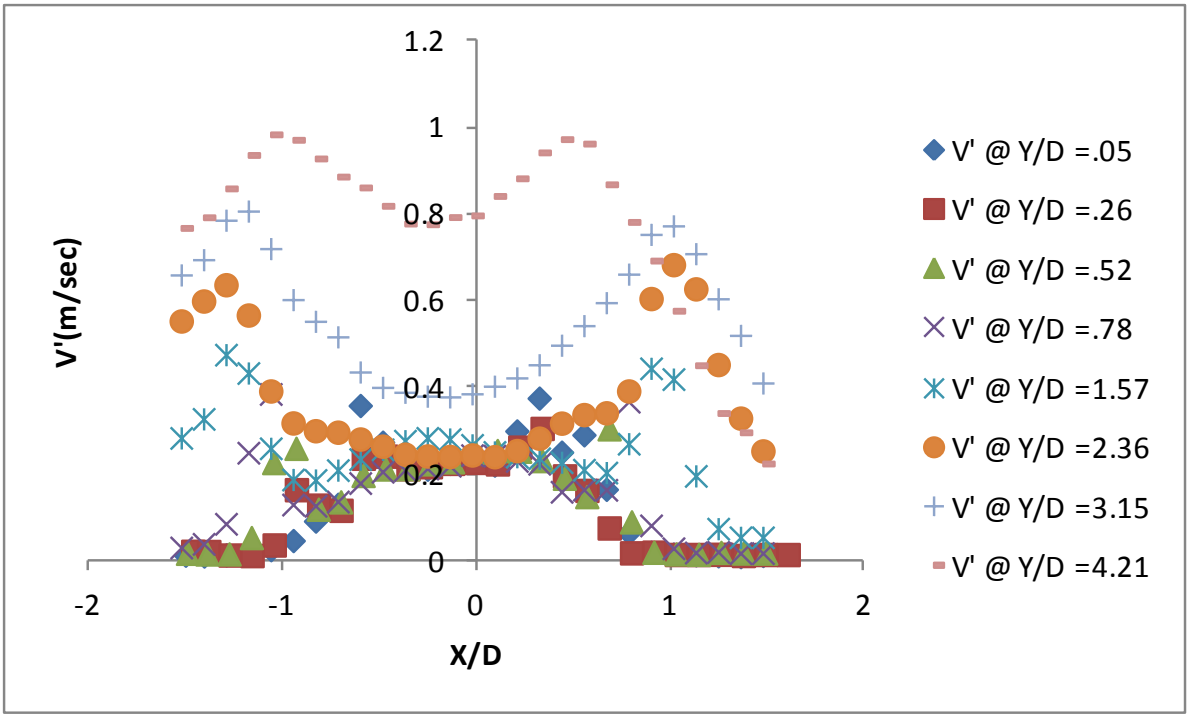

Figure 4.8.5 Radial RMS fluctuating velocity profiles at different axial distances for CH4-O2-CO2 flames at 93% blockage ratio

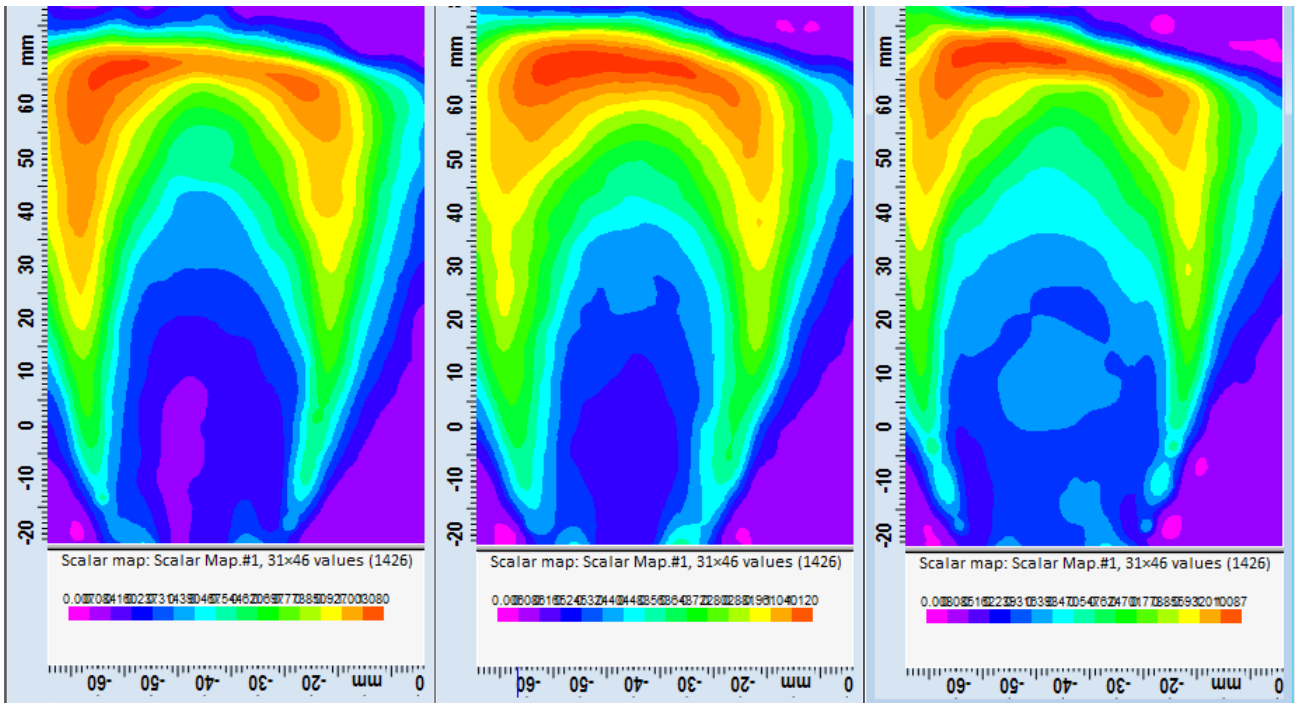

(a) (b) (c)

Figure 4.8.5 Scalar map of turbulent intensity for CH4-O2-CO2 flames at (a) BR of 73% (b) BR of 83% (c) BR of 93%

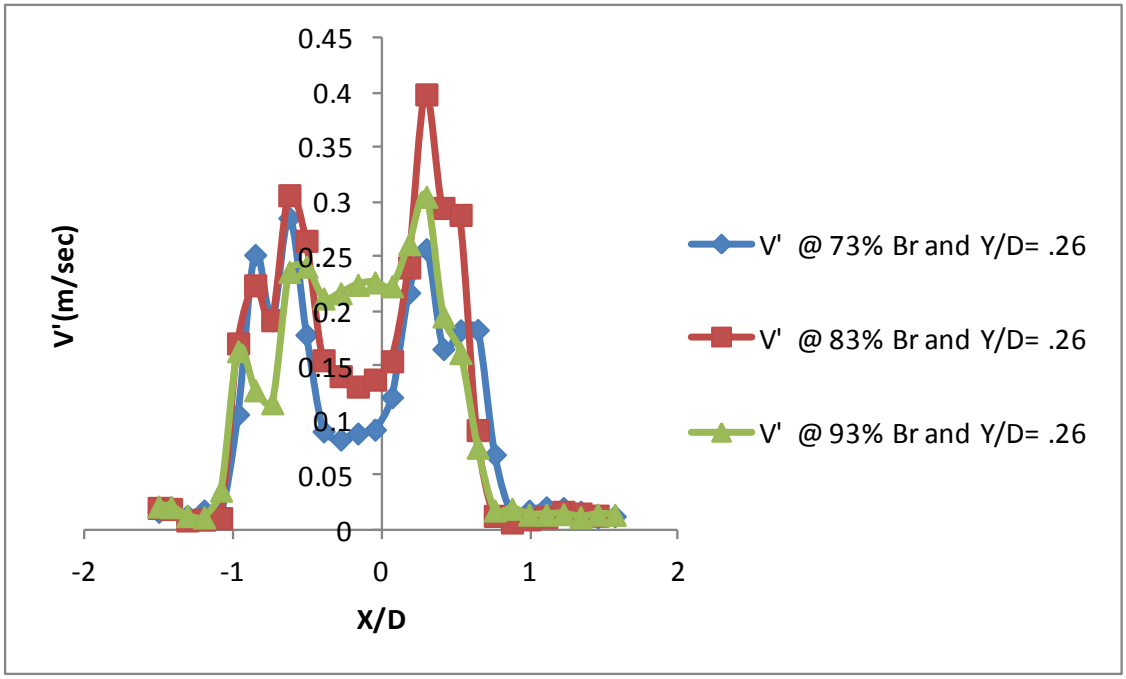

Figure 4.8.6 Comparison of Radial RMS fluctuating velocity profiles at different axial distances for CH4-O2-CO2 flames at (a) BR of 73% (b) BR of 83% (c) BR of 93%

Figure 4.8.6 shows the axial plot of velocity fluctuations of CH4-O2-CO2 flames at a constant Re (2500), Firing input (1.7 KW) and constant stoichiometric ratio (Φ=1). As we can see the velocity fluctuations increase with increase in the BR, as the turbulent intensity is increased by varying the BR from 73% to 93% the velocity fluctuations increased substantially at different axial distances (i.e Y/D = .26 and 1.57).

4.9 Effect of hydrogen content on the local flow field fluctuations of H2-CO-O2-CO2 flames at constant Re (2500), Firing input (1700 W) and Φ=1.

Figure 4.9.1 shows flow-field fluctuations for H2-CO-O2-CO2 combustion. The height of the premixed cone is decreased as the hydrogen content increased as shown in the figure (sequence from (a) to (b)), which clearly shows the effect of hydrogen on the effective flame surface area resulting in increase in the local propagation velocity for high hydrogen content fuels.

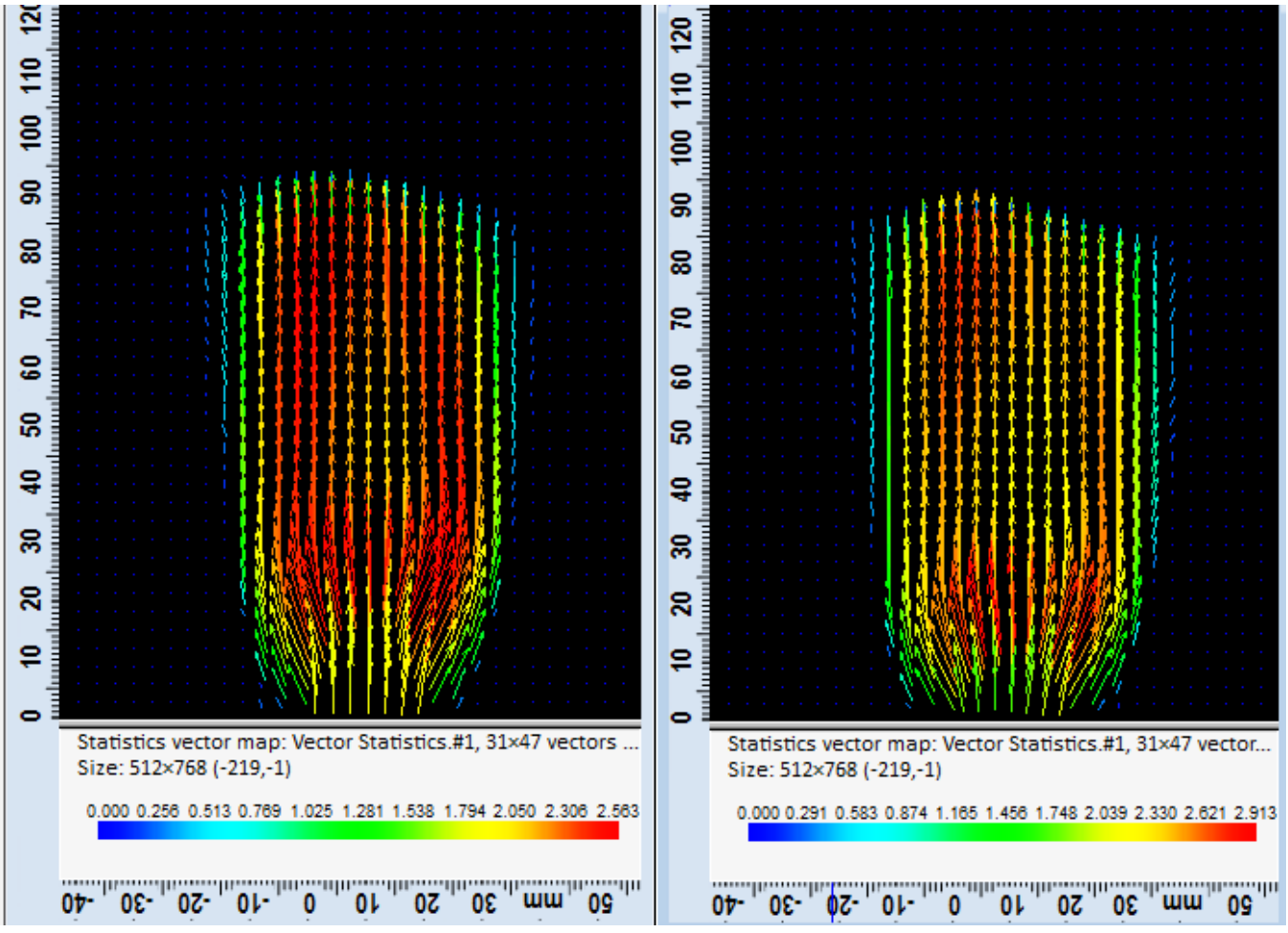

(a) (b)

Figure 4.9.1 Flow-Field for H2-CO-O2-CO2 flames (a) 10%H2-90%CO (b) 20% H2-80%CO

Figure 4.9.2 shows the scalar velocity maps of CH4-O2-CO2 flames at different blockage ratios (78%, 83% and 93%), constant firing input (1700), constant Re (2500) and ϕ=1.

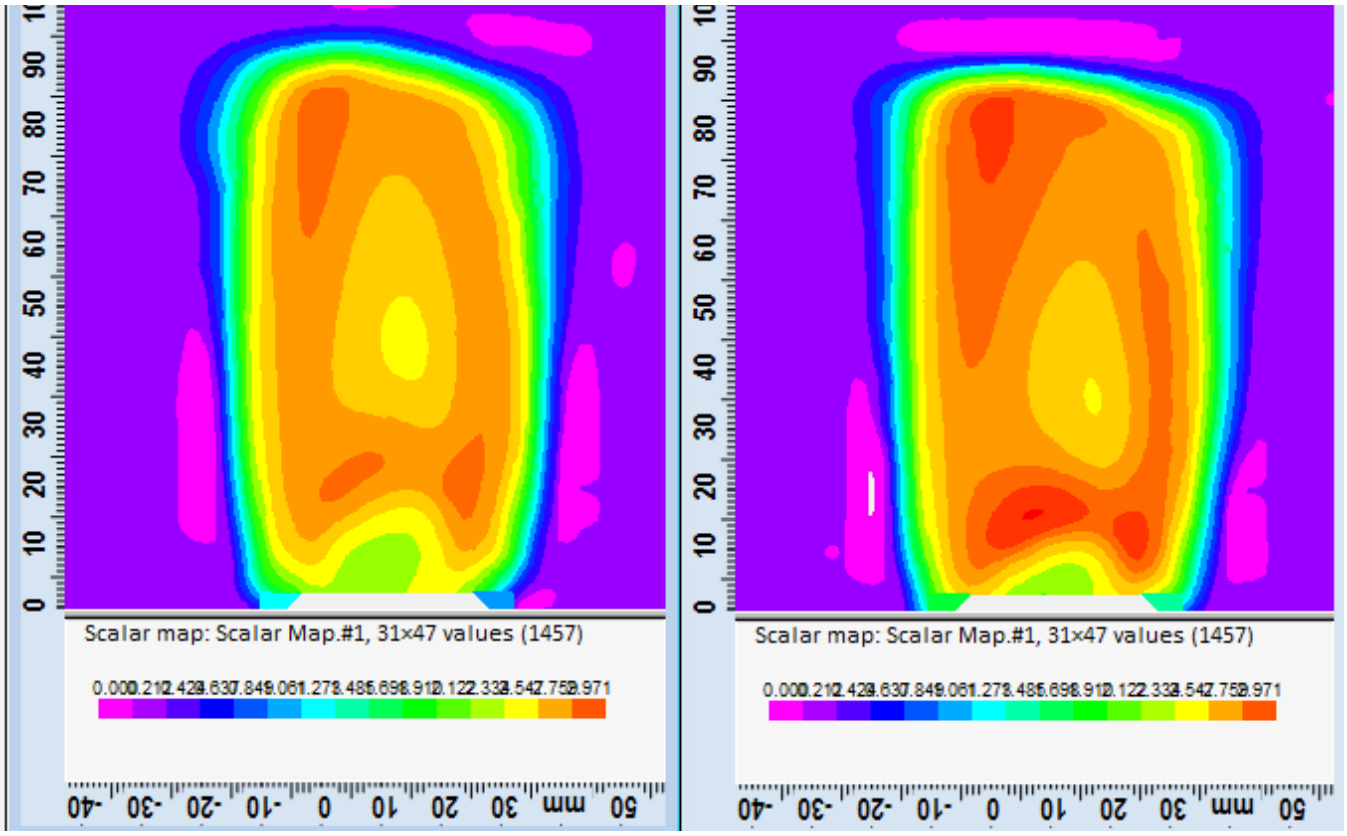

(a) (b)

Figure 4.9.2 Flow-Field for H2-CO-O2-CO2 flames (a) 10%H2-90%CO (b) 20% H2-80%CO

Figure 4.9.3 and 4.9.4 shows the plots of Radial RMS fluctuating velocity profiles at different axial distances for H2-CO-O2-CO2 flames at 10%H2-90%CO--O2-CO2 and 20% H2-80%CO-O2-CO2 respectively. Velocity fluctuations were recorded minimum at an axial distance X/D=.26 and then increased as we moved away from the burner exit.

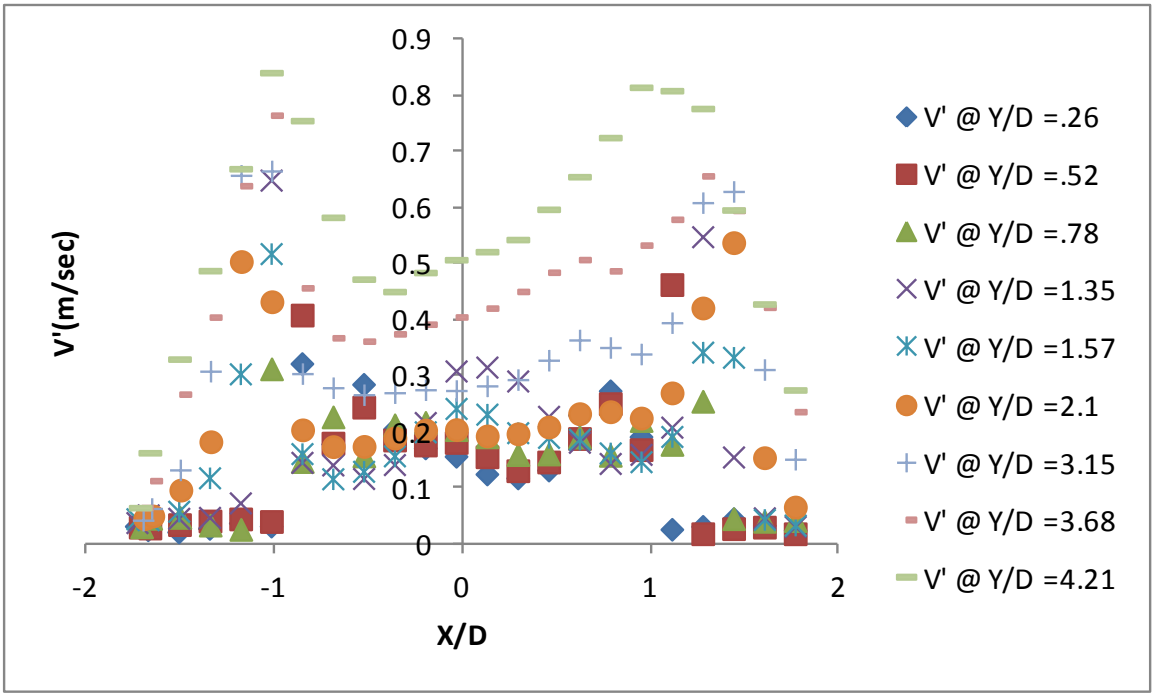

Figure 4.9.3 Radial RMS fluctuating velocity profiles at different axial distances for 10%H2-90%CO--O2-CO2 flames

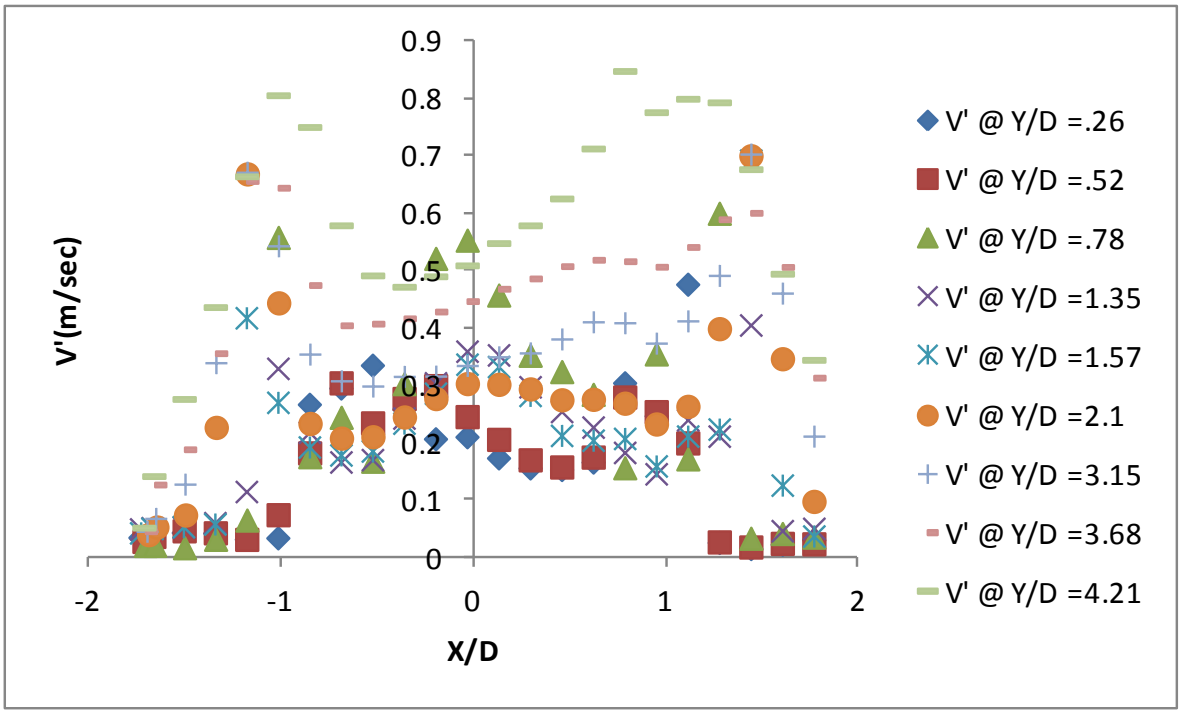

Figure 4.9.4 Radial RMS fluctuating velocity profiles at different axial distances for 20%H2-80%CO--O2-CO2 flames

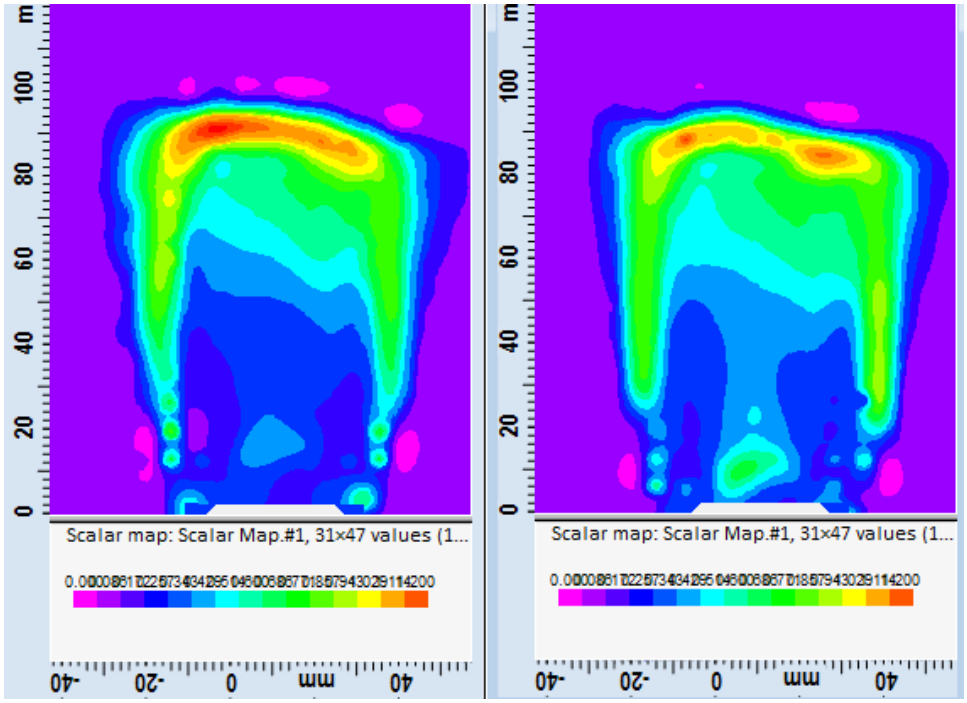

(a) (b)

Figure 4.9.5 Scalar maps of turbulent intensity for H2-CO-O2-CO2 flames (a) 10%H2-90%CO (b) 20% H2-80%CO

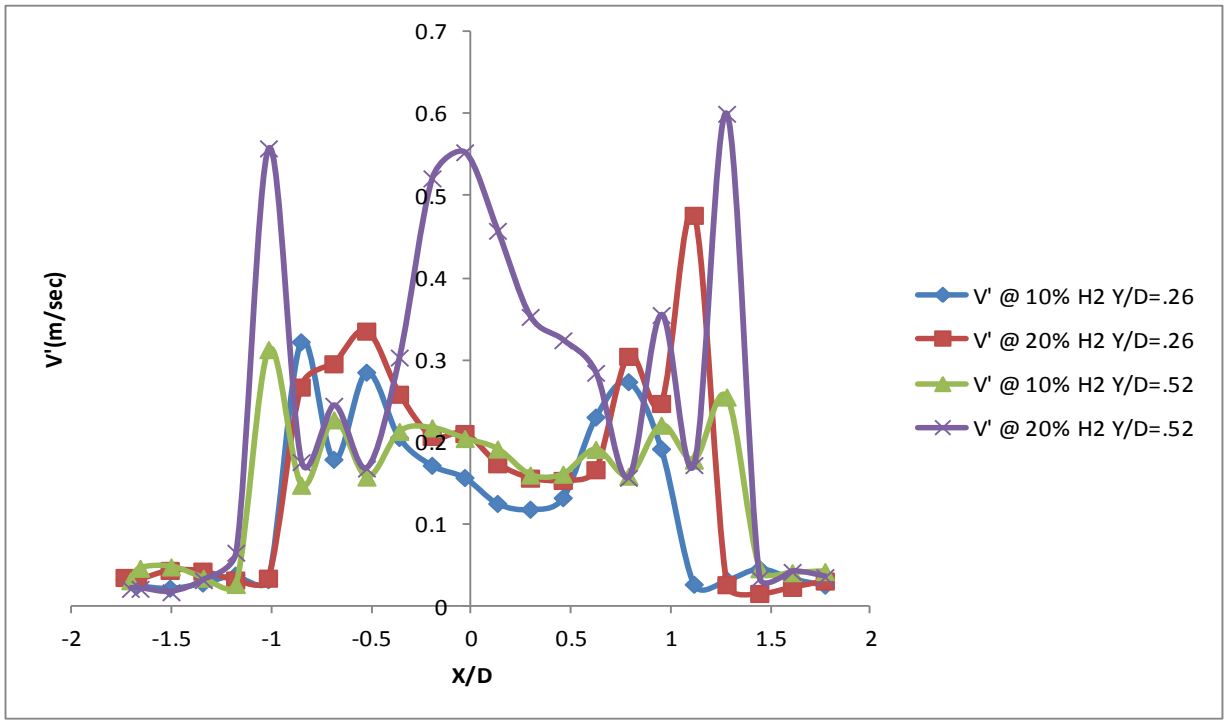

Figure 4.9.6: Comparison of radial RMS fluctuating velocity profiles at different axial distances (a) 10%H2-90%CO (b) 20% H2-80%CO

4.10 Effect of steam (H2O) on the local flow field fluctuations of CH4-O2-CO2-CO2 flames at constant Re (1500), Firing input (1700 W) and Φ=1.

A recirculation ratio $RR_{H_2O} = \frac{m_{H_2O}}{m_{O_2}+m_{CO_2}+m_{H_2O}}$ (RR_{H_2O}= 27%) were chosen for the current study. The gaseous mixture is preheated to 115 degrees centigrade prior to the combustion. Figure 4.10.1 shows the flow field fluctuations of CH4-O2-CO2-H2O flames at constant Re (1500), constant Firing input (1700 W) and constant stoichiometric ratio. To observe the effect of steam on flame stability, it is removed from the preheated mixture and an equal amount of CO2 (by mass) is added to maintain the Reynolds number constant. But, at the same Reynolds number the preheated CH4-O2-CO2 flame has flashback indicating that CH4-O2-CO2-H2O mixture absorbs more heat from the combustible mixture when compared to CO2. The result clearly states that steam is chemically active, as it has smaller diffusivity and enhances the backward reaction thereby reducing the flame temperature thereby reducing the local propagation velocity and decrease in the effective flame surface area.

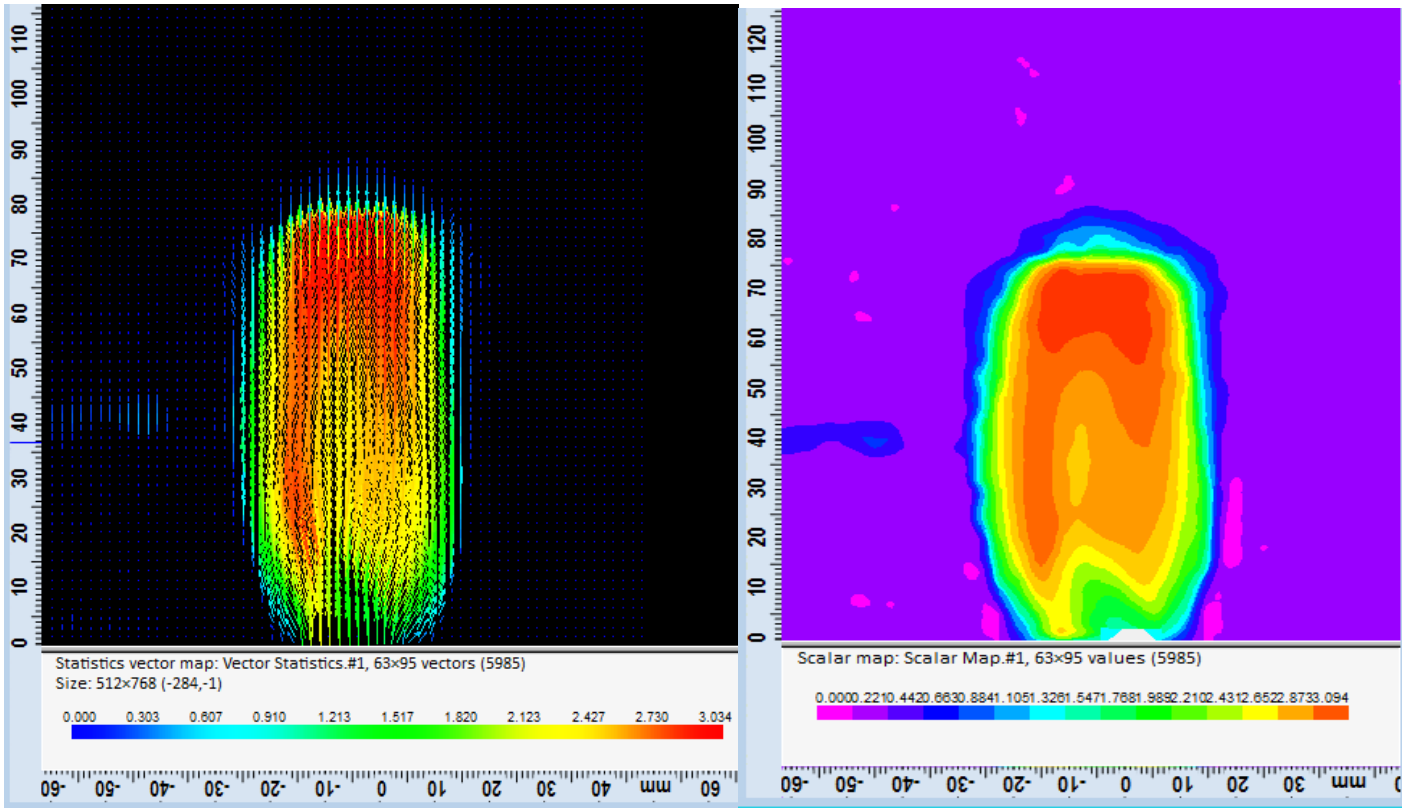

(a) (b)

Figure 4.10.1:(a) Flow-Field for CH4-O2-CO2-H2O flames (b) scalar map of velocity for CH4-O2-CO2-H2O flames

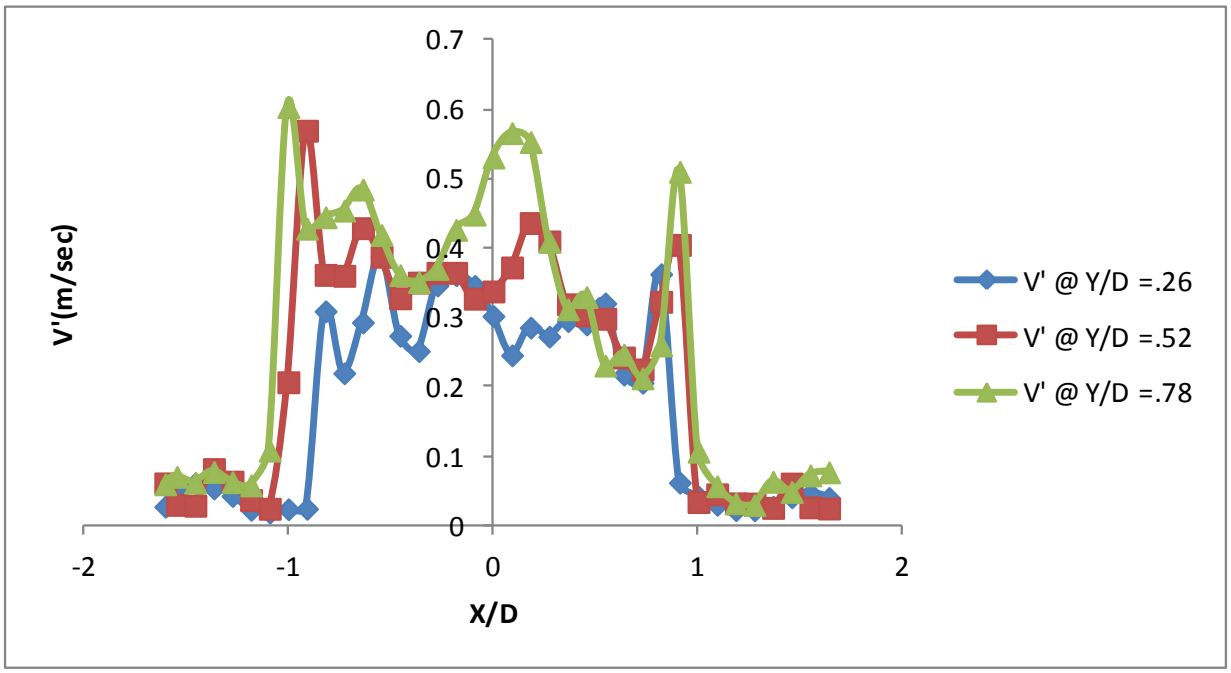

Figure 4.10.2 Radial RMS fluctuating velocity profiles at different axial distances for CH4-O2-CO2-H2O flames

Figure 4.10.2 shows the plots of Radial RMS fluctuating velocity profiles at different axial distances for CH4-O2-CO2-H2O flames. Velocity fluctuations were recorded minimum at an axial distance X/D=.26 and then increased as we moved away from the burner exit.

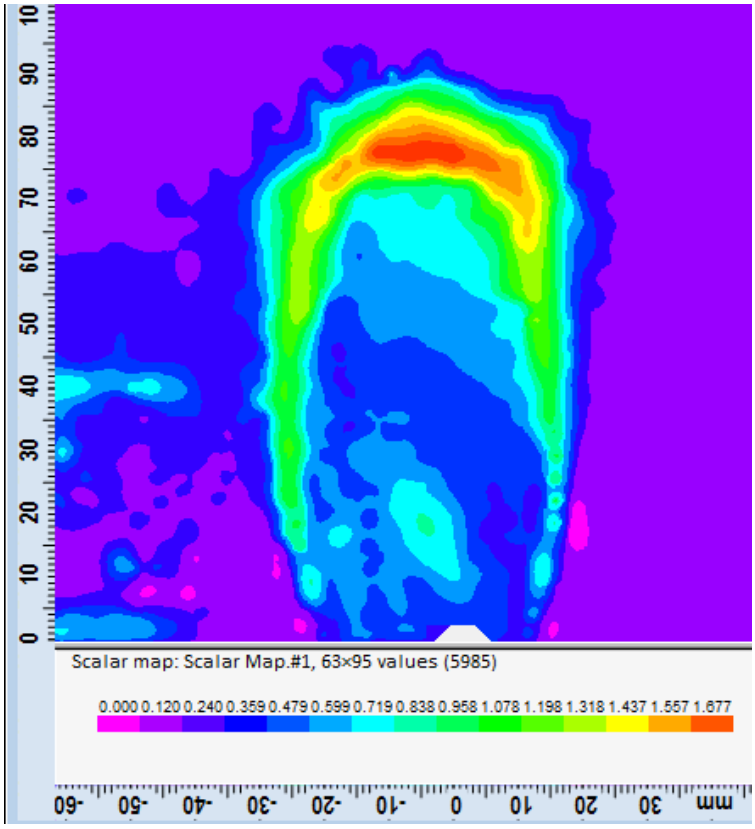

Figure 4.10.1 :(a) Scalar of turbulent intensity for CH4-O2-CO2-H2O flames at constant Re (1500), constant Firing input (1700 W) and ϕ=1

4.11 INVESTIGATION OF LOCAL FLOW-FIELD FLUCTUATIONS OF CH4-AIR FLAME IN A SWIRL STABILIZED COMBUSTOR AT STABLE CONDITION.

Comparison of burning velocity and local flow velocity profiles across the diameter of the combustion chamber were done at two positions x=5cm and x=10cm from the tip of the swirler. The profile for the local

longitudinal flow velocity, fluctuating velocity was generated by averaging over 4000 samples using the instantaneous velocity data extracted from the PIV measurement. The turbulent burning velocity, S_T was computed using the equation proposed by Damkohler[5]:

$$S_T = S_L + u' \quad (4.11.1)$$

where, S_L is the laminar burning velocity provided by the authors in a previous study[5] and u' is the RMS value of the fluctuating velocity component also extracted from the PIV measurement.

Figure 4.11.3 shows the vector flow field of methane air flames with a bulk velocity of 1.9 m/sec and S= 0.97. The high velocity regions which were located closer to the combustion chamber walls, provides enough space recirculation zones which helps the flame to stabilize right in front of the swirler. In recirculation zone, hot exhaust gases travel upstream heating up the un burnt gas mixtures. Eddies and vortices are formed and destroyed rapidly in the recirculation zone. Figure 4.11.4 also shows that turbulence intensity increases along the swirler axis up to certain distance and then decreases. Figure 4.11.5 shows the velocity profile of methane air flames at two different locations, x=5 and x= 10 cm from the tip of the swirler. Figure 4.11.6 shows the turbulent intensity increases as we move farther away from the centre of the

combustor. Figure 4.11.4 shows the turbulent burning velocity increases as we move farther away from the centre of the combustor for methane air flames.

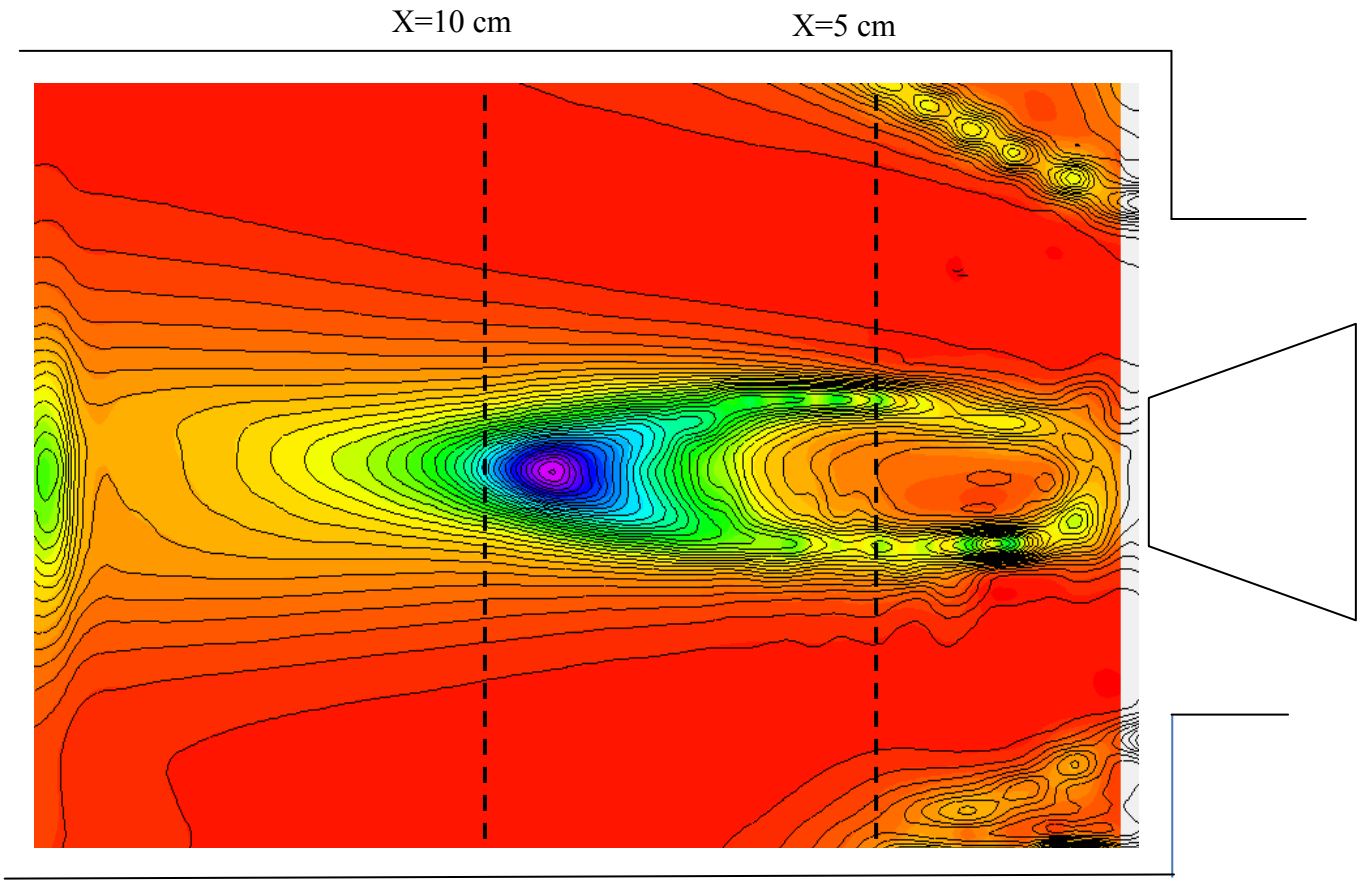

Figure 2: (a) scalar map of turbulence intensity of CH4-air flame at phi=1

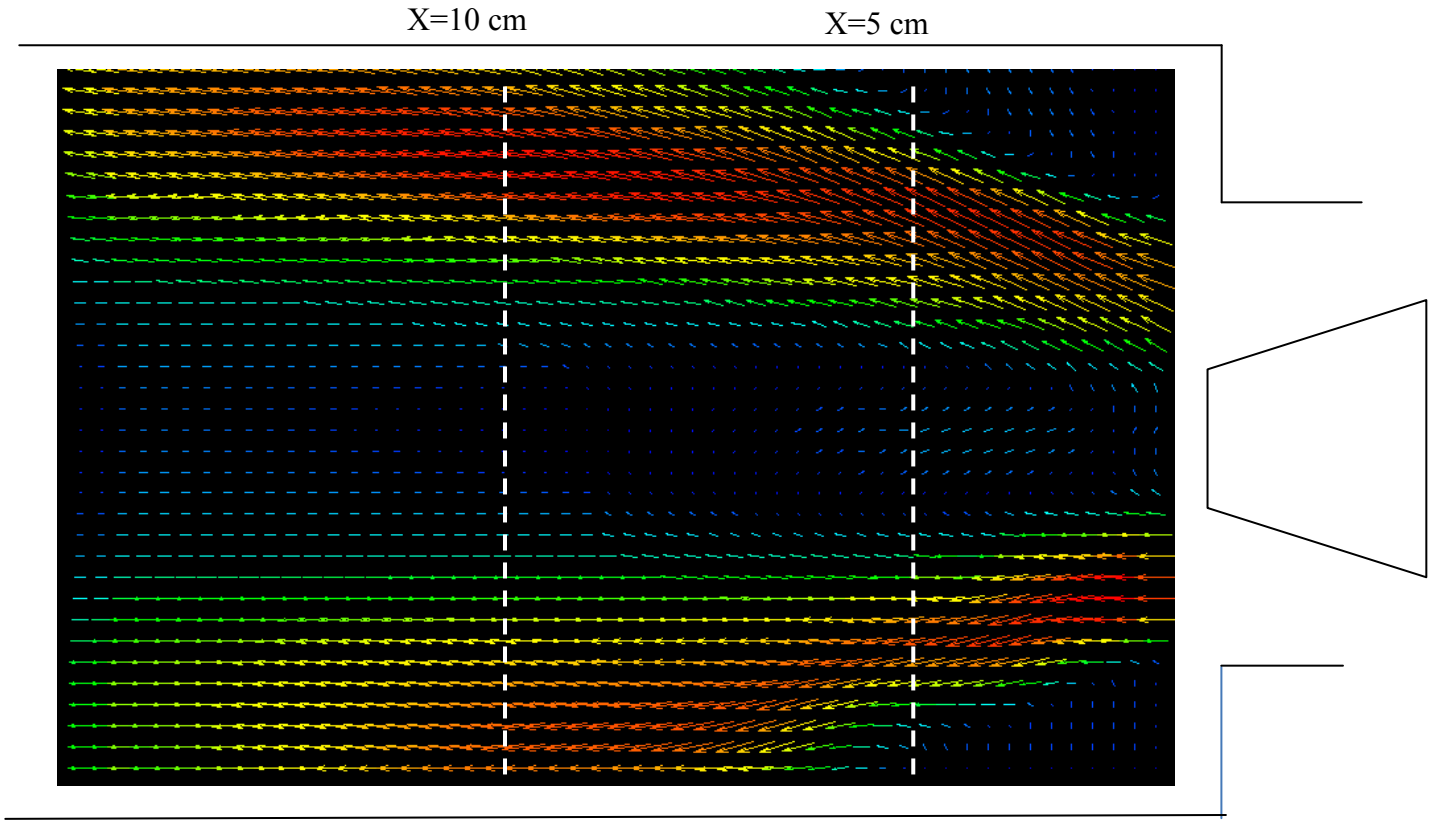

Figure 4.11.3: vector field of CH4- air flame at phi=1

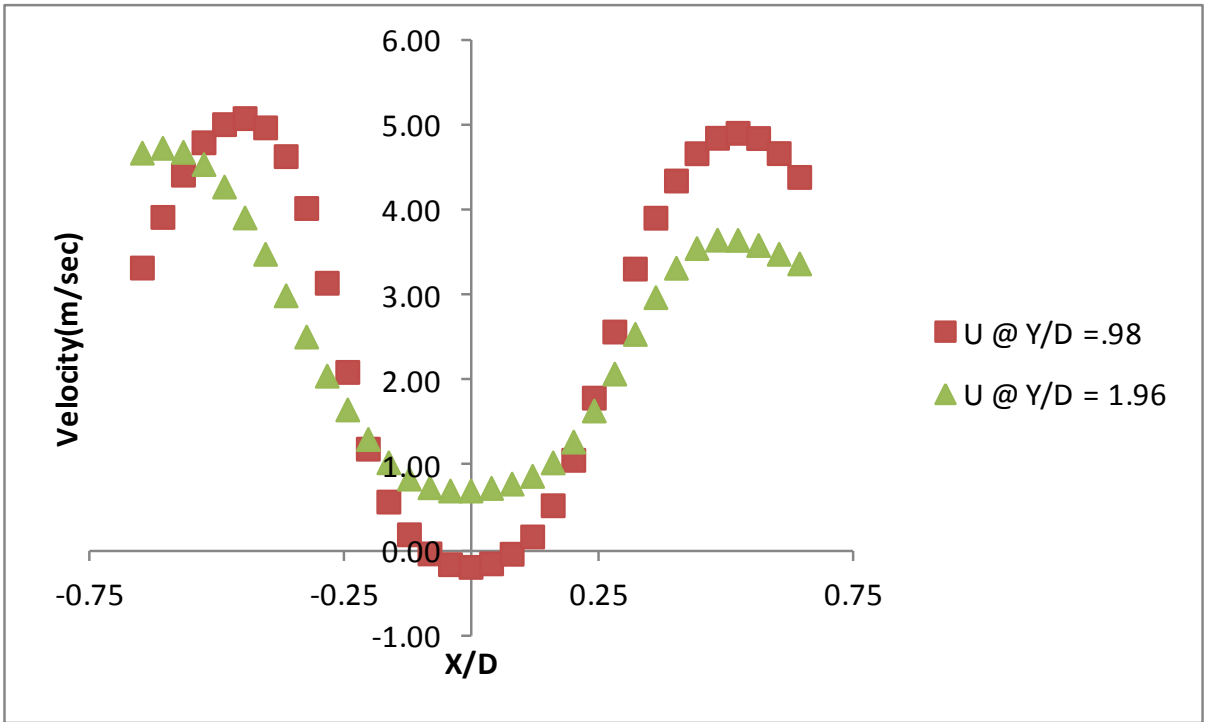

Figure 4.11.4: Local flow velocity profile at a distance x=5 cm and x=10cm from the centre of combustion chamber for methane air flame at Φ = 1

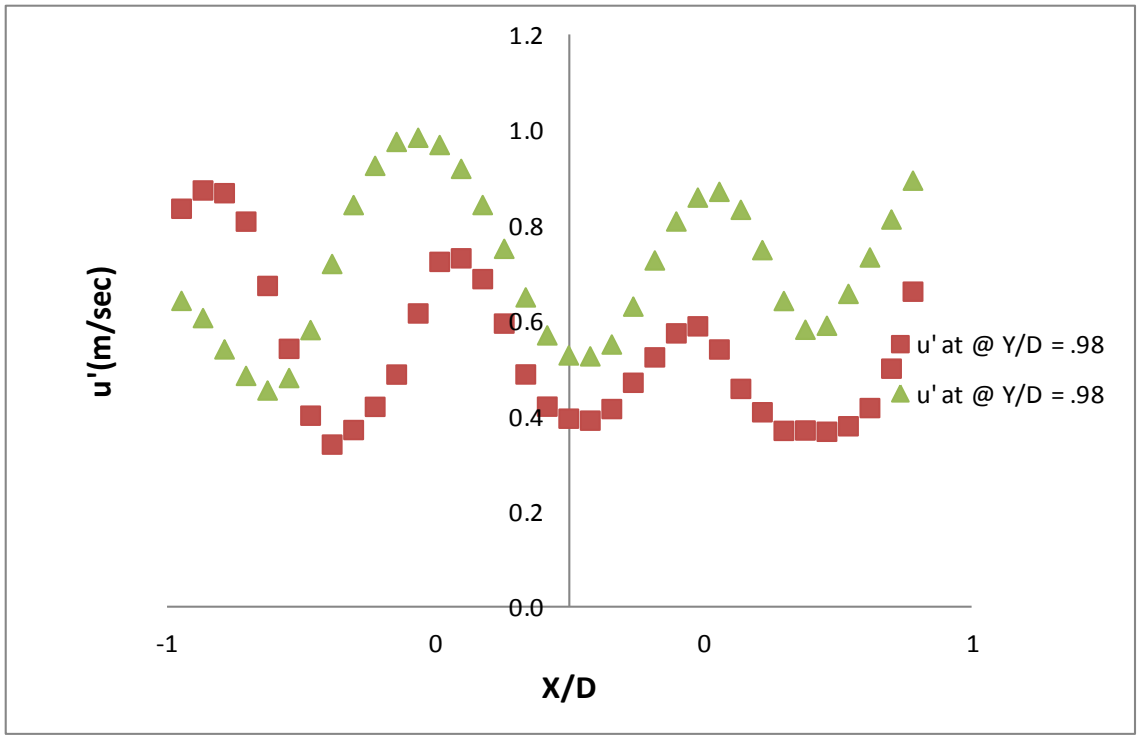

Figure 4.11.5 Turbulent intensity profile at a distance x=5 cm and x=10cm from the centre of combustion chamber for methane air flame at Φ = 1

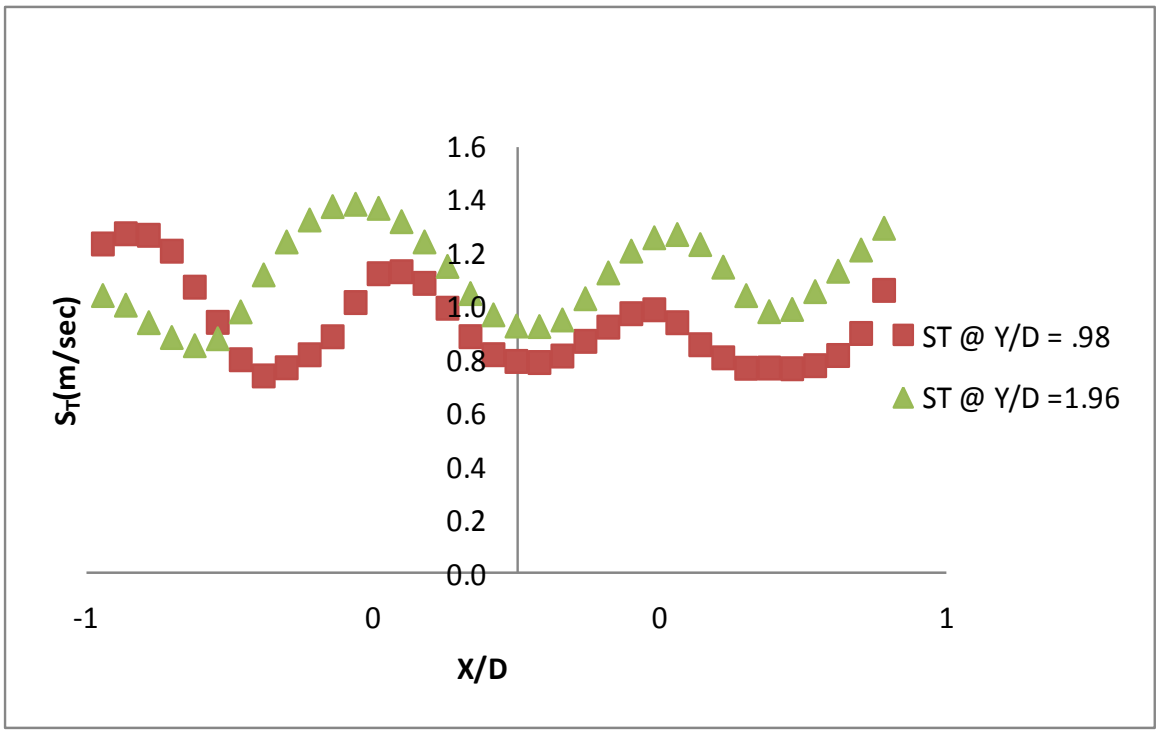

Figure 4.11.6 Turbulent burning velocity profile at a distance x=5 cm and x=10cm from the centre of combustion chamber for methane air flame at Φ = 1

4.12 TEMPERATURE DISTRIBUTION ALONG THE COMBUSTOR FOR VARIOUS OXY-FUEL FLAMES AT STABLE CONDITION

The temperature measurements are done at an offset distance of 5 cm away from the combustor axis. Figure 4.12.1 shows the temperature profile for methane and various compositions of syngas oxy combustion at a constant firing input of 5.5 Kw and the $\Phi = 1$.

Figure 4.12.1 shows that the higher CO2 concentrations are needed in the oxidizer mixture, to stabilize the flame as we move from methane to syngas fuels. The burning velocity of higher hydrogen fuels are higher when compared to low hydrogen content fuels, so higher amounts of CO2 is needed in the mixture to reduce the flame temperature thereby reducing the flame speed. The temperatures across the combustor remained constant as the firing input was maintained constant for all the mixtures.

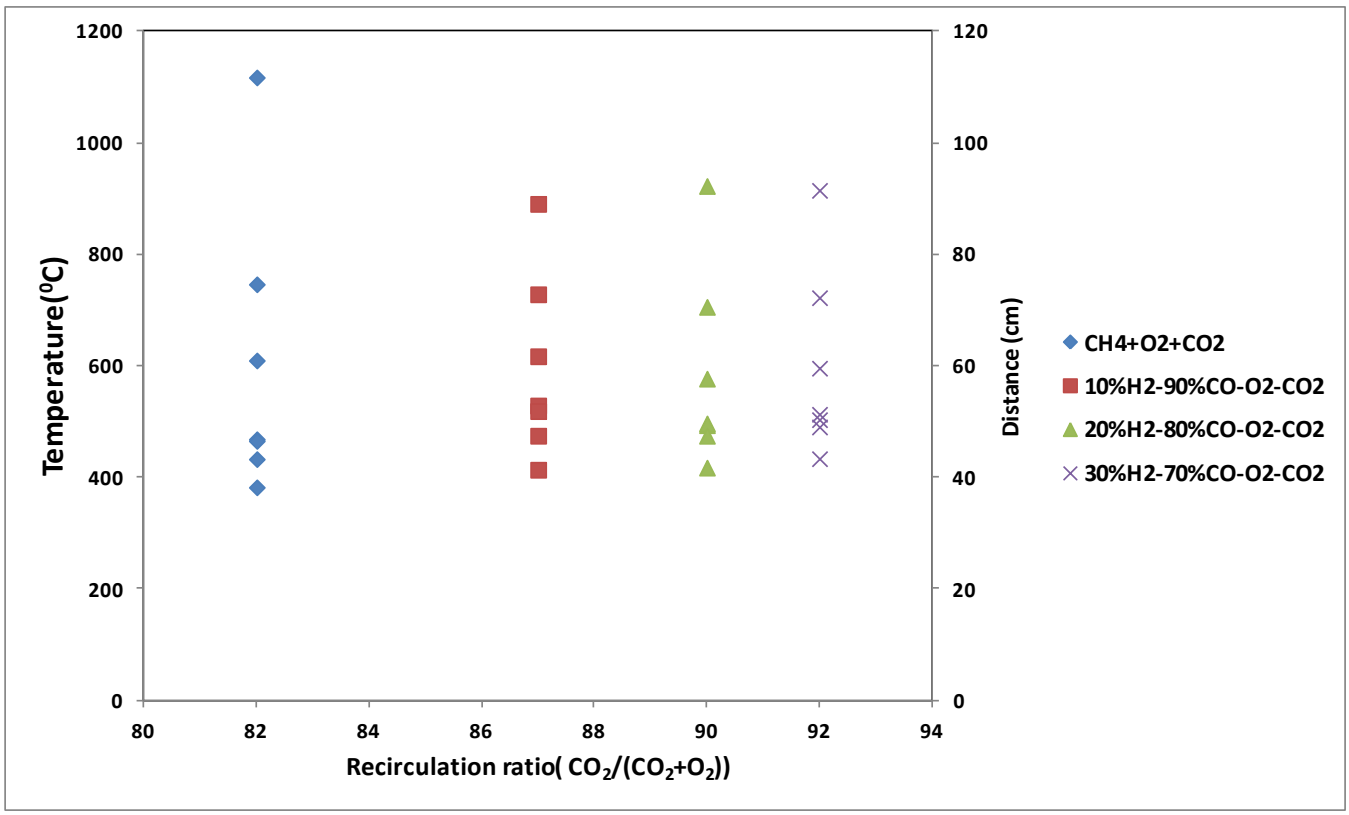

Figure 4.12.1: temperature distribution of methane and various compositions of syngas oxy combustion at a constant firing input of 5.5 Kw and the Φ = 1.

Chapter 5: Conclusions

For a constant equivalence ratio of 0.9 and RE of 2000 the turbulent burning velocities not only increased with increase in hydrogen content but also increased when the BR's increased .Turbulent burning velocities increased with increase in BR's as the hydrogen content increased in syngas mixture at a constant laminar burning velocity for syngas compositions varying from 10%H_2 to 30 % H_2. Turbulent burning velocities increased with increase in the BR's along with the increase in N_2 and CO_2 in Syngas mixtures.CO_2 as a diluents is more prominent than N_2 , the increase of CO_2 in the Syngas mixtures decrease the turbulent burning velocity.

For a constant equivalence ratio of 1 and RE of 2500 the local velocity fluctuations not only increased with increase in turbulent intensity but also increased with increase in when the firing input is increased along the burner axis. Local velocity fluctuations were higher for CH4-O2-CO2-Ar flames at RR_{CO_2} =70 when compared with CH4-O2-CO2 RR_{CO_2} =74% , since the heat released is high for CH4-O2-CO2-Ar flames as CO2 is chemically active and reduces the flame temperature whereas Argon is chemically inert and does not participate in any reaction.

For a swirl stabilized combustor, turbulence intensity increases along the swirler axis up to certain distance and then decreases. For a constant equivalence ratio of 1 and firing input of 5.5 Kw, the amount of CO2 needed in the oxidizer mixture to stabilize the flame is increased as we move from methane to syngas fuels.

References

Amato A, Hudak B, D'Souza P., D'Carlo P., Noble D., Scarbourough D., Seitzman J., Lieuwen T, "*Measurments and analysis of CO and O2 emissions in CH4/CO2/O2 flames*" Proceedings of Combustion Institute, Vol. 33. pp. 3399-3405, 2010.

Andersson K, Johansson R, Leckner B, "*Radiation intensity of propane-fired oxy-fuel flames: implications for soot formation.*" Vol. 22, pp.1523-41, 2008.

Ashman P.J, Haymes B.S, "*Rate coefficient of H+O2+M=>HO2+M (M=Ar,N2,CO2)*". Twenty-Seventh Symposium (International) on Combustion/The Combustion Institute, Australia, pp. 185-191,2006.

Brandl A, Tangermann E, Pfitzner M, "Validation of premixed combustion models using turbulent Bunsen flames at high pressure" 10thInternational Workshop on Premixed Turbulent Flames Mainz, germany, 2006.

Candel S. M and Poinsot T, "Flame stretch and the balance equation for the flame area."*Combust. Sci. Technol.*, 70:1-15, 1990.

Carbon sequestration Technologies Website, National Energy Technology Laboratory, Department of Energy, Web address: http://www.netl.doe.gov/technologies/carbon_seq/ 2007Roadmap; Accessed on 2007.

Damkohler G 1940, Der Einfl uss der Turbulenz auf die Flammengeschwindigkeit in Gasgemischen, *Zs, Electrochemie* 6(11):601–626

Davis S.G, Joshi A.V, Wang H, and Egolfopoulos F, "*An Optimized Kinetic Model of H2 /CO Combustion.* "Proceedings of Combustion Institute, Vol. 30.pp.1283.

Davison A, Thambiathu K, " *Technologies for capture of carbon dioxide*" Technical Review. Canada, 2005

Dardea A, Prabhakar R, Tranier J, Perrin N," *Air separation and flue gas compression and purification units for oxy-coal combustion systems*" 2009

Dickens P.G., Linett J.W, "*Efficiencies of third bodies in the reaction H+O2+M=> HO2+M.*" Chemistry and Phisics, Vol. 2.pp. 259.

Ditaranto M, Hals J, "*Combustion instabilities in sudden expansion of oxy-fuel flames.* Combustion and flame", Trondheim , Vol. 146, pp. 493-512, 2006.

Durst F, Melling A & Whitelaw J. H: "Principles and practice of Laser Doppler Anemometry", second edition, *Academic Press*, 1981.

Driscoll J. F, Turbulent premixed combustion –"Flamelet structure and turbulent burning velocities". *Prog. Energy Combust. Sci.*, 34:91-134, 2008.

Eggenspieler G and Menon S "Combustion and emission modelling near lean blow-out in a gas turbine engine." *Prog. Comput. Fluid. Dy.*, 5(6):281-297, 2005.

Ganapathisubramani B, Lakshminarasimhan K, Clemens NT (2007) "Determination of complete velocity gradient tensor by using cinematographic stereoscopic PIV in a turbulent jet. Exp Fluids 42(6):923–939

Glarborg P., Bentzen L.B.. "*Chemical effects of high CO2 concentration in Oxy-fuel combustion of Methane*" Energy and fuels, Vol. 22. pp. 291-296, 2008

Jarosinski, Jozef, and Bernard Veyssiere. Combustion Phenomena: Selected Mechanisms of Flame Formation, Propagation and Extinction. 1 ed. Boca Raton: CRC, 2009.

Koboyashi H., Hagiwara H ,Kaneko, Ogami H,Y" *Effects of CO2 dilution on turbulent premixed flames at high pressure and temperature"* Proceedings of the Combustion Institute, , Vol. 31. pp. 1451-1458, 2007

Law C. K and Sung C. J "Structure, aerodynamics, and geometry of premixed Flamelets." *Prog. Energy and Combustion. Science.*, 26:459-505, 2000.

Lieuwen, Tim C., Vigor Yang, and Richard Yetter. *Synthesis Gas Combustion: Fundamentals and Applications*. 1 ed. Boca Raton: CRC, 2009.

Liu F, Guo H, Smallwood G. J, and Gulder O. L, "The chemical effects of carbon dioxide as an additive in an ethylene diffusion flame: implications for soot and NOx formation," *Combustion and Flame*, vol. 125, pp. 778, 2001

Liu F., Guo H., Smallwood G.J. "*The chemical effect of CO2 replacement of N2 in air on the burning velocity of CH4 and H2 premixed flames*" Combustion and flame, vol. 133 pp.495-497, 2003.

Lumley, J. L., and Tennekes H. "1." In A First Course in Turbulence. London: The Mit Press, 1972. 1.

Mallard E and Le Chatelier H. L. *Annals of Mines*, 4:379-568, 1883

Matalon M." On flame stretch". *Combustion. Science. Technology.*, 31(3):169-181, 1983

Natarajan J, Lieuwen T, Seitzman J, 2005,"Laminar Flame Speeds of H_2/CO Mixtures: Effect of CO_2 Dilution, Preheat Temperature, and Pressure," *Combustion and Flame*, **151**, pp. 104–19.

Peters N. "*Turbulent Combustion*". Cambridge University Press, Cambridge, UK, 2000.

Pocheau A. "Front propagation in a turbulent medium". *Europhys. Lett.*, 20:401-406, 1992

Poinsot T and Veynante D. "*Theoretical and Numerical Combustion*". Edwards, Philadelphia,
PA, 2 edition, 2005.

Prabhakar Venkateswaran, Andrew D. Marshall, David R. Noble, Jose Antezana, Jerry M. Seitzman and Tim C. Liewen,"Global Turbulent Consumption Speeds of H_2/CO Blends" Proceedings of ASME Turbo Expo 2009,GT2009-59685

Ruan J, Kobayashy H, Niioka T,"*Combined effects of nongray radiation and pressure on premixed CH4/O2/CO2 Flames.*" Japan : s.n.

Upatnieks A, Driscoll JF, Ceccio SL, Rasmussen CC (2004) "Liftoff of turbulent jet flame assessment of edge flame and other concepts using cinema-PIV". Combust Flame 138(3):259–272

Vishwanath Ardha, Bidhan Dam and Ahsan Choudhuri."Laminar Burning Velocities of Syngas Fuels". Journal of Energy Resource Technology, JERT-10-1047

Wall TF," *Combustion processes for carbon capture*. s.l. : Proceedings of Combustion Institute, 2007, Vol. 31. 31-47.

Westbrook C.K., Dryer F.L,. *Chemical kinetic modelling of hydrocarbon combustion*. 1, s.l. : Progress in Energy and Combustion Science, Vol. 10, 1989

Zhang C, Atreya A, Lee K, "Sooting structure of methane counterflow diffusion flames with preheated reactants and dilution by products of combustion" Combustion and Flame, pp.1049,1992

"2D-PIV Reference Manual" 2nd edition Publication no: 9070U1752, Dantech Dynamics, 2005

Vita

Vishwanath Reddy Ardha earned his Bachelor of Science degree in Mechanical Engineering from Valluripalli Nageswara Rao Vignana Jyothi Institute of Engineering and Technology, India in 2007. He received his Master of Science degree in Mechanical Engineering in December, 2009 from University of Texas at El Paso. He joined the Doctoral program in 2010 through the Energy Science and Engineering track in Environmental Science and Engineering program at the University of Texas at El Paso (UTEP). Dr. Ardha has been recipient of State of Texas Public Education Grant (TPEG) for International Students 2011.While pursuing his degree, Dr. Ardha worked as a research assistant for the department of Mechanical Engineering and worked on funded projects for the US Department of Energy (DOE) which have being conducted at NASA Center for Space Exploration Technology Research (cSETR). He also worked as a Teaching Assistant for Mechanical Engineering department, UTEP.

Dr. Ardha has published his research findings in multiple refereed Journals and presented in multiple international conferences Dr. Ardha's dissertation entitled "Measurement and analysis of premixed turbulent Oxy-Fuel combustion" was supervised by Dr. Ahsan Choudhuri.

Permanent address: HNo#3505 Vidyut Nagar, Ramchandrapuram
Hyderabad, Andhra Pradesh, 502032, INDIA.

This thesis/dissertation was typed by Vishwanath Reddy Ardha.